A SYNTHETIC GENETIC SYSTEM TO INVESTIGATE BRAIN CONNECTIVITY AND GENETICALLY MANIPULATE INTERACTING CELLS

A Dissertation Presented

By

Ting-Hao Huang

Submitted to the Faculty of the

University of Massachusetts Graduate School of Biomedical Sciences, Worcester

in partial fulfillment of the requirements for the degree of

DOCTOR OF PHILOSOPHY

A SYNTHETIC GENETIC SYSTEM TO INVESTIGATE BRAIN CONNECTIVITY AND GENETICALLY MANIPULATE INTERACTING CELLS

A Dissertation Presented By

Ting-Hao Huang

This work was undertaken in the Graduate School of Biomedical Sciences
Program in Neuroscience

The signature of the Thesis Advisor signifies
validation of Dissertation content

_____
Carlos Lois, M.D., Ph.D., Thesis Advisor

The signatures of the Dissertation Defense Committee signify
completion and approval as to style and content of the Dissertation

_____
Kensuke Futai, Ph.D., Member of Committee

_____
Paul Garrity, Ph.D., Member of Committee

_____
Hong-Sheng Li, Ph.D., Member of Committee

_____
Yang Xiang, Ph.D., Member of Committee

The signature of the Chair of the Committee signifies that the written dissertation
meets the requirements of the Dissertation Committee

_____
Patrick Emery, Ph.D., Chair of Committee

The signature of the Dean of the Graduate School of Biomedical Sciences signifies
that the student has met all graduation requirements of the school.

_____
Anthony Carruthers, Ph.D.,
Dean of the Graduate School of Biomedical Sciences

March 7th, 2017

DEDICATION

To my grandparents in heaven! They will be always in my heart.

ACKWOLEDGEMENT

First I would like thank my advisor, Dr. Lois, for his mentoring and support throughout the years, not only to my research but also to broaden my vision in scientific fields. I aspire to be a scientist like him- always curious and full of ideas. I also thank him for being so supportive and thoughtful to me and my family. I also want to thank all my thesis research committee members Dr. Patrick Emery, Dr. Claire Benard, Dr. Marc Freeman and Dr. Kensuke Futai for their guidance and input for my research.

My research would not be possible without the help from the current and former colleagues in the lab, Tarciso Velho, Salome Antolin, Lius Sanchez, Bo Wang, Walter Gonzalez, Robert Agate, Antuca Callejas, Donghyung Lee, Aubrie De La Cruz, John Neary, Barbara Rymeski and Marie Maloof, for all the help and advice to my experiments, my career and my life. I also would like to thanks the colleagues in Neurobiology department, especially, in Dr. Benard lab and Dr. Alkema lab, for the support and teaching me how to handle worms, and Tobias Stork and Lukas Neukomm in Dr. Freeman lab for the precious comments and suggestions for my fly experiments.

Many thanks to all the friends in Massachusetts for helping my family and me, especially Kuan-Hung, Ping-I, Jen-Chieh, Amanda, Ming-Hung, Ya-Ting, Tsung-Han, Hsin-Jung, Yung-Chi, Tsai-Yi, Hui-Fang, Yu-Jie, Li-Ching, Tsun-Kai and Chia-Yu for the camaraderie and all the good times hanging out together; also

the people in BTCC for their care and their prayers.

I would like to give special thanks to my beloved family, my parents and my parents-in law for their supports so that I can have the opportunity to pursue my dream; my lovely daughter and my incoming son for their love so that I'm full of energy every day to face any task; my dearest wife for the support, especially during the time I was preparing my dissertation, and make me become a better person.

Finally, I would like to give thanks to the Lord for his blessing and guidance. More and more I studied, more and more I learned His mighty. "For since the creation of the world His invisible attributes, His eternal power and divine nature, have been clearly seen, being understood through what has been made, so that they are without excuse." Romans 1:20. May the Lord continue to bless everyone in my life!

ABSTRACT

The underlying goal of neuroscience research is to understand how the nervous system functions to bring about behavior. A detailed map of neural circuits is required for scientists to tackle this question. To this purpose, we developed a synthetic and genetically-encoded system, **TRanscellular ACtivation of Transcription (TRACT)** to monitor cell-cell contact. Upon ligand-receptor interaction at sites of cell-cell contact, the transmembrane domain of an engineered Notch receptor is cleaved by intramembrane proteolysis and releases a fragment that regulates transcription in the receptor-expressing cell. We demonstrate that in cultured cells, the synthetic receptor can be activated to drive reporter gene expression by co-incubation with ligand-expressing cell or by growth on ligand-coated surfaces. We further show that TRACT can detect interactions between neurons and glia in the Drosophila brain; expressing the ligand in spatially-restricted subsets of neurons leads to transcription of a reporter in the glial cells that interact with those neurons. To optimize TRACT for neural tracing, we attempted to target the synthetic receptor to post-synaptic sites by fusion with the intracellular domain of *Drosophila* neuroligin2. However, this modification only facilitate the receptor to be localized homogeneously throughout the neurites. The induction data of the modified receptor shows that the new receptor has better sensitivity compared to the original receptor, but the ligand-receptor interaction still happened at non-synaptic sites of membrane contact. To further target the ligand to pre-synaptic sites, we fused the ligand to

different pre-synaptic markers. We found the one fused with synaptobrevin is likely located at axon terminals, but only able to trigger moderate induction. Therefore, more examinations are required to further characterize the capability of this ligand. In summary, TRACT is useful for monitoring cell-cell interactions in animals and could also be used to genetically manipulate cells based on contact. Moreover, we believe that proper targeting of the ligand to synaptic sites will improve the specificity of TRACT for synaptic connections in the future.

TABLE OF CONTENTS:

List of Figures

List of Tables

List of Abbreviations

AAV: adeno-associated viruses

ALs: antennal lobes

AMMC: antennal mechanosensory and motor center

ATUM-SEM: automatic tape-collecting ultramicrotome scanning electron microscopy

AVPR2: arginine vasopressin receptor 2

BAC: bacterial artificial chromosome

Brp: Bruchpilot

ChAT: choline acetyltransferase

CLEM: Correlative Light Electron Microscopy

CNS: central nervous system

D: dorsal

DL: dorsolateral

DM: dorsomedial

ECD: extracellular domain

EM: electron microscopy

FACS: fluorescence-activated cell sorting

FIB: focused ion beam

FKBP: FK506 binding protein

FRT: FLP recognition target

FTCD: formimidoyltransferase-cyclodeaminase

GECIs: genetically encoded calcium indicators

GFP: green fluorescent protein

GPCRs: G protein-coupled receptors

GRASP: GFP Reconstitution Across Synaptic Partners

HA: histamine

HD: heterodimerization domains

HSV1: Herpes simplex virus type 1

iACT: inner antennal tract

ICD: intracellular domain

KCs: Kenyon cells

L: lateral

La: lamina

LM: Light Microscopy

LNs: local interneurons

LNRs: LIN-12/Notch repeats

LZ: leucine zipper

M: medial

mACT: middle antennal tract

MB: Mushroom body

Me: medulla

mPNs: multiglomerular PNs

NRR: Notch regulatory region

Nrx1: Neurexin1

nSyb: neural synaptobrevin

OLs: optic lobes

Ort: ora transientless

OSNs: olfactory sensory neurons

PA-GFP: photoactivatable green fluorescent protein

PALM: PhotoActivatable Light Microscopy

PNs: projection neurons

PRV: pseudorabies virus

RG: rabies glycoprotein

RV: rabies virus

S1LO: S1 loop-out

SBEM: Serial-block face scanning microscopy

SCAD: single chain antibody domain

ssTEM: serial-section transmission electron microscopy

STaR: Synaptic Tagging with Recombination

STED: STimulated Emission Depletion microscopy

STORM: STochastic Optical Reconstruction Microscopy

SNTGV: SCAD/NRR/TMD/GV

Syx: syntaxin

TACE: Tumor necrosis factor-□-Converting Enzyme

TAD: transcription activation domain

TCS: TEV Protease Cleavage Site

TEM: transmission electron microscopy

TEV: tobacco etch virus

TMD: transmembrane domain

TRACT: TRanscellular ACtivation of Transcription

uPNs: uniglomerular PNs

V: ventral

VL: ventrolateral

VM: ventromedial

VNC: ventral nerve cord

WGA: wheat germ agglutinin

CHAPTER 1 - Methods to investigate neuronal connectivity in the brain

This Chapter was adapted from the manuscript:

Methods to investigate the structure and connectivity of the nervous system.

Donghyung Lee, Ting-Hao Huang, Aubrie De La Cruz, Antuca Callejas, Carlos Lois. Fly (Austin). 2017 Feb 16:0. [Epub ahead of print]

THH and CL initiated the idea. DL, THH, ADLC, AC and CL prepared the manuscript. DL drew the figures. THH and CL coordinated and supervised the preparation of the manuscript.

Introduction

Understanding the computations that take place in neural circuits requires identifying how neurons in those circuits are connected to one another. In addition, recent research indicates that aberrant neuronal wiring may be the cause of several neurodevelopmental disorders, further emphasizing the importance of identifying the wiring diagrams of brain circuits. Therefore, in recent years, there has been a resurgence in interest in the analysis of the wiring diagrams of nervous systems, the so-called connectomics. The study of the connectome originated with the pioneering reconstruction of the entire *C. elegans* nervous system by electron microscopy (EM) in 1980, and has expanded to additional organisms, such as *Drosophila* and mice. The *C. elegans* nervous system, comprised of just over 1,000 neurons, is relatively simple to analyze. In addition, due to its fast generation time and reproductive peculiarities, *C. elegans* is an outstanding model for genetic analysis. However, there are a few issues that limit the usefulness of *C. elegans* for studies of the nervous system. First, *C. elegans* has a very limited behavioral repertoire. Second, *C. elegans* neurons lack voltage-gated sodium channels and consequently do not fire action potentials. Neurotransmitter release in *C. elegans* occurs via graded depolarizations mediated by voltage-gated calcium channels, a mechanism that is not shared by vertebrates or most invertebrates. Finally, electrophysiological recordings in *C. elegans* are notoriously challenging. Consequently, it is difficult

to establish correlations between synaptic activity and behavior in *C. elegans*.

The mouse is an attractive model for neuroscience. It is the most genetically tractable mammal, and there is strong conservation of physiology and anatomy between the rodent and human brain. In addition, despite its relatively slow generation time, techniques for genetic manipulation and electrophysiological recordings in mice are highly sophisticated. However, the mouse brain has more than 100,000,000 neurons, making it very difficult to analyze and understand the structure and dynamics of its nervous system.

The *Drosophila* brain, by comparison, only has around 100,000 neurons. The simplicity of its brain combined with the sophisticated tools available for genetic manipulation allow scientists to map entire circuits in *Drosophila* at the cellular level. At the same time, *Drosophila* exhibit more sophisticated behavior and circuitry than do *C. elegans*, making the study of its nervous system pertinent to understanding our own. In fact, some of its brain circuits, such as the olfactory circuit, show significant overlaps in organization and function with equivalent circuits in the mammalian brain. Ultimately, the *Drosophila* brain is an excellent model system for understanding how the connectome gives rise to function and behavior. As a result, many of the new methods to investigate the connectivity of neurons have been developed for use in *Drosophila*. These methods can be broadly divided into two groups: those based on electron microscopy (EM) analysis of brain tissue, and those based on genetic techniques.

(1-1) Analysis of synaptic organization by EM:

EM represents the gold standard for analysis of brain structure. Due to its high resolution, EM can unambiguously identify synapses. EM uses accelerated electron beams instead of light as its source of illumination and can consequently reveal the ultrastructure of biological tissue with xy-resolution as high as 2 nm. Chemical synapses can be visually identified from EM image because synaptic vesicles are concentrated at the presynaptic site and most *Drosophila* presynaptic sites have a morphological specialization called the T-bar as a pre-synaptic marker.

There are several variations of EM that can be used to study brain connectivity, but the one that has been used most extensively by neuroanatomists is serial-section transmission electron microscopy (ssTEM). For this technique, biological tissue is fixed, stained, embedded in resin, and then serially cut into sections around 40 nm thick with an ultramicrotome. The resulting slices are collected and visualized by transmission electron microscopy (TEM), which measures the electrons that pass through the sample. TEM offers the best xy-resolution of all EM methods. After images are generated from serial sections, they are first aligned along the xy-axis. Then, cellular membranes and organelles are identified and marked in a process known as segmentation. Finally, the segmented images are linked across the z-axis for 3D-reconstruction of neurons.

Though the initial steps (sectioning, imaging, alignment and segmentation) can be automated with varying degrees of success, reconstructing and proofreading a 3D-model from serial images requires hundreds of hours of skilled labor and represents the limiting step. Ongoing work seeks to streamline this process (Chklovskii et al., 2010; Schneider-Mizell et al., 2016).

The resolution of EM reconstructions offers two main advantages over other connectomic techniques. First, EM reconstructions can yield a comprehensive understanding of a small neuronal circuit. For example, the EM volume generated from the antennal lobe of *Drosophila* larva identified over 38,000 synapses among 160 neurons (Berck et al., 2016). Analysis of this connectome allowed the authors to build a circuit-level model that suggests how larva could move towards food sources while staying vigilant to predator-related olfactory cues. Additionally, the high resolution of EM leads to a quantitative assessment of neural circuits. Because EM reconstructions can reveal the size and the number of the synapses that exist between neurons, EM can provide an estimation of the strength of connection between neurons. This can be subsequently used to support theories of circuit function (Takemura et al., 2013). Although understanding circuit mechanisms rarely comes from its wiring diagram alone, the detail of connectomes generated by EM allow for models that can be subsequently tested with functional experiments.

EM is an extremely powerful method, but it suffers from several important limitations. First, for tissues to be analyzed by EM, they need to be fixed and

dehydrated. This process kills the cells in the tissue, preventing the direct combination of EM with functional analysis by electrophysiological or optical recordings. Second, EM is extremely time and labor-intensive. For reference, the seminal reconstruction of the *C. elegans* connectome took several years to complete for one single specimen. Similarly, EM reconstructions of the larval antennal lobe (Berck et al., 2016), the adult optic medulla (Takemura et al., 2013), and the A2 and A3 segments of VNC (Butcher et al., 2012) provide exhaustive connectomic data but only in localized circuits and for single samples. Even with the continuing optimization of automated reconstructions, EM will likely remain unsuitable for studying the connectivity of neurons with long-range projections. For example, when analyzing the structure of a brain circuit in Drosophila, it is impossible to identify the origin of the axons that belong to neurons located in the ventral nerve cord (VNC). Additionally, the variability of neural connections across time, between individuals, or with respect to directed mutations is unsuitable for analysis by EM.

1-1.A - Future advances for EM:

New advances in EM techniques promise to address some of the bottlenecks associated with traditional ssTEM. For example, automatic tape-collecting ultramicrotome scanning electron microscopy (ATUM-SEM) automates the process of collecting the serial sections created with an ultramicrotome.

Serial-block face scanning microscopy (SBEM), on the other hand, utilizes an electron microscope with a built-in ultramicrotome such that the sample is imaged as the top layer is serially sectioned and removed. Similarly, in focused ion beam (FIB) SBEM, the surface of the sample is imaged, and then vaporized with a focused ion-beam to allow for imaging of the next layer. SBEM techniques lead to flawlessly automated alignment across the z-axis. Though all of these techniques provide lower xy-resolution than ssTEM, FIB-SEM offers higher z-resolution than does ssTEM (10 nm vs. 40 nm). The superior z-resolution enables scientists to generate EM volumes with isotropic voxels that can be digitally resectioned for best graphical representation of neuritis (Hayworth et al., 2015). Such advancements in EM techniques, combined with ongoing efforts to automate 3D-reconstructions, offer the possibility of applying EM to larger volumes and larger sample size in the future.

Additionally, there is great interest in developing strategies for Correlative Light Electron Microscopy (CLEM) (Begemann and Galic, 2016). Traditionally, sample preparations for EM and LM have been incompatible, preventing the combination of EM and LM for the same sample. Several methods now exist to allow for CLEM. Optimized freeze-substitution embedding methods allow fluorescence imaging and EM imaging of the same sample in succession (Collman et al., 2015). In addition, a gene called miniSOG has been designed to act as a genetically encoded tag that can be visualized by LM and EM. miniSOG is a fluorescent protein that can be directly imaged by fluorescence microscopy,

and can be induced to produce singlet oxygens that generate an electron-dense material detectable by EM (Shu et al., 2011). Similarly, neurons of interest can be tagged with GFP, imaged *in vivo* with two-photon microscopy, and marked by etching with a near-infrared laser for identification at the EM level (Blazquez-Llorca et al., 2015). Parallel efforts in EM chemistry led to the development of multicolor EM (Adams et al., 2016). In this strategy, conjugated antibodies are used to locally deposit lanthanides that have distinct energy-loss spectra. The distribution of each lanthanide in the sample can be independently recorded with energy-filtered TEM to create pseudocolored images that are overlaid on a traditional EM image. Currently, there are 3 lanthanides that can be used to orthogonally mark molecules on an EM image. Application of multicolor EM to connectomic studies, in conjunction with advancements in CLEM, would allow scientists to conveniently integrate ultrastructural information about synapses with genetic tools that can readily label distinct subpopulations of neurons.

(1-2) Analysis of synaptic organization by LM:

As mentioned above, the main limitations of EM are that it cannot be used to examine live tissue, trace long distance connections, or investigate large numbers of samples. These bottlenecks of EM can be overcame by LM, which is considerably less time- and labor-intensive. Unfortunately, the resolution of LM is restricted to the wavelength of light used to illuminate the samples (400-600 nm). However, recently developed techniques such as STED (STimulated Emission

Depletion) microscopy (Hell and Wichmann, 1994; Klar et al., 2001), PALM (PhotoActivatable Light Microscopy), and STORM (STochastic Optical Reconstruction Microscopy) (Nienhaus and Nienhaus, 2014; Yamanaka et al., 2014) allow investigators to image the brain at subdiffraction limit resolution (10-50 nm for lateral resolution, Maglione and Sigrist 2013). STED uses patterned illumination to restrict light emission to a small region, while PALM and STORM use spare photoactivation of fluorophores to achieve a similar goal (Huang et al., 2010). At this resolution, subcellular structures such as individual neurotransmitter vesicles or T-bars can be discerned. Although the resolution of these methods is still lower than that of TEM, LM offers two major advantages. First, LM can be directly combined with genetic methods for labeling cells. The wealth of genetic tools in flies makes it possible to direct expression of fluorescent proteins or other transgenes to neuronal subpopulations. In conjunction with thousands of promoter elements that are widely available, there are three modular systems (Gal4/UAS, LexA/LexAop, and QF/QUAS) that can be used orthogonally to express pre- and postsynaptic markers in distinct sets of neurons, but also combinatorially to direct expression to highly precise subpopulations of neurons (del Valle Rodriguez et al., 2011). Additionally, LM can be used in live animals with parallel electrophysiological and optical imaging techniques. This allows researchers to combine structural and functional information in a way that EM cannot.

Several methods, including STaR (Synaptic Tagging with Recombination), use genetic labeling of synaptic sites to identify putative synaptic contacts between neurons (Chen et al., 2014; Christiansen et al., 2011; Kremer et al., 2010; Mosca and Luo, 2014) (Fig. 1-1). These methods have been used to study the variation in synaptic organization among individuals in different conditions and at different developmental stages, and to compare the changes in connectivity caused by mutations (Akin and Zipursky, 2016; Chen et al., 2014; Christiansen et al., 2011; Liu et al., 2016b; Mosca and Luo, 2014). In these methods, pre- and postsynaptic markers need to be genetically fused with different tags, such as fluorescent proteins, or tags that can be detected by immunocytochemical staining, such as the V5, HA, or OLLAS tag (Fig 1-1a). Therefore, by analyzing the proximity of pre- and postsynaptic markers, putative synaptic sites can be revealed directly by LM imaging (Fig. 1-1b). Moreover, as in most methods that depend on LM, fluorescent protein-tagged synaptic markers allow for the monitoring of changes in synapses in the same animal over time by live imaging using methods such as 2-photon microscopy (Chen et al., 2014).

The most common tagged marker to locate presynaptic sites is Bruchpilot (Brp), a large protein that selectively localizes to most active zones in the presynaptic site. However, it is important to note that several EM studies have shown that some (Robinson et al., 2002) presynaptic sites in the *Drosophila* brain, such as the calyx of the mushroom body, are devoid of the T-bar structure,

and the Brp protein level in some of the T-bars is either too low to be detected or completely absent (Butcher et al., 2012; Hamanaka and Meinertzhagen, 2010; Meinertzhagen and Lee, 2012). Therefore, it is necessary to validate the expression of the tagged Brp marker in different types of synapses in different brain regions before using this marker. As an alternative, tagged synaptic vesicular proteins, such as synaptobrevin and synaptotagmin, can be used to mark presynaptic sites (Robinson et al., 2002; Rolls et al., 2007; Uytterhoeven et al., 2011; Zhang et al., 2002). Because these two markers are located in the synaptic vesicular pools, they would likely label the entire presynaptic boutons, not just the active zones where the neurotransmitter release occurs. There is currently no pan-postsynaptic marker available for *Drosophila*. However, tagged neurotransmitter receptors can be used to label postsynaptic sites. Examples include the histamine-gated chloride channel, Ort, for some neurons in the optic lobe (Chen et al., 2014) and the acetylcholine receptor subunit, nAChRα7, in the antennal lobe and mushroom body (Christiansen et al., 2011; Leiss et al., 2009). However, it is important to note that using these neurotransmitter receptors will only detect the synapses that are mediated by those receptors. Thus, these strategies are useful to confirm the presence or absence of synaptic connections that are known (or suspected) *a priori*, but are not suitable to discover synaptic connections in an unbiased way.

Additionally, it is important to note that overexpression of full length Brp or

neurotransmitter receptors might disturb normal synaptic properties and neural circuits (Andretic et al., 2008; DiAntonio, 1999; Liu et al., 2009; Petersen et al., 1997; Tsurudome et al., 2010; Wagh et al., 2006). Close attention should be paid to the possible influences on native function of synapses when synaptic markers are overexpressed. Alternatively, using endogenous regulatory promoters of synaptic markers allows investigators to recapitulate normal expression levels and avoid overexpression. For example, for STaR, Chen et al. (2014) used the full length of genomic locus of Brp and Ort incorporated into a bacterial artificial chromosome (BAC) that included their endogenous regulatory promoter to keep the expression at physiological levels. In this case, a stop cassette flanked by FRT sites followed by the tag epitopes replaced the stop codon of Brp or was placed after the signal peptide of Ort. By crossing these flies to flies expressing the Flp recombinase in the desired neuronal types, the stop cassette was removed, and the tagged synaptic markers were selectively expressed in those neurons. Finally, instead of using the full-length tagged Brp, which is a very large protein, it is possible to use the C-terminal fragment of Brp fused with a fluorescent protein (Brp-short-FP) to label presynaptic sites (Berger-Muller et al., 2013; Christiansen et al., 2011; Mosca and Luo, 2014; Schmid et al., 2008; Sugie et al., 2015). The advantage of using Brp-short-FP is that it will bind to the endogenous Brp clusters in T-bars without forming aggregation, minimizing any potential changes to native synaptic properties (Fouquet et al., 2009; Kremer et al., 2010; Schmid et al., 2008).

To precisely analyze the proximity of pre- and postsynaptic markers, especially in regions with dense synapses, super-resolution microscopy methods (see above) may be required. Recently, these technologies have been used in *Drosophila* brain thin sections (8 µm) or whole brains (Spuhler et al., 2016). By using super-resolution microscopy in *Drosophila* brain sections, individual active zones labeled with Brp-short-mCherry could be clearly recognized. Moreover, combined with the proper image analysis methods, the spatial organization of the tagged synapses can be analyzed with resolving powers that approach those of EM. However, because of the influence of light scattering and spherical aberrations, only the top 1-3 µm of the sections can be imaged to obtain the optimal resolution. For this reason, reconstructing the connectome from a large piece of fly brain by super-resolution microscopy would still be time-consuming. If super-resolution microscopy could be combined with methods that allow for imaging in thick tissues, such as tissue clarification techniques, this would benefit the processes to analyze the synaptic organization in large brain regions or even whole brains in *Drosophila*. Recently, Ke et al. (Ke et al., 2016) used super-resolution microscopy to image the optic lobe neurons in whole *Drosophila* brains treated by a tissue-clearing method called SeeDBD2. Their approach allowed them to reconstruct the morphology of entire axon terminals of Mi1 medullary neurons at the resolution of 50-150nm.

1-2.A - GRASP (GFP Reconstitution Across Synaptic Partners):

GRASP is a genetic method used to identify cell contacts and synapses in living animals (Feinberg et al., 2008). It was initially developed in *C. elegans*, but it has been subsequently applied to the study of *Drosophila* brain connectivity. GRASP labels synapses based on the proximity of the pre- and postsynaptic plasma membranes. In CNS (central nervous system) synapses, the membranes of two synaptic partners are typically separated by less than 100 nm of extracellular space, which is known as the synaptic cleft. This distance can be spanned by transmembrane proteins expressed in the two interacting neurons. As the name implies, GRASP is based on the reconstitution of two fragments of the split-GFP across the synapses of interacting neurons. Each of the two non-fluorescent split-GFP fragments are added to carrier transmembrane proteins. The two fragments of the split GFP assemble into a fluorescent form only when the membranes are sufficiently close to permit carrier proteins to span the intercellular gap. One fragment of the split GFP, spGFP1-10, is 214 aa long while the second fragment, spGFP11, is just 16 residues long. The spGFP11 fragment can therefore be inserted into many different proteins without affecting their function.

In initial experiments in *C. elegans*, each fragment of GFP was fused to the extracellular domain of the cell adhesion molecule CD4 (Feinberg et al., 2008). However, this molecule is homogeneously distributed throughout the plasma

membrane, without any specificity for synaptic sites. As a result, this implementation of GRASP led to GFP reconstitution throughout the membrane including at sites of non-synaptic contact (Fig 1-2A). To improve the specificity of the system, one or both of the GRASP components were fused to synaptically localized proteins, restricting GFP reconstitution to synapses (Fig 1-2B).

Gordon and Scott (Gordon and Scott, 2009) demonstrated that GRASP works efficiently in flies by using it to detect cell-cell contact at the synapses between olfactory receptor neurons (OSNs) and projection neurons (PNs). The power of fly genetics has allowed the GRASP system to be expanded for studying neuron-muscle connections (Hasegawa et al., 2016; Itakura et al., 2015), the visual circuit (Lin et al., 2016), the circadian rhythm circuit (Cavanaugh et al., 2014; Gorostiza et al., 2014), the olfactory circuit (Masuda-Nakagawa et al., 2014), and even non-neural tissue, such as eggs and wing discs (Bosch et al., 2015; Huang and Kornberg, 2015). A recent modification of the GRASP system has taken advantage of the properties of some synaptic proteins that are displayed on the membrane only after the release of neurotransmitters (Macpherson et al., 2015). In order to limit GFP reconstitution to active synapses, the investigators fused spGFP1-10 to the extracellular domain of neural synaptobrevin (nSyb), which is exposed to the synaptic cleft only after vesicle release (nSyb::spGFP1-10). They tested this by expressing nSyb::spGFP1–10 in OSNs and its GRASP partner CD4::spGFP11 broadly in PNs. GFP was

reconstituted at synapses after artificial stimulation with KCl or natural stimulation with cognate odorants, demonstrating that NSyb::GRASP can preferentially label active synapses in the *Drosophila* brain.

Many useful fluorescent proteins, such as GFP itself or the calcium indicator GCaMP (Chen et al., 2013), cannot be used simultaneously with GRASP since initially it was only available in green. Recently developed variants such as CRASP (cyan) (Li et al., 2016) or YRASP (yellow) (Macpherson et al., 2015) allow investigators more flexibility because they do not overlap with GCaMP signal. In addition, the three reconstitution techniques can be used in parallel to study multiple synaptic connections orthogonally.

The GRASP system has also been adopted for use in mice (Kim et al., 2011). To specifically monitor the synaptic sites, the two fragments of split GFP are fused to Neurexin-1b and Neuroligin-1, which are known to localize at the pre- and post-synaptic sites, respectively. However, GRASP, unlike in Drosophila, has not been widely used in mice. This might be due to the difficulty of detecting the GRASP signal when analyzing the images (Feng et al., 2012), or the comparative lack of genetic tools to selectively label specific types of neurons in a complex brain.

The GRASP system is very powerful, but it suffers from three important limitations. First, the reconstituted fluorescence is often weak, making it difficult

to detect *in vivo*. The reconstitution of GFP can be detected in fixed tissue using immunofluorescence with different GFP antibodies that can selectively detect spGFP1-10, spGFP11, or the reconstituted GFP. However, immunostaining requires fixation of the tissue, and thus it precludes the combination with functional methods such as electrophysiological or optical recordings. Recently, to solve this problem, several new strategies based on the concept of GRASP have been developed, which use neuroligin and neurexin conjugated with enzymes to amplify the signals by catalytic reactions, such as iBlinc (*B*iotin *L*abeling of *IN*tercellular *C*ontacts) (Desbois et al., 2015). iBlinc can generate the detectable signals without further immunostaibning and have been applied in live C. elegans. However, the application in other species hasn't been reported yet. Second, the interaction between the sp11 and sp1-10 fragments is irreversible, and can artificially render permanent cell-cell contacts that are natively transient. Third, GRASP reveals the point of contact between cells, but it does not allow for genetic manipulation of synaptically connected neurons, a feature that would be invaluable for functional analysis of circuitry.

1-2.B - Photoactivatable fluorescent protein:

When using GRASP or STaR to analyze synaptic contacts, putative pre- and postsynaptic neurons have to be known *a priori* so that the transgenic proteins can be expressed precisely in these neurons. Therefore, these strategies cannot be used to discover novel synaptic partners in an unbiased

manner. In contrast, photoactivatable green fluorescent protein (PA-GFP) is an ideal tool for discovering novel synapses, and has been successfully used in *Drosophila* (Clowney et al., 2015; Fisek and Wilson, 2014; Lai et al., 2012; Ruta et al., 2010). To implement this tool, a neuron of interest (first-order neuron) must be marked with dye or fluorescent proteins to outline its neurites. PA-GFP is genetically expressed pan-neuronally, or more narrowly in candidate subsets of neurons that are hypothesized to be connected to the first-order neuron. By spatially restricting the application of UV light to specific dendrite or axon arborizations of the first-order neuron, only the PA-GFP in neurites of partner neurons is converted from a weakly fluorescent state to a strongly fluorescent state (~100 fold increase) (Patterson and Lippincott-Schwartz, 2002). Gradually, the activated PA-GFP diffuses from the neurites to the cell body to highlight the morphology of the entire neuron (Fig. 1-3A). Recently, two new enhanced variants of PA-GFP, SPA-GFP and C3PA-GFP, have been generated, with the latter having the strongest fluorescence (Ruta et al., 2010).

One caveat of this approach is that it can highlight any neuron that has arborizations within the illuminated region, including neurons that have passing axons or dendrites which do not synapse with the first-order neuron (Fig. 1-3B). Therefore, electrophysiological recordings or genetically encoded calcium indicators (GECIs) are required to confirm the existence of synaptic connections between the highlighted neurons and the first-order neuron. The recently

developed PA-GECIs have the features of PA-GFP (high-contrast of fluorescence intensity after photoactivation) and GECIs (high-sensitivity of calcium detection) (Berlin et al., 2015). PA-GECIs could provide a more convenient way of investigating connectivity by allowing investigators to initially identify the potential synaptic partners and subsequently test their functional connectivity in the same animals.

1-2.C - Transsynaptic tracers:

Transneuronal tracing in mammals has benefited from the availability of specific neurotropic viruses that are selectively transported across synapses. Herpes simplex virus type 1 (HSV1), pseudorabies virus (PRV), and rabies virus (RV) have all successfully been used to elucidate neural connections in mice (Nassi et al., 2015). Recently HSV1 and PRV have been genetically modified to selectively tracing neuronal circuit in mice in a Cre-dependent manner (DeFalco et al., 2001; Lo and Anderson, 2011). Wickersham et al., 2007 (Marshel et al., 2010) have genetically engineered and generated a replication-incompetent RV by replacing its envelope glycoprotein gene (RG) in the genome, which is crucial for RV transsynaptic spread from neurons to neurons, to a fluorescent protein, and was also pseudotyped by a different envelope protein, EnvA. Without the RG gene in the genome, this modified RV can only infect the neurons expressing EnvA receptor, TVA, but cannot reproduce more viral particles to infect other

neurons. Therefore, by coexpression of RG and TVA in particular types of neurons, it allows the replication-incompetent RV selectively infects that given types of neurons, and mono-transsynaptically spreads to their retrograde synaptic partners. This genetically modified RV provide a useful tool to study neuronal micro-circuit at single cell resolution (Miyamichi et al., 2011; Wickersham et al., 2007). However, to deliver these neurotropic viruses requires brain surgery and stereotaxic injection, which are prone to inconsistency. Moreover, these viruses can cause cytotoxicity, which may influence the functions of labeled neurons, and limit the time period during which neurons can be analyzed (Callaway and Luo, 2015). Finally, it remains to be seen whether RV's ability for transynaptic transport is equally efficient across different types of synapses (Callaway and Luo, 2015). According our experiences, the replication-incompetent RV worked inefficiently in dendrodendritic synapses between the granule cells and the mitral cells in mouse olfactory bulbs.

Unfortunately, none of the transsynaptic viruses that have been used in mammals work in *Drosophila*, presumably due to the lack of receptors or host cellular machinery that these viruses require for entry and replication. Non-viral tracers such as C-fragment of tetanus toxin or wheat germ agglutinin (WGA), can be expressed as transgenes into specific "source" neurons, and transferred across their synapses (Huh et al., 2010). The transfer of tracing agents may occur in an anterograde (from the source neuron's axon to its postsynaptic

partner) or retrograde (from the source neuron's dendrite to its presynaptic partner) manner. WGA, in particular, has been used successfully as a transneuronal tracer in multiple species including *Drosophila* (Tabuchi et al., 2000).

WGA is a lectin protein that binds certain sugar moieties of glycoproteins covering eukaryotic cell membranes (Gabius et al., 2011). WGA is transported preferentially to the axon terminal, where it is secreted and endocytosed by the postsynaptic partner of the source neuron (Broadwell and Balin, 1985; Fabian and Coulter, 1985). WGA can then be visualized by staining or by conjugation to horseradish peroxidase (Broadwell and Balin, 1985). After being produced by a source neuron, secreted into the synaptic cleft and endocytosed by a postsynaptic partner, WGA can be repeatedly passed along a circuit of connected neurons. However, this multi-synaptic transport of WGA may not give a clear interpretation of data. Because only a small fraction of the WGA from the source neurons jumps across the synapse, and WGA does not replicate, the little WGA that reaches the synaptic partner can be difficult to detect. To solve this problem, adeno-associated viruses (AAV) encoding WGA fused with Cre recombinase, WGA-Cre, has been used in combination with Cre-dependent reporters in mice to amplify the WGA signal (Gradinaru et al., 2010; Libbrecht et al., 2016). However, this strategy does not seem to work robustly in mammals, and it remains to be tested whether parallel strategies such as WGA-Flp or

WGA-GAL4 can be used in *Drosophila.*

1-2.D - Tango:

The Tango assay is one such tool derived from the molecular logic of Delta-Notch signaling. It was initially developed to monitor the interaction of a receptor of interest with its ligand or agonist in the extracellular space. In the Tango assay, three exogenous genetic elements are introduced into a “receiver” cell. The first element is a protein fusion consisting of a transmembrane receptor fused to an intracellular transcription factor. The transmembrane domain and intracellular domain are separated by a cleavage site that is targeted by a site-specific protease, such as tobacco etch virus (TEV) protease. The second element is a protein fusion consisting of the aforementioned protease linked to a protein that associates with the receptor upon agonist-binding. The third element is a reporter gene that can be activated by the transcription factor. The binding of the agonist recruits the protease to the receptor. The protease then frees the transcription factor from its membrane anchoring, allowing it to reach the nucleus and activate transcription of the reporter cassette. This results in a visual indication of receptor activation.

Initially, to test as proof of concept, Barnea et al. have adopted Tango into receptor tyrosine kinases, steroid hormone receptors, and G protein-coupled receptors (GPCRs) (Barnea et al., 2008). In the design of the Tango assay for GPCRs, the human arginine vasopressin receptor 2 (AVPR2) was used as a

model. The receptor was fused to a transcription factor by a TEV Protease Cleavage Site (TCS), and the TEV protease was fused to human β-arrestin2, which associates with AVPR2 upon receptor activation. When these two chimeric constructs and a reporter gene were introduced into a cell line, the Tango-modified AVPR2 was able to induce the reporter gene expression upon binding to its respective agonist. The GPCR Tango assay has since been adopted for use in the Drosophila nervous system. The assay can be used to both screen which circuits are responsive to a specific neurotransmitter (Tango-map) and identify the postsynaptic partners of known neurons (Tango-Trace) that use GPCRs as neurotransmitter receptors.

Inagaki et al. (2012) applied the Tango-map assay to dopamine receptors in the Drosophila nervous system to investigate the neural circuits on which dopamine acts. In transgenic flies, they expressed the Tango-modified dopamine receptor, arrestin-TEV protease, and a reporter transgene in all neurons, to assess its functionality as a mapping system (Tango-map) (Fig. 1-4). They were able to detect expression of the GFP reporter in receiver cells that expressed the modified dopamine receptor upon their activation by dopamine. Next, they used this technique to explore which neurons received dopamine signaling following starvation periods, to determine how hunger affects the action of neuromodulators, like dopamine.

The Tango-based technique called Tango-Trace was further used to to

trace the synaptic connections of photoreceptor neurons in the Drosophila visual system (Jagadish et al., 2014). Here the Tango assay was adopted to the histamine (HA) receptor, since Drosophila photoreceptor neurons use HA as their main neurotransmitter. As in the previous study, two fusion proteins were constructed (HA receptor-TCS-Gal4 and Arrestin-TEV protease) and expressed in flies with a reporter. In this variant of the Tango method, there was very little activation of the receptor by the endogenous levels of HA in the brain. However, by artificially stimulating HA release in specific photoreceptor neurons with a temperature-sensitive cation channel (trpA1), they were able to visualize the postsynaptic partners to the trpA1-expressing cells.

The Tango assay as described here has several benefits that make it a versatile, useful tool for visually detecting cell-cell interactions. The assay can be applied to 89 members of the GPCR class, making it suitable for many different cell types. In addition, since all three components of the receptor and reporter are exogenous, there is very little risk that endogenous proteases or transcription factors will cross-react with the system. Also, although the native receptor is modified with the protease cleavage site and transcription factor intracellular domain, the specificity of the ligand binding is unaffected, allowing receptor activation to remain specific to its respective ligand. Additionally, if neurotransmitter release can be controlled specifically in presynaptic neurons of interest, as with the trpA1 channel, Tango can allow for identification of its

functional postsynaptic partners.

Tango also has several limitations. First, although Tango can be adapted for many members of the GPCR family, it is currently restricted to the study of cell-cell interactions mediated by GPCRs. This precludes the use of Tango for studying synapses mediated by gap-junctions or intercellular interactions mediated by anchored proteins. Furthermore, Tango requires a priori knowledge of the neurotransmitter used by the presynaptic neuron of interest, preventing its application for unbiased identification of uncharacterized synapses. Second, Tango has caveats that could possibly lead to false identification of connectivity. Theoretically, if the neurotransmitters diffuse outside of the synaptic cleft, neighboring neurons that express the receptor, but are not synaptically connected to the source neuron may be activated. To overcome these limitations, Tango-based systems used for future applications could be modified such that a membrane-tethered ligand localized to a presynaptic site could activate a Tango-modified receptor located in its postsynaptic partner.

(1-3) Summary

As mentioned above, each of the methods for tracing the neuronal connections has its advantages and disadvantages (Table 1-1). To overcome some of the limitations of currently available methods, we developed a new tool, which (i) can be genetically encoded in transgenic animals; (ii) does not exhibit cytotoxicity; and (iii), allow researchers to monitor cell-cell contacts and

manipulate the transcriptional profiles of the labeled cells in an unbiased fasion. This new genetic system, TRACT, is based on the molecular logic of the Notch receptor and provides a record of cell-cell interaction based on regulation of transcription by intramembrane proteolysis. The results have shown this new genetic system can monitor cell-cell contacts in cell lines in vitro, and selectively detect neuron-glia or neuron-neuron contacts in transgenic Drosophila in vivo. We anticipate, in the future, that TRACT could be used to unbiasedly trace neural circuits and manipulate the circuit functions to provide insights to how circuits provide behavior.

FIGURES

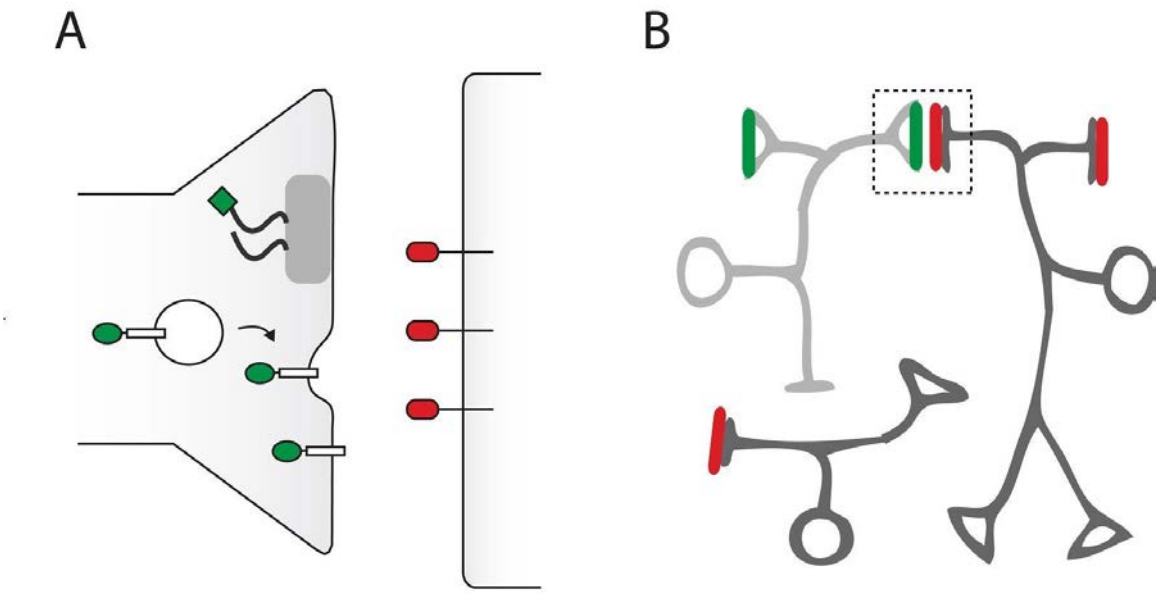

FIGURE 1-1. Visualization of synapse by genetically tagging synaptic proteins. (A) Fluorescent proteins or epitope tags can be targeted to synaptic membranes by fusion to synaptically localized proteins. For example, tags fused to Brp (curly black line) or synaptic vesicular proteins (white rectangle) will localize to the presynaptic terminal (left). There are no pan-neuronal postsynaptic markers, but tags (red oval) fused to neurotransmitter receptors such as Ort have been successfully used in the past. **(B).** The axon terminal (triangle) of the presynaptic neuron of interest (light gray) is marked with tags that are fused to presynaptic proteins (green). A different tag (red) is expressed at the postsynaptic sites of candidate partner neurons (dark gray). The proximity of these two distinct tags (green, red) is assessed to verify synaptic connection.

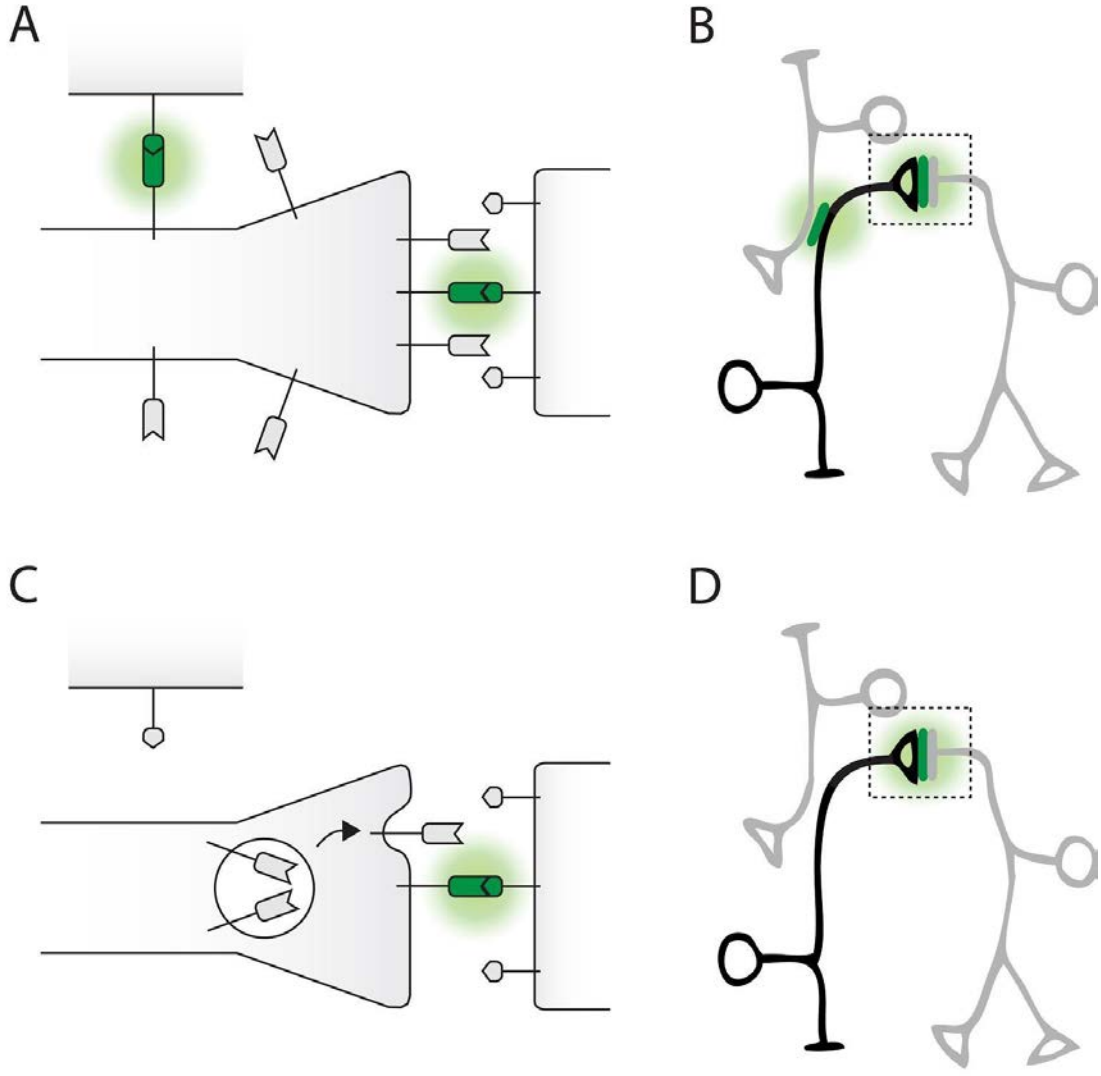
A
B
C
D

FIGURE 1-2. GFP Reconstitution Across Synaptic Partners (GRASP). (A). CD4::spGFP1-10 (dented rectangle) is distributed homogeneously throughout the membrane of the presynaptic neuron. As a result, GFP reconstitution (green) can occur at the synapse (right) as well as at sites of non-synaptic contact (top). **(B).** A presynaptic neuron (black) expressing CD4::spGFP1-10 makes contact with two neurons (gray) expressing CD4::spGFP11. GFP reconstitution occurs at all sites of membrane contact and is not specific to synapses. **(C).** NSyb::spGFP1-10 (dented rectangle) is localized to synaptic vesicles. Upon synaptic release, NSyb::spGFP1-10 is exposed specifically to the synaptic cleft. As a result, GFP reconstitution (green) only occurs at synaptic sites when synaptic vesicles fuse. **(D).** A presynaptic neuron (black) expressing NSyb::spGFP1-10 makes contact with two neurons (gray) expressing CD4::spGFP11. GFP reconstitution occurs at the synapse but not at the site of nonsynaptic contact.

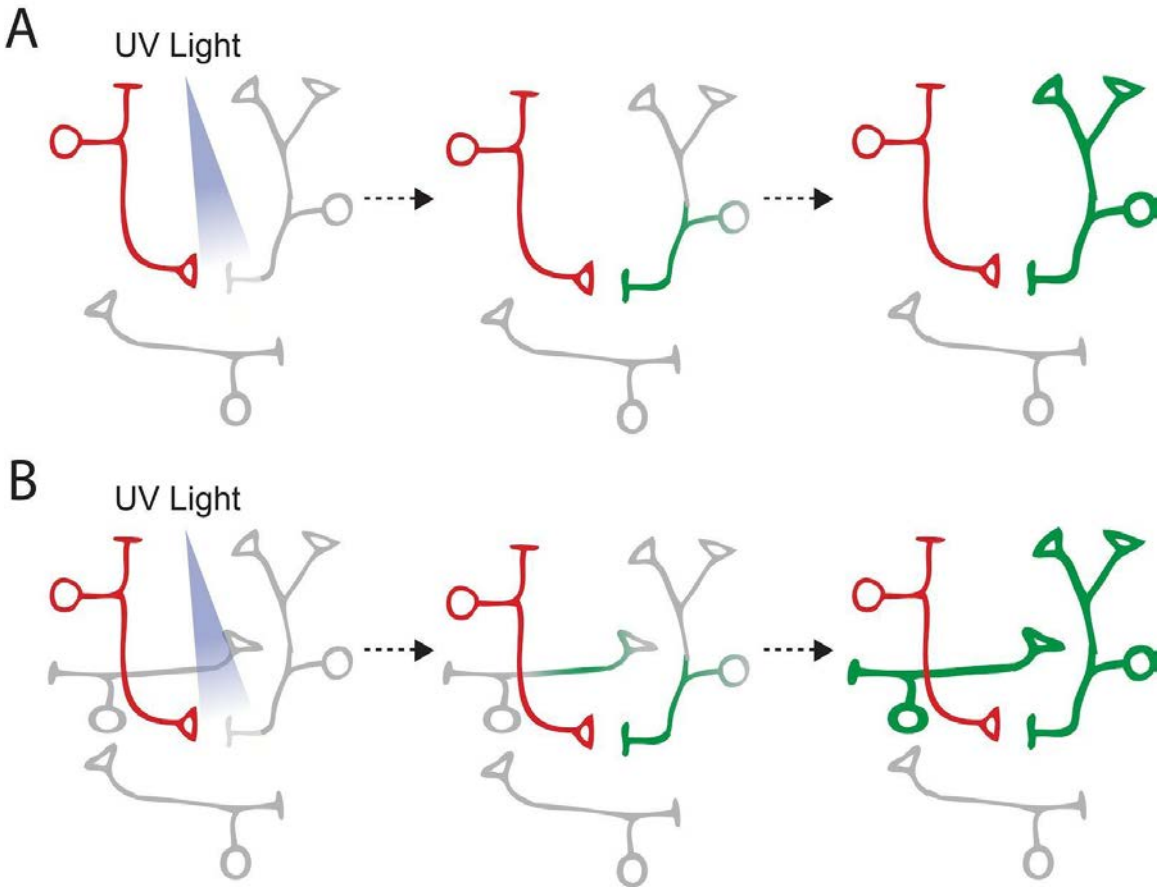
A
UV Light
B
UV Light

FIGURE 1-3. Detection of synaptic partners by PhotoActivatable GFP (PA-GFP). (A). A neuron of interest (red) is first highlighted with dye or fluorescent proteins to mark its neurites while PA-GFP is expressed in all candidate partner neurons (gray). When UV light is applied just outside the neurite of the highlighted neuron, PA-GFP in its synaptic partner (green) is converted to a strongly fluorescent state. The converted PA-GFP then diffuses throughout the partner neuron, highlighting its entire morphology. **(B).** One of the pitfalls of this technique is that UV light stimulation can also activate PA-GFP in bystander neurons. In this scenario, PA-GFP in two neurons (green) is activated but only one of these is synaptically connected to the neuron of interest (red). In practice, functional studies need to be carried out to confirm the candidate synaptic connections identified with PA-GFP.

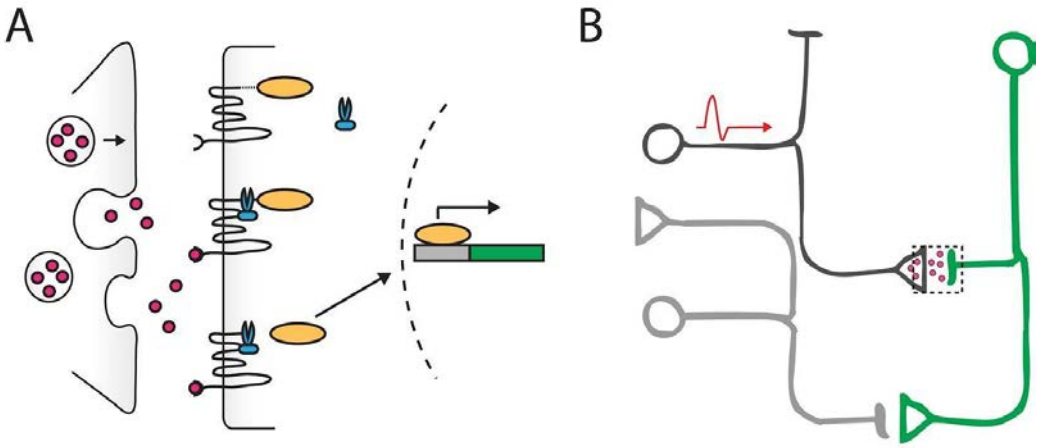
A
B

FIGURE 1-4. Identifying functional synaptic contact using Tango-modified GPCRs. (A). When neurotransmitters (red) are released from the active zone of the presynaptic neuron (left), they bind Tango-modified GPCRs on the postsynaptic neuron (right). The binding of neurotransmitter recruits an intracellular protease (blue) that cleaves the transcription factor (orange) which is tethered to the GPCR. This transcription factor then translocates to the nucleus to activate transcription of reporter genes such as *GFP* (green rectangle). **(B).** After the presynaptic neuron of interest (dark gray) fires an action potential, it releases neurotransmitters (pink) that bind to the Tango-modified GPCRs expressed in the postsynaptic neuron. This induces GFP expression in the postsynaptic neuron (green) but not in the bystander neuron (light gray).

Table 1-1. An overview of the advantages and disadvantages associated with each method of identifying synaptic connections.

Technique	Advantages	Disadvantages
Electron Microscopy	Provides detailed wiring diagram of small volumes.	Time and labor-intensive. Impractical for long-range connections or for many samples.
Synaptic Tagging	Can monitor synapses *in vivo*.	For regions dense with synapses, super-resolution microscopy may be required. Need genetic drivers for putative synaptic partners.
GRASP	Can monitor synapses *in vivo*. With NSyb::GRASP, can specifically detect active synapses.	May be not sensitive enough for *in vivo* detection. Can induce irreversible binding at natively transient synapses.
PA-GFP	Can be used for unbiased identification of novel synapses.	Not conclusive by itself. Requires functional studies to confirm.
WGA	Only requires a single transgene. Simple to implement.	Can result in labeling of higher-order synapses. The signal can be difficult to detect because it gets diluted.
Tango-Trace	Can identify functional synapses. Allows genetic manipulation based on synaptic input.	Requires prior knowledge of neurotransmitters. Requires a way of artificially stimulating the presynaptic neuron of interest.

CHAPTER 2

TRACT (transcellular activation of transcription), a genetic system to investigate cell-cell interactions in vitro

This Chapter was adapted from Ting-Hao Huang's publication and unpublished data:

Monitoring cell-cell contacts in vivo in transgenic animals.

Ting-Hao Huang, Tarciso Velho, Carlos, Lois. Development. 2016 Nov 1;143(21):4073-4084.

ABSTRACT

To generate a new genetically-encoded system to trace the connections in the nervous system, we took advantage of the molecular mechanism of Delta-Notch signaling to design a pair of ligand and receptor. The design of the synthetic receptor includes Notch negative regulatory region (NRR) and transmembrane domain (TMD), where metalloproteases and γ-secretase proteolytically cleave after Delta-Notch binding. Once the synthetic receptor interacts with its ligand, anchored on a surface or expressed in cells, couple of sequentially proteolytic cleavages are triggered to release its intracellular fragment and to regulate the expression of the downstream reporter gene. However, we noticed that (1) most of the receptor proteins are retained inside the cell, and (2), without the ligand, the synthetic receptor by itself generates moderate ligand-independent background activity in the reporter cells. Both of these characteristics might impede the future application of this system in vivo. To improve this system, we tested several modifications in the NRR, the TMD or the intracellular transcription factor to reduce background and, at the same time, to improve cell surface expression. So far we have found two variants of the receptor that have relative low ligand-independent background, which are further used in Chapter 2 and 3.

INTRODUCTION

Neuronal cells form a specialized type of cell-cell interaction, the synapse, which enables the transmission of information through brain circuits. There are few methods currently available to analyze cell-cell contacts, most of them designed to study interactions between neurons. As discussed at length in the previous session, the most commonly used methods are co-localization of fluorescent tags by light microscopy, serial electron microscopy (Denk and Horstmann, 2004), and GRASP (GFP Reconstitution Across SynaPses) (Feinberg et al., 2008). While each of these methods has its strengths and weaknesses, none of these methods enable long-term genetic modifications of the interacting cells. We have developed a new genetically-encoded tool based on the molecular logic of Notch that can not only analyze cell-cell contacts but also allow for transcriptional regulation of cells based on contact.

The Notch-Delta pathway controls cell fate during development through cell-cell interactions (Artavanis-Tsakonas and Muskavitch, 2010). Delta is one of the ligands for Notch receptors (other ligands in vertebrates are Jagged and Serrate) (Kopan and Ilagan, 2009). Previous works have demonstrated that the key element controlling the activation of the Notch receptor is the Notch regulatory region (NRR), a 200 aa fragment of the Notch extracellular domain (ECD) located immediately before the transmembrane domain (TMD) (Gordon et al., 2007). The NRR includes three LIN-12/Notch repeats (LNRs) followed by the

heterodimerization domains (HD). During the synthesis process of Notch proteins, their precursors in the Golgi are first proteolytically cleaved by a furin-like convertase at the S1 site inside the HD. After the S1 cleavage, the two parts of Notch heterodimerize noncovalently to form a mature Notch protein (Blaumueller et al., 1997; Logeat et al., 1998). The NRR is folded in such a way that, in the absence of Delta binding, a cleavage site (called S2) located between the TMD and S1 site is inaccessible to the action of ubiquitous metalloproteases such as Kuzbanian (in Drosophila) or TACE (Tumor necrosis factor--Converting Enzyme) in vertebrates (Tiyanont et al., 2011). Upon Delta-Notch binding, it is hypothesized that the NRR partially unfolds, increasing the accessibility of the S2 site and permitting cleavage by the metalloproteases (Gordon et al., 2015; Meloty-Kapella et al., 2012; Stephenson and Avis, 2012; Tiyanont et al., 2011). After S2 cleavage, a subsequent cleavage (called S3) by the ubiquitous metazoan γ-secretase complex occurs in the TMD, within the cell membrane (Brou et al., 2000) (Mumm et al., 2000). After S3 cleavage, the intracellular domain (ICD) of Notch loses its membrane anchorage and translocates to the nucleus where it regulates transcription of cell fate-related genes (Struhl and Adachi, 1998, 2000) (Fig. 2-1a and 2b).

Previous experiments have demonstrated that the Notch receptor can be engineered by maintaining the ECD and TMD of the native Notch while replacing the ICD with artificial gene regulatory modules such as the transcriptional

activator Gal4 (Sprinzak et al., 2010; Struhl and Adachi, 2000) or the recombinase Cre (Vooijs et al., 2007). These experiments demonstrate that the molecular mechanism of the Delta-Notch system can be used to monitor cell-cell interactions. However, the Delta-Notch system cannot be used in animals without further modifications because it is highly conserved throughout the animal kingdom, and it is likely that there could be cross-talk between Notch and Delta ECDs from different species. Thus, exogenous expression of the native ECDs of Notch or Delta is problematic because it may severely perturb development due to dominant-negative effects of the engineered ligands and receptors. In addition, the potential interaction between endogenous Delta (plus Jagged and Serrate) and the native ECD of an engineered Notch receptor would lead to high background levels of signaling.

In this chapter, we demonstrate that a synthetic receptor, which contains the NRR and TMD of Notch fused to an orthogonal ligand-binding domain and a transcription factor, is able to monitor contact among cells in culture when the ligand is present either on the surface of objects or on membranes of co-incubated cells. However, the primary design of TRACT exhibited problems of ligand-independent activation. Therefore, we attempted to further optimize the receptor to improve its signal-to-noise ratio by modifying its NRR and TMD. We were able to design two modified receptors with reduced ligand-independent activation that maintain high fold-inducibility by ligand. These receptors were

implemented for use *in vivo*.

RESULTS

Monitoring cell-cell interactions in vitro

To develop a robust system that would allow for the monitoring of cell-cell interactions in animals we engineered an artificial receptor called SCAD/NRR/TMD/GV (SNTGV). This design for the artificial notch receptor is similar to those described recently (Gordon et al., 2015; Morsut et al., 2016). The SNTGV receptor retains the wild-type Notch NRR and TMD, but both the Notch EGF-like repeats and ICD have been replaced by a single-chain antibody domain (SCAD) (Kochenderfer et al., 2009) and the transcriptional regulator, Gal4VP16 (GV), respectively (Fig. 2-1b). The SCAD recognizes the ECD of murine CD19 (CD19), therefore functioning as a receptor for this antigen (2-1c). To preliminarily test this system, we generated stable CHO cell lines carrying both the UAS-Histone2B-mcitrine (H2Bmcit) reporter (Sprinzak et al., 2010; mcitrine is a YFP variant (Griesbeck et al., 2001)) and the SNTGV receptor (SNTGV/UAS-H2Bmcit cells) by lentiviral transduction. First, to prove the induction triggered by the ligand-receptor binding is through the contacts between the neighboring cells, CD19 cells and SNTGV/UAS-H2Bmcit cells were co-cultured sparsely and allowed to expand. In this case, only the cells at the periphery of each clonal colony were able to make contacts with ligand-expressing cells in adjacent colonies. As expected, only the outer border cells adjacent to the CD19 colonies had robust induction of H2Bmcit expression. This result indicates that the

induction requires direct cell-cell contacts (Fig. 2-2).

In the absence of CD19 (the ligand) positive cells, the SNTGV/UAS-H2Bmcit cells had variable but moderate levels of H2Bmcit expression (in the remaining of this dissertation the ligand-independent cleavage of Notch will be referred as the ligand-independent background) (Fig 2-4a, top panel). To minimize the noise of the system, single cell SNTGV/UAS-H2Bmcit clones with negligible level of background H2Bmcit expression were isolated by fluorescence-activated cell sorting (FACS). A single cell clone line was selected to be used in the following experiments. When SNTGV/UAS-H2Bmcit cells from the single cell clone lines are co-cultured with emitter cells expressing CD19, there is robust induction of H2Bmcit expression, but no induction was observed when co-cultured with CD19 negative control cells (Fig. 2-3a). H2Bmcit expression can be detected as early as 12hrs after co-culture. After 48 hours, H2Bmcit expression peaks at 30-fold expression compared to uninduced controls (Fig. 2-3a). Importantly, co-culturing of SNTGV/UAS-H2Bmcit cells with CHO cells expressing rat Delta did not lead to H2Bmcit expression (data not shown), indicating that the activation of SNTGV requires binding to its ligand, CD19.

It is hypothesized that the activation of Notch upon ligand binding involves a pulling force that exposes the NRR S2 site to metalloproteases (Gordon et al., 2015; Meloty-Kapella et al., 2012; Nichols et al., 2007; Stephenson and Avis, 2012). Consistent with previous works (Varnum-Finney et al., 2000) we have

observed that SNTGV can be activated by ligands presented on the cell surface (Fig. 2-3a) or attached to a plastic substrate (Fig. 2-3b). However, we did not observe SNTGV activation when the antibody recognizing SCAD was applied in soluble form to the culture medium (data not shown). These results suggest that the mere binding of ligand (CD19) to the receptor (SNTGV) is not sufficient to expose the NRR S2 site. In contrast, our results are consistent with a model in which NRR acts as a mechanosensor that is partially unfolded by tension generated by the binding of an immobilized ligand (cell- or substrate-bound) to its receptor (Kopan and Ilagan, 2009; Stephenson and Avis, 2012; Meloty-Kapella et al, 2012; Gordon et al; 2015). In addition, incubating cells with the metalloprotease inhibitors, batismastat, GM6001, and TAPI (which block the S2 site cleavage (Brou et al., 2000; Mumm et al., 2000)), or with the γ-secretase inhibitor, DAPT (which blocks the S3 site cleavage (Brou et al., 2000; Mumm et al., 2000)), reduced or eliminated, respectively, the induction of H2Bmcit expression observed by mixing the “emitter” and “receiver” cells (Fig. 2-3c). These observations suggest that the activation of SNTGV by CD19 binding likely recapitulates the S2 and S3 cleavages that occur when Delta and Notch interact, as recently described (Gordon et al., 2015).

Improving signal-noise ratio of SNTGV

To further characterize SNTGV proteins, we first attempted to analyze the

protein products by western blot and immucytochemistry. However, SNTGV proteins could not be detected from virally transduced CHO cells or single cell clone lines by Western blot. Therefore, immunostaining in CHO cell lines against Gal4 DNA binding domain or VP16 was used to investigate SNTGV protein expression. Surprisingly, we found that SNTGV proteins are mostly accumulated in perinuclear region (Fig. 2-5b top panels). Since SNTGV protein appears to be at least in part retained inside the cells, very likely in the ER and Golgi, we used the antibody against the extracellular component of SNTGV (SCAD) under non-permeabilized condition to determine cell-surface expression. Under these conditions the antibodies are not able to penetrate the cells, and can only recognize antigens present on the outer surface. This surface staining show only weak expression of SNTGV on the plasma membrane of CHO cells (Fig. 2-4a left panel). In summary, the SNTGV protein seems to be transported to the cell surface inefficiently with the majority likely retained in the ER/Golgi.

In optimizing TRACT, we came to recognize good membrane expression of the SNTGV protein as a key factor. Because the system is activated by the interaction of SNTGV and CD19 across two plasma membranes, the inducibility of the receptor is predicted to be limited to the number of SNTGV molecules present on the cell surface. Simply increasing the expression level of SNTGV transgene to make the system more sensitive is not an option as overexpression of the receptor leads to ligand-independent activation (data not shown). To

improve the capability of SNTGV to monitor cell-cell contacts, we focused on approaching two important issues, surface transportation and ligand-independent activity.

Gordon el al., (2009) found that S1 cleavage plays different roles on the surface expression of Notch1 and Notch2. Deleting the loop containing the S1 site, called S1 loop-out (S1LO) helps both Notch1 and Notch2 to resist the proteolytic process by Furin-like convertase without changing the NRR structures substantially. They also found that, in Notch1, S1LO modification decreases protein surface expression and ligand-dependent activity. In contrast, S1LO Notch2 has more efficient surface transportation and better ligand-induced activity. To improve the surface expression of SNTGV, we first generated a new receptor construct by switching the original NRR and TMD of SNTGV from hNotch1 to the S1LO NRR and TMD of hNotch2 (hN2S1LO-SNTGV). The UAS-H2Bmcit CHO cells expressing hN2S1LO-SNTGV has weaker mcitrine intensity compared with the ones expressing SNTGV, which indicates that hN2S1LO-SNTGV might have low ligand-independent activity (Fig. 2-4a the middle panels). When the hN2S1LO-SNTGV/UAS-H2Bmcit cells were co-cultured with CD19 cells, a significant induction of H2Bmcit expression was observed (Fig.2-4c the bottom panels). To verify whether this modification does help the receptor proteins transport to the cell surface, surface staining with the same antibody recognizing SCAD was performed for both SNTGV and hN2S1LO-SNTGV cells.

Surprisingly, we found that the surface expression of hN2S1LO-SNTGV was worse than the one of SNTGV (Fig. 2-5a the middle panel). The fact that hN2S1LO-SNTGV still has the inducibility (perhaps weaker) despite the poor surface expression indicates that TRACT only requires minute amounts of the receptor in the plasma membrane for activation.

Several studies have shown that, in addition to the intracellular domains of membrane proteins, the properties of transmembrane domains, such as the charge and length, also play important roles in the sorting and transport across different subcellular compartments, which influence the subcellular localizations of membrane proteins (Sharpe et al., 2010; Singh and Mittal, 2016). Moreover, our FACS data shows that the ligand-independent background in SNTGV/UAS-H2Bmcit cells was reduced by TAPI and DAPT (data not shown), suggesting their involvement in the ligand-independent cleavage of the NRR and the TMD. To further attempt to improve the surface expression and to decrease the ligand-independent activity of the synthetic receptor, we focused on modifying the TMD of SNTGV. Struhl and Adachi, 2000 have done elegant work to characterize the role of γ-secretase in Notch and other transmembrane proteins in Drosophila embryos. In their studies, the replacement of the Notch TMD by the TMD of sevenless (sev), another transmembrane proteins, results in lower ligand-independent background when native ECDs of Notch was replaced by exogenous motifs such as multiples of Myc tags; meanwhile, full length Notch

with sev TMD is still capable to be activated by its ligand, Delta. Moreover, their results also show that the dimerization caused by the leucine zipper domain of GCN4 (LZ) and notch PEST domain (polypeptide enriched in proline, glutamate, serine and threonine, degradation signal) can reduce ligand-independent background. Therefore, we made the following new receptor constructs based on these findings (Table 2-1):

(1) **hN2S1LO-SNT$_{sev}$GV:** hNotch2 TMD of hN2S1LO-SNTGV was replaced by the sev TMD;

(2) **hN2S1LO-SNTGV-PEST**: hNotch1 PEST domain was fused after Gal4VP16;
(3) **S(LZ)NTGV** and (4) **hN2S1LO-S(LZ)NTGV**: the GCN4 LZ motif was inserted between the SCAD and the NRR of both SNTGV and hN2S1LO-SNTGV.

in addition to the Sevenless TMD, we also tried the TMD domain from human CD4, which is known to be transported to the plasma membrane efficiently.

(5) **hN2S1LO-SNT$_{CD4}$GV**: the TMD of S1LO-SNTGV was replaced by the human CD4 TMD.

Because the CD4 TMD has never been tested in Notch protein, it is crucial to consider the stability of the ICD fragment after S3 cleavage based on the N-end rule, which mean that the half-lives of peptides are determined by the first amino acid of their N-terminal (Bachmair et al., 1986). For instance in mammalians, peptides which start with Val, Met and Gly have half-lives that

exceed 30hrs, but the ones that end with Glu, Arg and Gln have half-lives that are only about 1hr (Gonda et al., 1989). Therefore, other receptor constructs were generated in which the CD4 TMD was either hybridized with hNotch2 TMD or substituted to more stable residues:

(6) hN2S1LO-SNT$_{CD4/N2}$GV: the last six amino acids of CD4 TMD C-terminal, GIFFCV, were substituted with the last six amino acids of hNotch2 TMD C-terminal, LGVIMA, which are downstream of the S3 site;

(7) hN2S1LO-SNT$_{CD4IF-->GV}$GV: the last 5th and 4th a.a. of CD4 TMD, I and F, were substituted with G and V, respectively.

For cells that express either hN2S1LO-SNT$_{sev}$GV or hN2S1LO-SNT$_{CD4}$GV, there is no background expression of H2Bmcit; however, H2Bmcit expression cannot be induced after co-culturing with mCD19+ cells. hN2S1LO-SNTGV-PEST not only has very strong background activity, but also seems to accumulate inside the Golgi. For S(LZ)NTGV or hN2S1LO-S(LZ)NTGV, the S1LO with LZ has similar subcellular expression with original hN2S1LO-SNTGV, while S(LZ)NTGV has better cell surface expression. Expression pattern of S(LZ)NTGV after non-permeabilized immunostaining is stronger than that of SNTGV (Fig. 2-5a right and 2-5b bottom panels). However, S(LZ)NTGV cause even higher background compared to SNTGV although they still have the ability to respond to ligand and induce more H2Bmcit expression (Fig. 2-4a the bottom panels and b). For the last three constructs, those chimeric proteins have similar

subcellular localization with hN2s1LO-SNTGV. The chimeric protein with CD4/N2 TMD has comparable level of the background and inducibility to hN2s1LO-SNTGV. The background of hN2S1LO-$SNT_{CD4IF-->GV}$GV is lower than that of hN2s1LO-SNTGV; however, its inducibility is also weaker. In summary, the surface expression of SNTGV can only be improved when the LZ domain was present. However, none of the modifications led to better signal-noise ratio than SNTGV.

To test whether Gal4VP16 influences the stability and internalization of SNTGV, we replaced the Gal4VP16 with other known GAL4-based transcription factors. It has been shown that many transcription factors are rapidly degraded by ubiquitin-mediated proteolysis to tightly regulate their functions. Salghetti et al., (2000) have reported a correlation between the activity and degradation signal of an acidic transcription activation domain (TAD). Because ubiquitination is the key step for membrane proteins to be internalized by endocytosis, we asked if the ubiquitination of Gal4VP16 could affect SNTGV stability or internalization. Therefore, we generated several new receptor constructs by swapping the VP16 with TADs of CTF and Gal4, based on the results in Salghetti et al., 2000. Compared with SNTGV, the receptors with the TAD of CTF or Gal4, ShNTGCTF or ShNTG4, respectively, both exhibited lower ligand-independent activities. Furthermore, when the CD19 cells were co-cultured with the cells expressing either one of these two receptors, cells with ShNTG4 showed a

higher level of the H2Bmcit induction than that with ShNTGCTF, albeit still lower than the original SNTGV (Fig. 2-6a). ShNTG4 in HEK293T cells mostly colocalized with ER and Golgi markers, calreticulin and formimidoyltransferase-cyclodeaminase (FTCD), respectively, but not with the lysosome markers, Lamp-1 (Fig. 2-6b). Therefore, the reduction of ligand-independent activity in ShNTG4 might merely result from the weaker transcription activity of Gal4 TAD than VP16.

DISCUSSION

Cell-cell contacts are fundamental to the development and function of multicellular organisms. Cell-cell interactions are critical, for example, for the specification of embryonic tissues, the maintenance of stem cell niches, and cell migration. In addition, abnormal cell-cell interactions are fundamental to the pathogenesis of several diseases, most notably, to the escape of metastatic cells from tumors (Wang et al., 2005). Our experiments demonstrate that it is possible to take advantage of the molecular logic of the Notch pathway to transcriptionally record cell-cell interactions, without incurring the risks associated with using the native ECDs of Delta or Notch in animals. This new system, TRACT, can monitor cell-cell contacts when the ligand is expressed in cells or detect the ligand presented on artificial surfaces.

A few elegant studies with similar designs have been published while we were developing TRACT (Gordon et al., 2015; Morsut et al., 2016; Roybal et al., 2016). These publications have shown the potential of similar systems to monitor cell-cell interactions *in vitro*. The synthetic receptor in this type of system has been adopted for variety of combinations, which provides a range of flexibility to study a complex biological network by multiple layers of signaling regulations of these system. First, the ligands and its corresponding binding motifs have been switched to different protein combinations, including GFP/anti-GFP nanobody, cancer endogenous antigen HER2 or mesothelin /anti-HER2 or mesothelin

SCAD, the FK506 binding protein (FKBP)/the FRB domain of mTor, anti-Myc antibody/Myc epitope. It is important to notice that, in most cases, SCAD was used in the receptor part. We have previously swapped SCAD and CD19 to the ligand and the receptor, respectively. Unexpectedly, the receptor carrying CD19, instead of SCAD, generates very strong ligand-independent background, and no detectable inducibility once co-cultured with the cells expressing SCAD transmembrane proteins. This might imply that somehow the extracellular ligand binding domain is also important for TRACT to function normally. Second, the intracellular transcription factors can also be switched with other binary transcription systems, such as LexA, QF, tetA, split Gal4, or KRAB repressor. Third, instead of fluorescent proteins, the released transcription factors can activate the expression of the ligands of TRACT, endogenous transcription factors, cytokines and antibodies. These modifications provide useful tools to investigate the Notch molecular mechanism, to bioengineer immune cells to precisely target tumor cells and program the differentiation to specific cell types.

In the future, we anticipate that, to control cell fate or function, these systems including TRACT could be used to delete or knock-down genes through nuclear translocation of recombinases in the receptor ICD such as cre, flp, or inducing the expression of downsteam RNAi. Furthermore, this synthetic genetic system will be useful to investigate cell-cell interactions during development *in vivo*, to investigate the dynamics of cancer invasion during metastasis, to

engineer artificial tissues *in vitro* (Sasai, 2013), and to unveil wiring diagrams of neurons in brain circuits.

Although all these *in vitro* studies using systems similar to our design show wonderful results with low signal-noise ratio of the receptors, after testing one of those receptors in the UAS-H2BmCit CHO cells, Antuca Callejas, a graduate student in Dr. Lois lab, found this receptor provided very strong ligand-independent background (Antuca Callejas unpublished data). It indicates that the background expression of the reporter genes is the combination of the ligand-independent activity of the receptors and the sensitivity of the reporter cells that were used.

Several possible problems on this synthetic receptor could lead the ligand-independent background activity. First, several mutations associated with leukemia in the notch heterodimerization domains have been identified (Grabher et al., 2006; Malecki et al., 2006). The studies have shown that those mutations generate unstable heterodimerization of Notch on plasma membrane, which lead to ligand-independent activity of Notch signaling pathway. Perhaps part of the synthetic SNTGV protein is misfolded, and failed to form proper heterodimerization after S1 cleavage. Therefore, it causes the synthetic SNTGV susceptible to metalloprotease. Second, it has been shown that the ligand-independent activity can also occur in wildtype Notch proteins, which is caused by the endocytosis of Notch proteins from plasma membrane (Palmer and Deng,

2015). Once Notch is internalized through endocytosis, it will either be recycled back to the plasma membrane or be transported to the lysosomes. In the lysosomes the Notch ECD will be shredded by lysosomal protease, which triggers the following γ-secretase cleavage and release of the ICD.

The ligand-independent activity and inefficient cell surface expression of the receptors may limit the possible application of TRACT. If TRACT is used to induce genetic factors, such as mutant proteins or RNAi, to modify the functions or cell fates of the contacting cells, the ligand-independent background might cause ectopic effects. Another reason that the ligand-independent background of SNTGV might impede the future application *in vivo* is due to the difficulty of screening and identifying individuals with low ligand-independent background. Moreover, as opposed to in vitro, it may be more complicated to balance the signal-noise ratio in vivo for several reasons. First, it's difficult to maintain the expression of the receptor at the same level by promoters across different cell types of interest to keep the amount of free receptor ICD is always below the threshold of the induction of the response gene expressions. Although more and more cell type specific promoters are available now, the expression level driven by a given promoter may differ across cell types. Moreover, the promoter activity might be not homogenous in all the positive cells or throughout different developmental stages. Therefore, this receptor with high ligand-independent activity might work properly with one promoter, but might fail if switched to a

stronger promoter. Second, the sensitivity of the response cassettes might vary between tissues or cell types caused by the chromatin effects of the insertion site in genomes. Therefore, it is possible that the background expression of the response genes occur in one cell type, but not another, even though they both have comparable levels of the receptor expression. Finally, the cell properties of different cell types might also change the ligand-independent activity of the receptors, such as the protease activities or the endocytosis rate in cells. Although our counter-staining does not show that SNTGV and the lysosome marker, Lamp1, co-localize, this does not rule out the possibility that some portion of SNTGV protein gets directed to lysosomes for degradation. SNTGV in the lysosome might be degraded too rapidly to be detected by immunostaining. Therefore, a more sophisticated experiment with the inhibition of lysosomal enzymes should be tested.

To improve the signal-noise ratio of the TRACT, we have managed to increase the surface expression level of SNTGV on plasma membrane and reduce its ligand-independent activity. However, after testing several modifications in the NRR and the TMD of SNTGV, none of them provided a significant improvement to the signal-noise ratio. S1LO NRR of hNotch2 impedes the transportation of the receptor proteins to the cell surface although this modification seems to reduce the ligand-independent background. Moreover, putting the PEST domain of Notch at the C-terminal of h2S1LO-SNTGV

increases the background while replacing the Notch2 TMD with the ones from other type I transmembrane proteins, including the CD4/hNotch1 hybrid TMD, decreases the inducibility while the ligand is present. In contrast, forcing SNTGV to dimerize by adding the LZ motif from GCN4 helps the receptor to be transported to the cell surface. However, this modification also increases the ligand-independent background. Recently Antuca Callejas in Dr. Lois lab has continued testing different modifications to reduce the ligand-independent background based on ShNTG4 (Antuca Callejas unpublish data). First, according to the study, which suggests that transmembrane proteins with a long TMD tend to locate on plasma membrane (Sharpe et al., 2010; Singh and Mittal, 2016), they had tested different length (24 and 28 residuals of amino acids) of the TMD as well as CD4/hN1 hybrid TMD on ShNTG4. Only ShNTG4 with CD4/hN1 hybrid TMD ($SNT_{CD4/hN1}G4$) provides low ligand independent background and still can induce the downstream reporter gene expression. Second, Morsut et al., (2016) claimed that including extra EGF repeats before the NRR in synNotch receptor can help to reduce its ligand-independent activity. My colleague has also tested several new ShNTG4 receptor with different length of most C-terminal EGF-like repeats (30th-36th, 33rd-36th and 36th only) in front of the NRR. Only the one having only 36th EGF-like repeats showed good level of inducibility, but still weaker compared to SNTGV. Finally, Antuca also tested a receptor with the NRR and the TMD of human Notch2. Several studies suggest the human Notch2 NRR is resistant to the mutations that cause constitutive

activation of Notch1. Moreover, more force is required to open human Notch2 NRR than to open human Notch1 NRR (Stephenson and Avis, 2015). Those results indicate that the structure of human Notch 2 NRR is more stable than human Notch 1 NRR. However, ShNTG4 with human Notch2 NRR generates even stronger ligand-independent background compared with the original ShNTG4. In summary, none of the receptors we tested has good surface expression with low ligand-independent activity and strong induction. It indicates that the ligand-independent activity of SNTGV or ShNTG4 might be a complicated issue with complex regulation of its processing, transport and activity. Although we are continuing to test additional receptor modifications, we chose ShNTG4 and $SNT_{CD4/hN1}G4$, which have low background and good inducibility, to generate transgenic flies to test our system in vivo. These experiments are described in the next two chapters.

MATERIALS AND METHODS:

Generation of genetic constructs and production of viral particles. SNTGV was constructed by fusing a single chain antibody (SCAD) that recognizes the mouse CD19, the NRR and TMD from human notch1, and Gal4VP16. The SCAD included amino acids 1-289 from the monoclonal 1D3-28z.1-3 (Kochenderfer et al., 2009). The NRR domain and TMD comprised amino acid 1446-1880 of human Notch-1. Gal4VP16 was then fused after the notch1 TMD, and the entire SNTGV was subcloned into the FUW lentiviral backbone (Lois et al., 2002), FU-SNTGV-W.

Lentiviral particles encoding SNTGV were generated as previously described (Lois et al., 2002). For generating retroviral particles expressing mouse CD19, the MSGV-CD19 plasmid (Kochenderfer et al., 2009) was co-transfected with pCL-Eco and VSVg as previously described (Lin et al., 2010).

Different modifications on SNTGV to improve TRACT function are listed in the followings:

- hN2S1LO-SNTGV: S1LO NRR of hN2 was generated by PCR from s1-LO N1/N2 construct, which generally gifted from Dr. Blacklow. The PCR fragment including the hN2S1LO was, then, subcloned into FU-SNTGV-W digested by BamHI and RsrII.
- S(LZ)NTGV and hN2S1LO-S(LZ)NTGV: the GCN4 LZ motif was generated by

PCR from pUC57-GCN. The PCR fragment was subcloned into either FU-SNTGV-W or FU-hN2S1LO-SNTGV-W digested by BamHI.

- hN2S1LO-SNTGV-PEST: the GAL4DBD and PEST domain of hN1 (including transcription activation domain) were generated by PCR from FU-hN2S1LO-SNTGV-W and the original s1LO-N2/N1 constructs, respectively. FU-hN2S1LO-SNTGV-W was digested by RsrII and AscI. Two PCR fragments and the digested vector were ligated by Gibson Assembly® Cloning Kit (NEB).

-hN2S1LO-SNT_{CD4}GV or hN2S1LO-SNT_{sev}GV: hN2S1LO-SNTGV was PCRed by the reverse primer containing CD4 TMD or sev TMD sequence and the linker to generate the fragment of hN2S1LO-CD4TMD or hN2S1LO-sevTMD. These fragments were subcloned into FU-hN2S1LO-SNTGV-W digested by BamHI and RsrII by Gibson Assembly® Cloning Kit.

-hN2S1LO-$SNT_{CD4IF\text{-}\text{-}>GV}$GV or hN2S1LO-$SNT_{CD4/N2}$GV: hN2S1LO-SNTGV was amplified by the reverse primer containing CD4 TMD with sequences to substitute the amino acid residues and the linker to generate the fragment of hN2S1LO-CD4/hN2TMD or hN2S1LO-$CD4TMD_{CD4IF\text{-}\text{-}>GV}$. These fragments were subcloned into FU-hN2S1LO-SNTGV-W digested by BamHI and RsrII by Gibson Assembly® Cloning Kit.

- ShNTGCTF and ShNTG4: The fragment containing SCAD was generated by PCR from FU-hN2S1LO-SNTGV-W; the hN1NRR was generated by PCR from FU-SNTGV-W with the reverse primer having the hN1NRR sequence directly after SCAD. The fragments carrying hN1TMD and Gal4VP16, Gal4esn or

Gal4CTF were generated by PCR from FU-SNTGV-W, G4CTF, or hNECD-G4esn, respectively, with the reverse primer having the hN1TMD sequence. These three fragments, SCAD, hN1NRR and hN1TMD with different transcription factors, were ligated together with the FUW vector digested by XbaI/AscI by Gibson Assembly® Cloning Kit.

Generation of stable cell lines. The UAS-H2B-citrine reporter CHO cell line was kindly provided by Dr. Elowitz (Caltech). Citrine is a variant of YFP, and we will refer to this reporter as UAS-H2Bmcit. UAS-H2Bmcit cells were grown as described previously (Sprinzak et al., 2010). To stably express SNTGV, UAS-H2Bmcit cells were infected with a SNTGV lentivirus. SNTGV/UAS-H2Bmcit cells were sorted into single cells in a 96 well plate to generate clonal cell lines. Clones with low fluorescence background and high inducibility were chosen for further experiments. To generate stable lines of control emitter cells, CHO cells were first infected by retrovirus expressing mcherry fluorescent protein, and grown in bulk. Control CHO cells are defined as “mcherry+ cells”. To generate stable lines expressing mouse CD19, control mcherry+ cells were infected with a retrovirus expressing CD19 and grown in bulk. Emitter CHO cells expressing CD19 are defined as “CD19/mcherry+ cells”.

Induction of SGNTV by coculture with CD19 cells. SNTGV/H2Bmcit cells were co-cultured with CD19+/mcherry+ cells at 1:1 ratio in 24-well plates. Cells were incubated with the S3 inhibitor, DAPT (10μM), for 30 hrs to synchronize the

timing of induction, and collected at 12, 24 and 48 hours after removal of DAPT.

Western blot: Cells were lysed for 5 minutes at room temperature in a lysis buffer (25 mM Tris-HCl [pH 7.6], 150 mM sodium chloride, 1% sodium deoxycholate, 1% Nonidet P-40, 0.1% sodium dodecyl sulfate [SDS]), supplemented with a protease inhibitor cocktail (Roche). Cellular extracts were boiled for 5 minutes and centrifuged at 14,000 rpm for 5 minutes. Equal protein amounts were subjected to SDS-polyacrylamide gel electrophoresis and transferred to nylon membranes. The membranes were incubated for 1hr in blocking buffer

(3% dry skin milk in tris-buffered saline, TBST), incubated for 2 hrs with a rabbit anti-GFP antibody (Millipore, 1:750 dilution in blocking buffer), washed three times for 10 minutes in TBST buffer, incubated for 2 hrs with a peroxidase conjugated goat anti- rabbit IgG antibody (1:2000 dilution in BB), and washed three times for 10 min in TBST buffer. Protein expression was detected by chemiluminescence autoradiography. Blotting membranes were stripped and processed for β-tubulin as a loading control (Sigma, mouse anti- β-tubulin 1:2000 dilution). Incubations and washes were all performed at room temperature.

Flow cytometry analysis. Co-cultured cells were trypsinized from the plate, diluted in PBS, fixed in 4% PFA, and analyzed for FITC and mcherry fluorescence using a BD LSR II flow cytometer with standard protocols. Relative total fluorescence intensity in Q3 (bottom right quadrant) was quantified by multiplying percentage of cells with mean FITC fluorescence intensity in Q3.

S2 and S3 inhibitors: For inhibitor treatment, batimastat (BB94, 50μM), GM6001 (50μM), TAPI (100μM) and DAPT (10μM) were added into growth medium when co-cultured cells were plated. Co-cultured cells were collected at 48 hours after the cells were plated.

Induction by substrate-attached ligand on ELISA plates and image analysis. Rabbit anti-rat IgG F(ab')2 (312-005-047, Jackson ImmunoResearch) and anti-goat IgG (BA-5000, Vector Labs) antibodies were diluted at different concentrations in PBS. Diluted antibodies were used to coat 96-well ELISA plates (442404, Thermo Scientific) at 4°C overnight. Next day the ELISA plates were gently washed by PBS, 10mg/ml BSA was added to block the plates at 37°C for 1hr, and SNTGV/UAS-H2Bmcit cells (2 × 104) were then plated. Photographs were taken under an inverted fluorescence microscope with 10× objective lenses. Integrated density of each photograph was analyzed by ImageJ.

Statistical significance was determined using a two-tailed unpaired test (t-test). Data are shown as mean ± s.e.m. In all cases, 3 replicates of the experiments were analyzed (n=3).

Cell surface and regular immunostaining. The cell for immunostaining were first seeded on coverslip glasses that pre-coated by poly-D-lysine in water for 24hrs before the seeding in 37c incubator. For cell surface staining, the cells were first pre-treated with dynasore (100um, sigma) for 30mins in the incubator

to block the endocytosis. The cells, then, were washed by the surface staining buffer (1xPBS with 2% fetal brovine serum (FBS), 0.1% sodium azide and dynasore) for 5mins on ice. After the wash, the cells were incubated with the primary antibody, rabbit anti-rat IgG F(ab')2 (1:10 dilution in the surface staining buffer, 312-005-047 Jackson ImmunoResearch) for 45mins on ice. The cells were wash by surface staining buffer three times and 5mins each time on ice after the antibody incubation. The cells were incubated with the secondary antibody, goat anti -rabbit Alexa555, (1:750 dilution) for 45 mins on ice. After this, the cells were washed three times again. After the cell surface staining, the cells were fixed by 4% paraformaldehyde for 10 mins in RT, and followed by the regular immunostaining procedures. For the regular immunostaining, after fixation, the cells were first permeabilized by 0.1% triton X-100 in 1xPBS (PBST) for 10mins and blocked with the blocking solution (1% FBS in PBST) for 30mins. The cells were, then, incubated with primary antibodies (1:500 dilution in the blocking solution for mouse anti-VP16 1-21, sc-7545 Santa Cruz Biotechnology; 1:300 mouse anti-GAL4DBD RK5C1, sc-510 Santa Cruz Biotechnology; 1:300 dilution rabbit anti-CALR, LS-B9387 LSBio; 1:100 dilution rabbit anti-LAMP1 H-228, sc-5570 Santa Cruz Biotechnology; 1:300 dilution mouse anti-FTCD 58K-9, LS-C143027 LSBio)

FIGURES

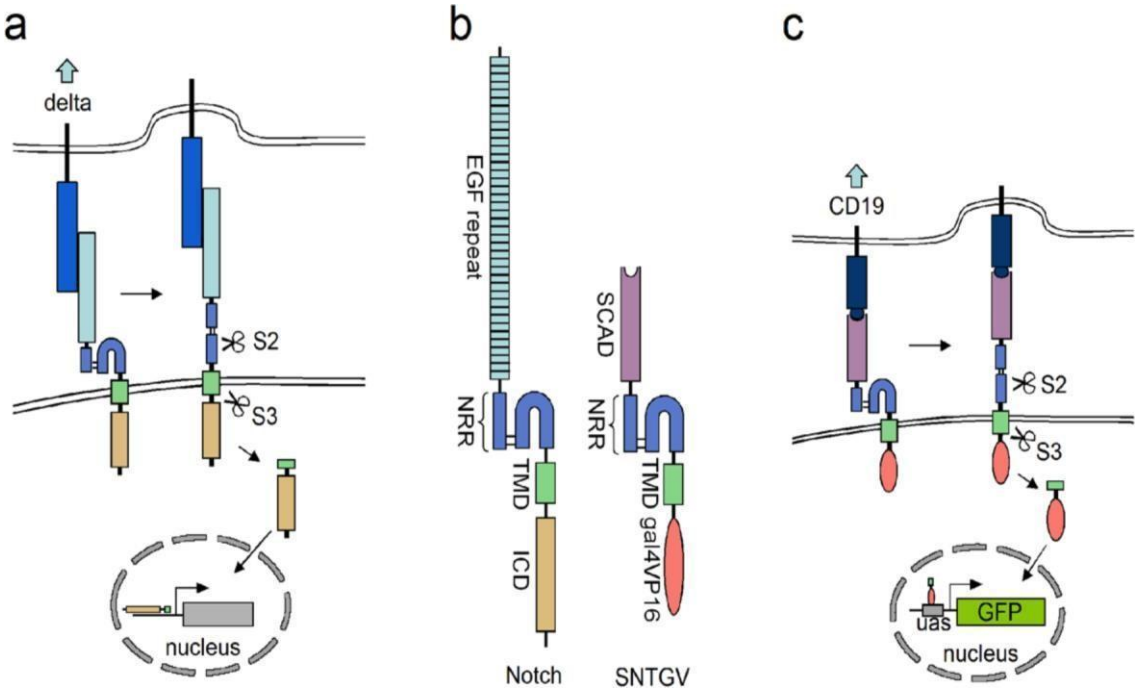
a
delta
S2
S3
nucleus
b
EGF repeat
NRR
TMD
ICD
Notch
SCAD
NRR
TMD
gal4VP16
SNTGV
c
CD19
S2
S3
GFP
uas
nucleus

FIGURE 2-1. A synthetic genetic system to record cell-cell contacts and manipulate interacting cells

(a) Molecular mechanism of Delta-Notch signaling. Upon ligand (Delta) binding, the NRR domain of the Notch receptor is partially unfolded, exposing the S2 site. Thereafter, it is sequentially cleaved, first in NRR (S2 site) and then in TMD (S3 site). After TMD cleavage, the ICD moves into the nucleus and activates transcription. (b) Diagram depicting the domains of Notch and the engineered receptor, SNTGV. (c) SNTGV activation uses the molecular mechanism of the Delta-Notch signaling pathway. Upon CD19 binding, SNTGV is cleaved both in the NRR and TMD, and, then, GAL4VP16 moves into the nucleus of the receiver cell to activate transcription of UAS- dependent genes, such as GFP, in this example.

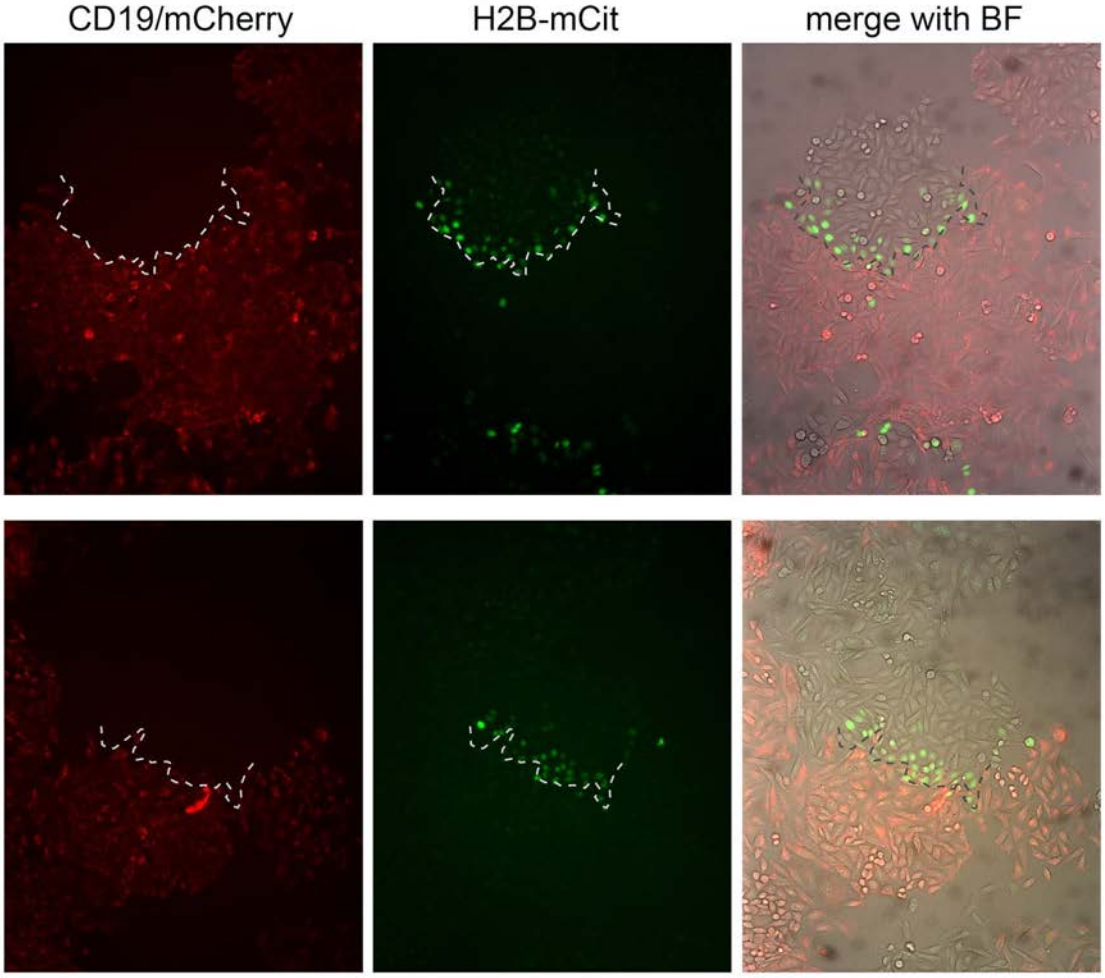
CD19/mCherry
H2B-mCit
merge with BF

FIGURE 2-2. The induction of the reporter gene expression by TRACT to monitor cell-cell contacts in CHO cells.

Two examples (top and bottom panels) of the images from sparsely co-culturing of CD19 cells (red cells in the left panel) and SNTGV/UAS-H2Bmcit cells are shown in this figure. In the middle panel, only the cells of the SNTGV/UAS-H2BmCit colonies, which were close to and made contacts with the CD19 colonies, had H2Bmcit expression increase, but not the cells far from the CD19 colonies. The stippled lines mark the boundaries between CD19 cell colonies and SNTGV/UAS-H2Bmcit cell colonies.

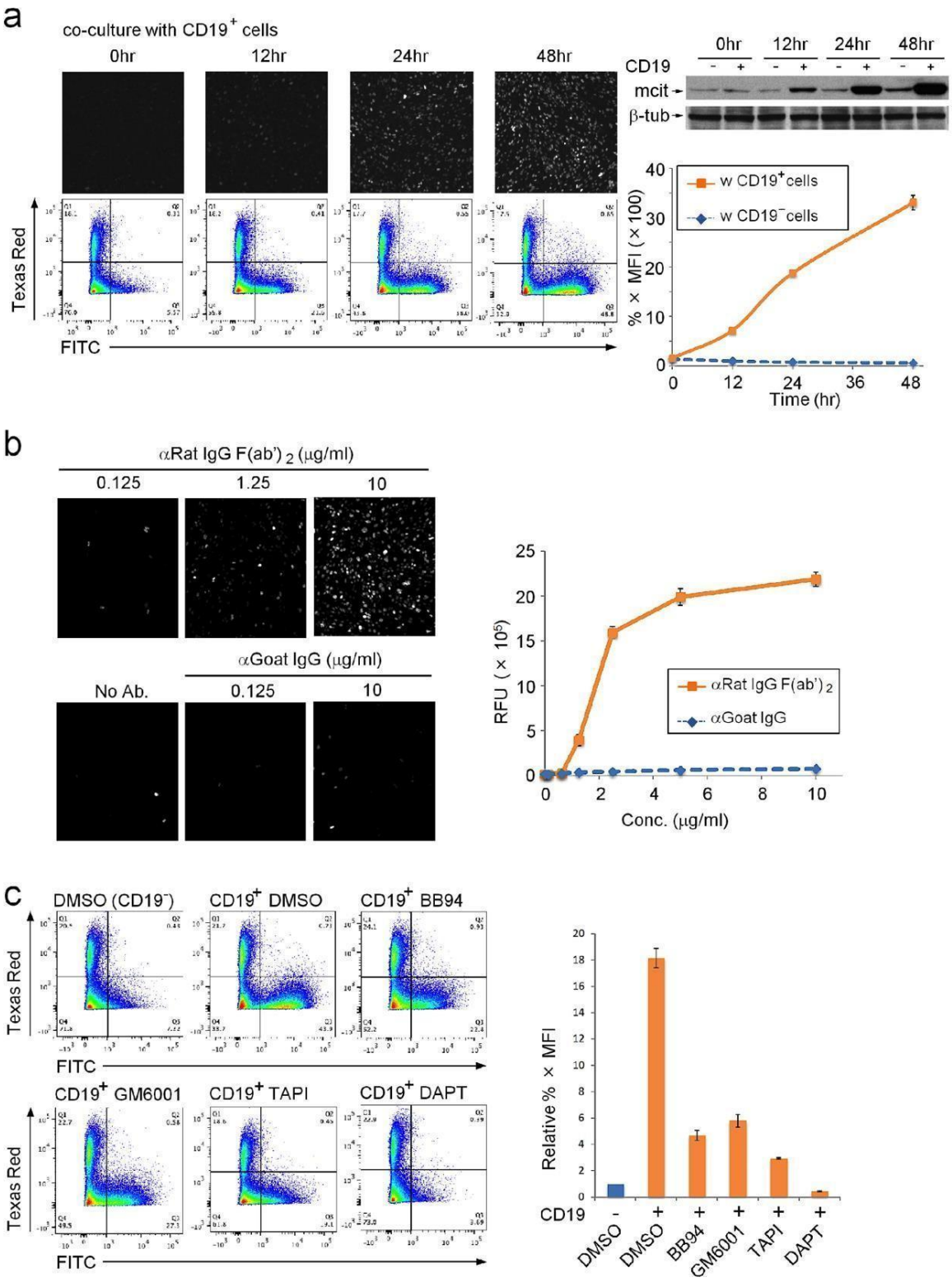
a
co-culture with CD19+ cells
0hr
12hr
24hr
48hr
CD19
mcit
β-tub
Texas Red
FITC
w CD19+cells
w CD19−cells
% × MFI (×100)
Time (hr)
b
αRat IgG F(ab')2 (μg/ml)
0.125
1.25
10
αGoat IgG (μg/ml)
No Ab.
RFU (× 10^5)
Conc. (μg/ml)
αRat IgG F(ab')2
αGoat IgG
c
DMSO (CD19−)
CD19+ DMSO
CD19+ BB94
CD19+ GM6001
CD19+ TAPI
CD19+ DAPT
Relative % × MFI
DMSO
BB94
GM6001
TAPI
DAPT

FIGURE 2-3. Induction of reporter gene expression in vitro by cell-cell and cell-substrate interaction.

(a) Induction of nuclear YFP expression (from a UAS-H2Bmcitrine (UAS-H2Bmcit) reporter cassette) at different time points after co-culturing SNTGV/UAS-H2Bmcit cells with CD19+/mcherry+ cells. Top left: microscopy images showing H2Bmcit expression. Top right: Western blot analysis of H2Bmcit expression induced by co-culturing emitter and receiver cells. Bottom left: FACS plots showing the increase in H2Bmcit expression (X-axis) in SNTGV/UAS-H2Bmcit cells in bottom right quadrant. Y-axis shows the intensity of red fluorescent protein in CHO cells. CD19+/mcherry+ emitter cells are located in the top left quadrant. Bottom right: Quantification of the relative H2Bmcit fluorescence intensity (bottom right quadrant) from the FACS analysis. Induction at 12 versus 0 hours: 4.6 fold ($p<0.0001$), 48 versus 0 hrs = 20.9 fold ($p<0.0001$). (b) Immobilized ligand activates SNGTV signaling. Top left: Anti-rat IgG F(ab')2 antibody (which binds to SCAD) attached to plastic induces H2Bmcit expression in SNTGV/UAS-H2Bmcit cells. Bottom left: Plastic-attached control antibody (which does not binds to SCAD) does not activate SNTGV signaling. Right: Quantification of induction of H2Bmcit expression of SNGTV/UAS-H2Bmcit cells by immobilized Anti-rat IgG F(ab')2. Induction fold of anti-rat (positive ligand) versus anti-goat (negative control) antibodies: 1.25 µg/ml= 11.5 fold ($p<0.005$), 2.5 µg/ml= 38.3 fold ($p<0.0001$), 5 µg/ml= 34.6 fold ($p<0.0001$), 10 µg/ml= 29.8

fold ($p<0.0001$) (c) The induction of SNGTV by its ligand (CD19) requires metalloprotease and γ-secretase. Left: FACS analysis plots showing the effects of metalloprotease (batismastat, GM6001 and TAPI) and γ-secretase (DAPT) inhibitors on H2Bmcit induction by interaction between SNTGV/UAS-H2Bmcit and CD19+/mcherry+ cells. The condition “DMSO (CD19–)” illustrates the lack of H2Bmcit expression when co-culturing SNTGV/UAS-H2Bmcit cells with control mcherry+ (CD19 negative) cells. All the other conditions include SNTGV/UAS-H2Bmcit and CD19+/mcherry+ cells. Right: Quantification of the relative fluorescence intensity from the FACS analysis shown on left. The values of the experimental conditions are normalized to the control “DMSO (CD19–)”. Batismastat versus DMSO: 3.86 fold reduction, $p<0.0001$, GM6001 versus DMSO: 3.1 fold reduction ($p<0.0001$), TAPI versus DMSO: 6.25 fold reduction ($p<0.0001$), DAPT versus DMSO: 50 fold reduction ($p<0.0001$).

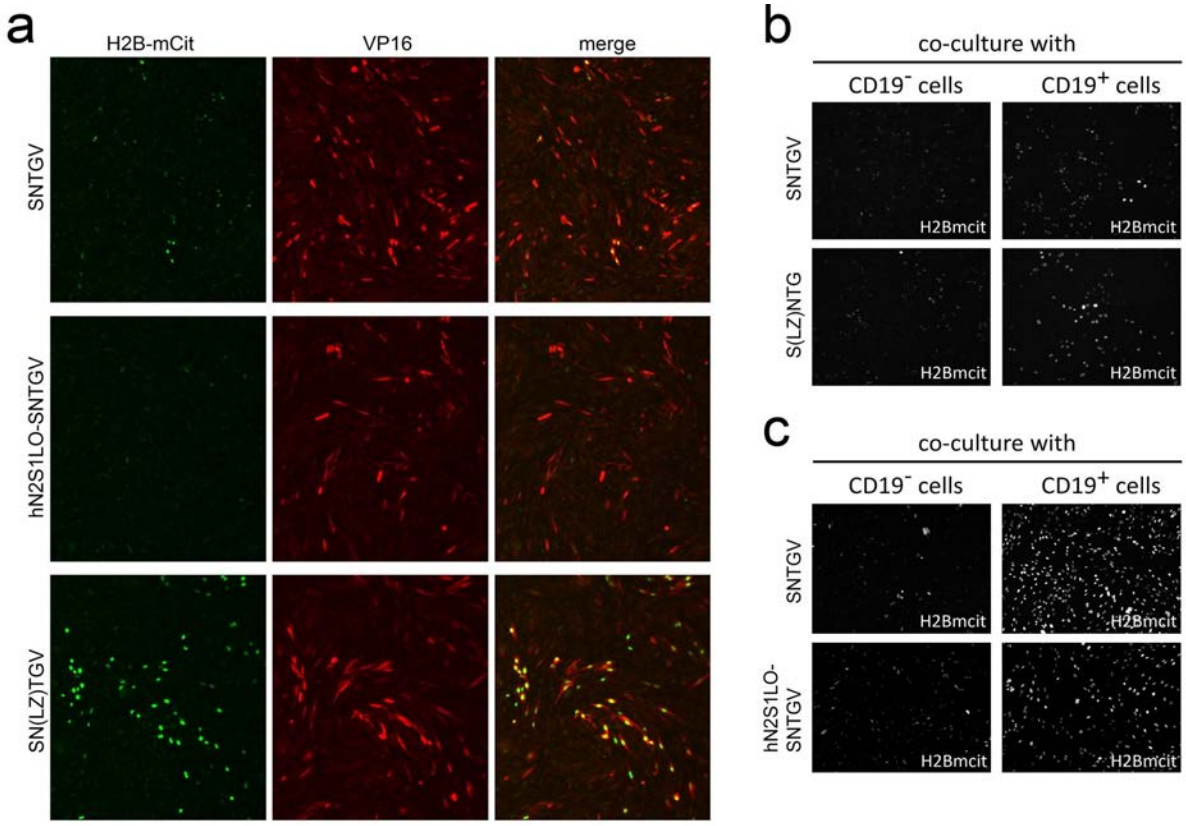
a
H2B-mCit
VP16
merge
SNTGV
hN2S1LO-SNTGV
SN(LZ)TGV
b
co-culture with
CD19- cells
CD19+ cells
SNTGV
S(LZ)NTG
H2Bmcit
c
co-culture with
CD19- cells
CD19+ cells
SNTGV
hN2S1LO-SNTGV
H2Bmcit

FIGURE 2-4. The ligand-independent background generated from different receptors and their capabilities to induce the reporter gene expression by cell-cell interaction.

(a) To show the ligand-independent background from SNTGV (the top panel), hN2S1LO-SNTGV (the middle panel) and S(LZ)NTGV (the bottom panel), three different lentiviruses encoding these receptor proteins were sparsely transduced into UAS-H2Bmcit CHO cells with a similar viral particle concentration. By immunostaining against VP16 (the middle panel) to reveal the receptor positive cells, it clearly shows that around half of the SNTGV cells have detectable H2Bmcit intensities (top left) while most of the hN2S1LO-SNTGV cells do not (middle left). In contrast, most of the S(LZ)NTGV cells have relatively strong ligand-independent background (bottom left). The right panels show merged images of VP16 (red), H2Bmcit (green). (b and c) The capabilities of S(LN)NTGV (b) and hN2S1LO-SNTGV (c) are compared to the one of SNTGV side by side when they were co-cultured with either the CD19 negative control cells (the left panel) or the CD19 positive emitter cells (the right panel). In (b), both SNTGV and S(LZ)NTGV are capable of inducing H2Bmcit expression increase when the emitter cells are present (comparing the right to the left panel). The overall intensity of S(LN)TGV after the induction seems higher than the one of SNTGV, but it might be due to the higher basal level of the ligand-independent ground. In (c), it also shows that the expression level of H2Bmcit can be induced by the

trans-interaction of CD19 and hN2S1LO-SNTGV (comparing the bottom right to the bottom left). However, the inductions from hN2S1LO-SNTGV are relative weaker than from SNTGV.

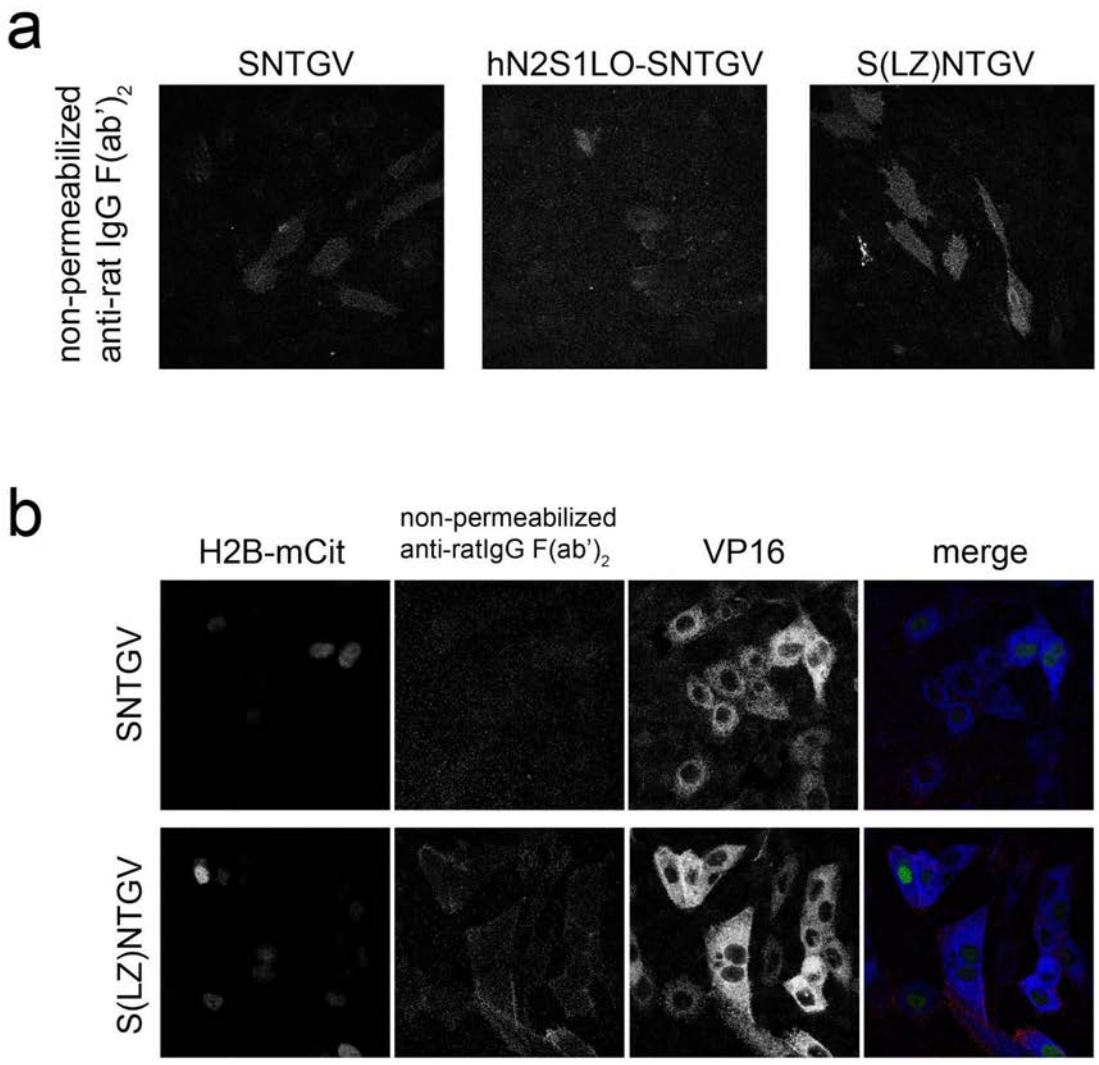
a
SNTGV
hN2S1LO-SNTGV
S(LZ)NTGV
non-permeabilized
anti-rat IgG F(ab')2
b
H2B-mCit
non-permeabilized
anti-ratIgG F(ab')2
VP16
merge
SNTGV
S(LZ)NTGV

FIGURE 2-5. The cell surface expression of different receptors in CHO cells.

(a) To detect the cell surface expression of SNTGV (right), hN2S1LO-SNTGV (middle) and S(LZ)NTGV (left), the immunostaining was performed under the non-permeabilized condition (without detergent) by using the antibody against SCAD (Anti-rat IgG F(ab')2). SNTGV shows moderate level of surface expression compared to hN2S1LO-SNTGV and S(LZ)NTGV. In hN2S1LO-SNTGV, the signal of the surface expression is hardly to be observed while S(LZ)NTGV provide the strongest surface expression among these three receptors. (b) To carefully characterize the cell surface expression between SNTGV (top panel) and S(LZ)NTGV (bottom panel), the surface immunostaining samples were imaged by confocal microscope, and the images from single optical sections are shown here. In addition, to compare the total expression of the receptor proteins, the surface immunostaining (the second panel from the left) was followed by the regular immunostaining against VP16 under permeabilized condition. In the results of VP16 immunostaining,S(LZ)NTGV (bottom) in the cells is homogeneously localized throughout the cytosol to the plasma membrane while SNTGV (top) is retained close to the nucleus. Although the total expression levels (the third panel from the left) of SNTGV and S(LZ)NTGV are comparable, the surface expression signal of SNTGV (top second) is much weaker or barely detectable than the one of S(LN)NTGV (bottom second). In the merged images (rightest panels), the H2Bmcit signals

show in green; the surface staining signals in red; and VP16 signals in blue.

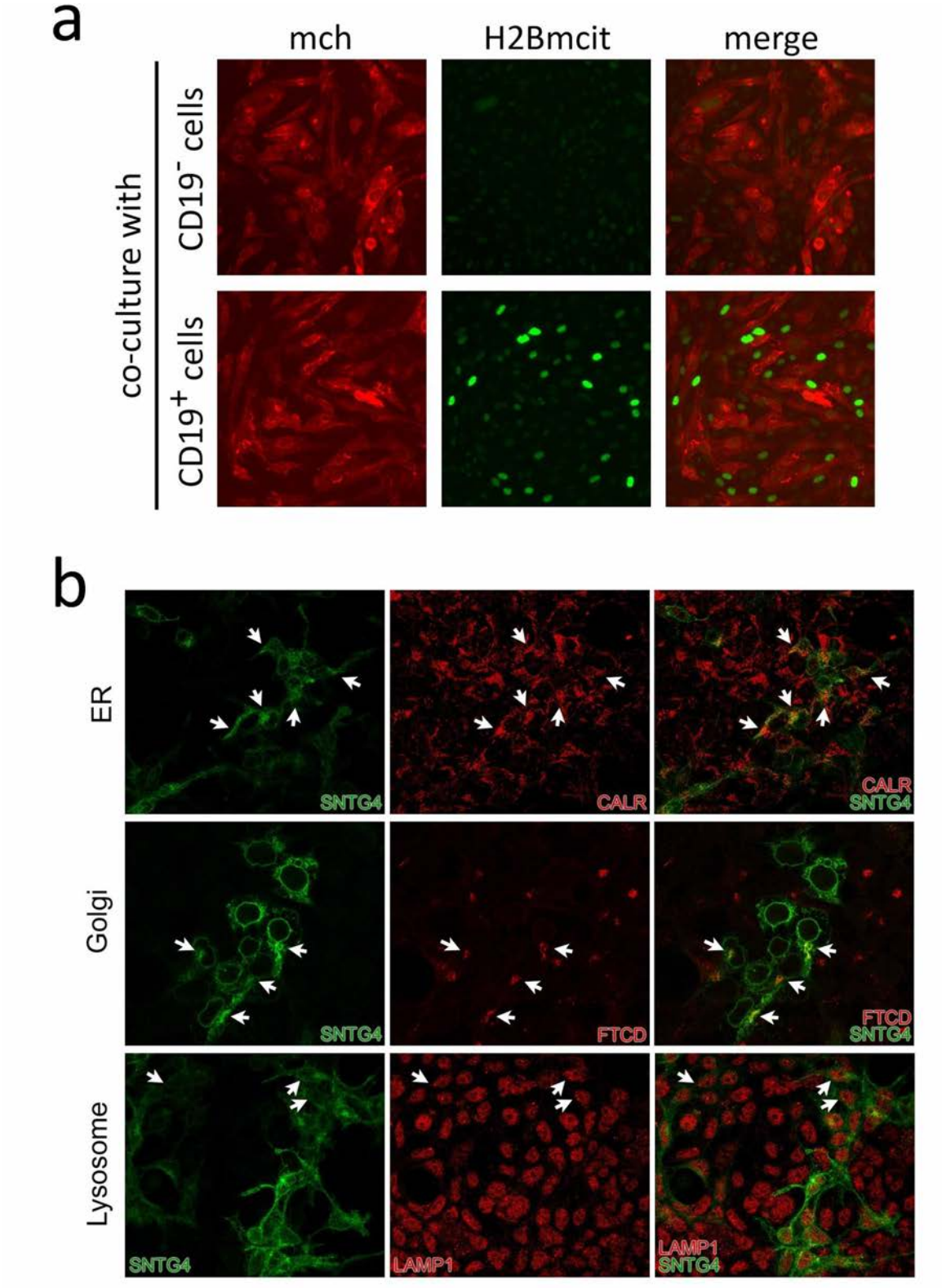
a
mch
H2Bmcit
merge
co-culture with
CD19⁻ cells
CD19⁺ cells
b
ER
Golgi
Lysosome
SNTG4
CALR
CALR
SNTG4
SNTG4
FTCD
FTCD
SNTG4
SNTG4
LAMP1
LAMP1
SNTG4

FIGURE 2-6. Induction of reporter gene expression in CHO cells by cell-cell interaction through ShNTG4 and the subcellular localizations of ShNTG4 in HEK293 cells.

(a) When CD19 is not present, ShNTG4 has merely detectable ligand-independent background (top central). Once the ShNTG4 cells were co-cultured with the CD19+ cells, the expression level of H2Bmcit was dramatically increased (bottom central). The CD19- and CD19+ cells co-express mcherry fluorescent proteins to be visualized (the left panel). (b) The ShNTG4 HEK293 cells were co-immunostained with GAL4 DNA binding domain (green in the left panel) and other cellular organelle markers, CALR for the ER (top central), FTCD for the Golgi (middle central) and LAMP1 for the lysosomes (bottom central). The arrows indicate the positive signals of the organelle markers. In top and middle panels, ShNTG4 is mostly co-localized with CALR (top panel) and TFCD signals (middle panel). However, ShNTG4 is not co-localized with LAMP1 (bottom panel).

Table 2-1. The list of the modified receptor constructs and the summary of their ligand-independent backgrounds and inducibilities

	Modified domain	ligand-independent background	inducibility
SNTGV		++	Y
hN2S1LO-SNTGV	NRR and TMD	+	Y
hN2S1LO-$SNT_{sev}GV$	TMD	-	N
hN2S1LO-SNTGV-PEST	ICD	+++	ND
S(LZ)NTGV	ECD	+++	Y
hN2S1LO-S(LZ)NTGV	ECD	+++	ND
hN2S1LO-$SNT_{CD4}GV$	TMD	-	N
hN2S1LO-$SNT_{CD4/N2}GV$	TMD	+	Y (weak)
hN2S1LO-$SNT_{CD4IF-->GV}GV$	TMD	+	Y (weak)
ShNTGCTF	Transcription factor	-	Y (weak)
ShNTG4	Transcription factor	+	Y

Chapter 3 - Application of TRACT to investigate interactions between neurons and glia in the Drosophila nervous system

This Chapter was adapted from Ting-Hao Huang's publication

Monitoring cell-cell contacts in vivo in transgenic animals.

Ting-Hao Huang, Tarciso Velho, Carlos, Lois. Development. 2016 Nov 1;143(21): 4073-4084.

ABSTRACT

Neurons and glial cells are the two major types of cells in nervous system. Several evidence have demonstrated that glial cells play important roles in regulating neuronal functions and animal behaviors. However, a powerful genetic tool is still required to facilitate the research on glial cells. We, therefore, applied our system, TRACT, in Drosophila to monitor the contacts between neurons and glial cells. First, when the ligand was expressed in different types of glial cells with pan-neuronally expressed receptor, we observed different populations of neurons labeled in the larval central nervous system. It indicates that TRACT is capable to detect the contacts between neurons and glial cells. We further used TRACT to selectively label a group of astrocytes depending on their contacts with ligand positive neurons. From these results, we found astrocytes contacting the OSN axon terminals are stereotypically located at certain regions near the antennal lobes, and some of them occasionally infiltrate into other brain regions as well. Moreover, we also noticed that their cell body sizes are slightly smaller than those of astrocytes interacting with mushroom body Kenyon cells. Therefore, TRACT provides a reliable tool to spatially and consistently target a given group of glial cells, even if there is no specific promoter or driver available. We anticipate that, in the future, it can be used to manipulate glial cells genetically to further study their roles in regulating neural circuits.

INTRODUCTION

In Chapter II and the publications from other groups, many variations of the Notch-Delta mechanism have been used to genetically modify interacting cells (Gordon et al. 2015; Morsut et al. 2016; Roybal et al. 2016). This strategy has been used in vitro to investigate the mechanism of Notch-Delta signaling, to recognize tumors by T cells and engineer cell interactions between cultured cells (Gordon et al. 2015; Morsut et al. 2016; Roybal et al. 2016). However, it remains to be shown whether ligand-induced intramembrane proteolysis can be used to monitor cell-cell interactions in vivo.

The nervous system is composed of two main types of cells, neurons and glial cells. Glial cells are abundant in the nervous system, and were originally thought as supporting cells for neurons. However, more and more evidence has shown that the communication between neurons and glial cells plays an important role in the development and functions of the nervous system, including brain-blood barrier, myelination, nutrient support, neurite outgrowth guidance, synaptic formation and plasticity, and cell debris and neurotransmitter clearance (Banerjee and Bhat, 2007; Clarke and Barres, 2013; Fields, 2015; Freeman, 2015; Kriegstein and Alvarez-Buylla, 2009; Oland and Tolbert, 2011; Volterra et al., 2014). Many of these functions depend on the interactions between the glial and neuronal membranes. Moreover, malfunction of glial cells has also been linked to several neural diseases (Jacobs and Doering, 2010; Lioy et al., 2011;

Prinz and Priller, 2014).

Understanding the development and function of the brain will require the ability to monitor, and eventually modify, the interactions between neurons and glia. There are several different glial cell types in the Drosophila CNS, including surface glia (perineural and subperineural glia), cortex glia, and neuropil glia (ensheathing glia and astrocytes). Each of these glial types have characteristic morphologies and functions, which are similar to the mammalian glial cells. In addition, they also interact with neurons in different ways. Surface glia form two layers of sheath, which are similar to the vertebrate blood-brain barrier, with the glia on the surface of the CNS to insulate it from the hemolymph (Edwards and Meinertzhagen, 2010; Freeman, 2015; Stork et al., 2012). The outer layer is composed of perineural glia, in which Volkenhoff et al., (2015) found an active sugar transporter expressed to provide the energy resource to the CNS. The inner layer of subperineural glia, tightly contacting each other by septate junctions, are thought to participate as the major insulator in the blood-brain barrier, and only have limited contact with neurons (Edwards and Meinertzhagen, 2010). In contrast with the surface glia, cortex glia and neuropil glia are highly associated with neurons. Cortex glia surround and make contact with neuron cell bodies. Each cortex glia can ensheath multiple neuron cell bodies, and are thought to provide the nutrients and support to neurons (Edwards and Meinertzhagen, 2010; Freeman, 2015; Stork et al., 2012). Ensheathing glia are

wrapping the neuropils to provide the structural boundaries between neuropils (Edwards and Meinertzhagen, 2010; Freeman, 2015; Stork et al., 2012). Ensheathing glia can also respond to axonal injury and clean up the debris of the injured axons by phagocytosis (Doherty et al., 2009). Drosophila astrocytes have extensive membrane-membrane contact with neurons as the highly branched astrocyte processes infiltrate into the synaptic neuropils and interact with synapses in the so-called “tri-partite synapse” (Edwards and Meinertzhagen, 2010). One of the important functions of Drosophila astrocytes is to clear the neurotransmitter by the transporters from the synaptic clefts to avoid the prolonged effects (Edwards and Meinertzhagen, 2010; Freeman, 2015; Stork et al., 2012). Recently, several studies in Drosophila also found that calcium signaling or activity in astrocytes might be involved in regulating synaptic functions (Liu et al., 2014; Ng et al., 2011). Moreover, Drosophila astrocytes also play important roles in pruning the neurites and synaptic formation during the metamorphosis stage, especially in the olfactory circuit (Hakim et al., 2014).

Although several drivers and tools in Drosophila, like flip-out or MARCM (Lee and Luo, 2001), are available to characterize the morphologies or functions of different glia types, none of them can precisely and consistently target selected subpopulations of glia cells involved in a specific neural circuit. The lack of reliable genetic drivers for subpopulations of glia makes it difficult to precisely assess their functional role in neural circuits. For instance, it might take intensive

efforts to screen and find an individual with a single clone of labeled glial cells in or nearby the neuropils of interest (Peco et al., 2016). Moreover, pan-glial cell promoters were often used to manipulate the functions of glial cells to study the roles of glial cells on particular behaviors in Drosophila, which might also influence other circuits simultaneously. Without narrowing down the effect to the glial cells in the specific circuit, the results can be misleading and convoluted. Recognizing the need for a better genetic tool in glia cell research, we attempted to utilize TRACT for spatially restricted transcriptional control of glial cell subpopulations.

As an initial test we used TRACT to investigate cell-cell interactions between glial cells and neurons in the brains of transgenic Drosophila. This method has revealed new insights into neuron-glia interactions, and shows potential to allow experiments that are not possible with currently available methods. First, we demonstrate that TRACT can be used to activate gene expression in glial cells that contact specific subsets of neurons by restricting ligand expression to those neurons. This is an important feature as it allows TRACT to genetically identify (and eventually manipulate) cells in a selective manner even if no specific promoters exist for them. For example, we show that it is possible to selectively label a subset of glial cells that interact with olfactory neurons even though there are no specific drivers for these glial cells. Second, using TRACT we have observed that the distribution of glial cells can have a high

degree of stereotypy. For example, we have observed that the astrocytes that interact with olfactory sensory neurons are preferentially localized in certain sectors of the antennal lobe. Third, we have observed that some astrocytes extend branches into two different functional areas of the brain (the antennal lobe and the subesophageal zone). This observation suggests that these particular astrocytes may bridge the functions of these two brain areas, consistent with previous publications (Omoto et al., 2015).

RESULTS

Monitoring glia-neuron interactions in the brain

To monitor contacts between neurons and glia in the Drosophila nervous system we generated constructs tailored for expression in transgenic flies, namely a receptor called SNTG4 and CD19mch (see Material and Methods for detailed description). To express the CD19mch ligand into specific glial types we used the LexA/LexAop bipartite expression system (del Valle Rodriguez et al., 2011; Venken et al., 2011) which allows for modular gene expression. We placed the CD19mch ligand under LexAop-dependent control and used two different LexA drivers, alrm-LexA::GAD or repo-LexA::GAD, to direct ligand expression into different glial types in Drosophila (Fig. 3-1). The alrm driver is strongly active in astrocytes and weak in most other glial cell types (Stork et al., 2012). The repo driver, on the other hand, is active in wrapping glia, subperineurial glia, perineurial glia, cortex glia, but weak in astrocytes (Freeman et al., 2003). Finally, we also included a UAS-GFP allele to report SNTG4 activation and combined these alleles by conventional genetic crosses (elav-SNTG4; repo>CD19mch; UAS-GFP and elav-SNTG4; repo>CD19mch; UAS-GFP). In the absence of CD19mch there was low level ligand-independent background, with some weakly GFP positive cells localized to the eye discs (Fig. 3-1d).

The different glial cell types interact with neurons different ways. Thus, we examined whether directing expression of CD19mch into specific sets of glial

types with the repo and alrm drivers would lead to distinct patterns of reporter expression in neurons. The alrm promoter drove CD19mch expression in astrocytes throughout many regions of the late 3rd instar larva nervous system, particularly in the central brain and the neuropils of the abdominal and thoracic neuromeres (Fig. 3-1b). GFP was induced in neurons throughout the nervous system in the same regions as those in which CD19mch was observed (Fig. 3-1b, and Fig. 3-2a1-a8). The repo driver also led to CD19mch expression throughout many regions of the nervous system including the central brain, thoracic, and abdominal neuromeres , and in glial cells that wrap the peripheral nerves (red fibers in Fig. 3-1c and Fig. 3-2b1-b8). This pattern of ligand expression led to GFP+ neurons in the same or adjacent areas where CD19mch was observed. No GFP expression was observed in any of these areas in the absence of the LexA driver for the ligand (Fig. 3-1d) or the SNTG4 receptor (data not shown). These data indicate that the GFP signal observed upon co-expressing CD19mch and SNTG4 receptor is based on the physical interaction between neurons and glia.

The GFP expression pattern induced by repo-driven ligand overlaps with that of alrm driven ligand in certain areas of the nervous system (namely the mushroom body and the neuropils of the thoracic and abdominal neuromeres). However, as expected given the different types of glial cells targeted by the repo and alrm drivers (Stork et al., 2012), there were also some differences between

the regions in which GFP was induced in neurons when the ligand was directed by alrm and repo (Fig. 3-1 and Fig. 3-2). For example, in the optic lobe the GFP induction in neurons was very strong with the repo, but very weak with the alrm driver (Fig. 3-1 and Fig. 3-3). This observation is consistent with the robust expression of CD19mch in the optic lobe by the repo, but very weak with the alrm driver (Fig. 3-1 and Fig. 3-3). These data show that expressing ligand in discrete subpopulations of glia can reveal different cell-cell interactions, highlighting the specificity and versatility of TRACT.

In the adult brains, however, TRACT failed to detect the contacts between glial cells and neurons. While CD19mch in astrocytes was not able to induce any GFP expression in adult neurons, CD19mch, expressed in most of the glial cells by the repo driver, induced strong GFP inductions only in the adult optic lobes and the mushroom bodies.

The repo and alrm drivers directed expression of the ligand in glial cells broadly distributed throughout the nervous system. Consequently, we observed broad activation of GFP in a large number neurons throughout the brain and ventral nerve cord, as there was no regional specificity for either the emitter or receiver cells. This made it difficult to study in detail or quantify the interactions between neurons and glia. To overcome this limitation, we attempted to investigate the interactions between highly specific subsets of neurons and the glia that contact them.

Monitoring interactions between glia and specific types of neurons

As shown in figure 3-1, the interactions between glia and neurons are ubiquitous throughout the nervous system. Glial promoters such as alrm and repo will direct transgene expression into glial cells in all areas of the nervous system, and consequently, these glial cells will interact with widely distributed neurons. Thus, any genetic manipulation that depends on general promoters such as alrm or repo would be difficult to interpret, because they would affect the interaction between neurons and glia in a global manner. For many experiments it would be necessary to selectively target populations of glial cells located in discrete areas of the nervous system to achieve highly specific manipulations. Interestingly, there are many neuron-specific promoters (in Drosophila, zebrafish, or mice) that can be used to direct transgene expression into selected brain areas. For example, in Drosophila there are promoters or drivers that can be used to selectively express transgenes into projection neurons in the antennal lobe (Stocker et al., 1997) or specific photoreceptors in the compound eyes (Bowtell et al., 1991). Similarly, in mammals, there are promoters to direct expression of transgenes into mitral cells of the olfactory bulb (Nagai et al., 2005) or Purkinje neurons in the cerebellum (Oberdick et al., 1990). In contrast, currently there are no known promoters that can be used to selectively direct transgene expression into glial cells located in discrete areas of the nervous

system. Therefore, to manipulate the astrocytes that contact subsets of neurons in discrete areas of the Drosophila nervous system, we utilized the highly specific drivers that direct expression of the CD19 ligand into specific neuronal types, while the SNTG4 receptor was expressed in astrocytes driven by alrm promoter. We used three different drivers to direct ligand expression into specific subsets of neurons: (i) MB247-LexA::VP16 for Kenyon cells (KCs) of the mushroom body, (ii) orco-LexA::VP16 for olfactory sensory neurons (OSNs) , and (iii) pdf-LexA for Pigment Dispersing Factor (PDF) neurons in ventral nerve cord and central brain. We analyzed the contacts between these selective subsets of neurons and the glia with which they interact during the wandering larval stage, and we observed that selective subsets of astrocytes were induced to express GFP in different CNS regions as expected from the position of the ligand expressing neurons (Figs. 3-4 to 3-6).

First, when mCD19mch was expressed in central brain neurons (including KCs) by the MB247 driver, there were more than 20 astrocytes labeled in the central brain surrounding the mushroom body, the antennal lobe and subesophageal zone (Fig. 3-4a) in wandering larvae. We observed that GFP+ astrocytes near the mushroom bodies infiltrated their processes into the calyx and lobes of mushroom bodies (Fig. 3-4b). In addition, we noticed that the MB247 driver also directed CD19 expression in other neurons outside the mushroom bodies (arrows and arrowheads in Fig. 3-4), and accordingly, there

was GFP induction in astrocytes at the antennal lobe and subesophageal zone of the MB247 animals (Fig. 3-4d, arrow).

When CD19mch was expressed in OSNs, we observed selective GFP expression in astrocytes near the antennal lobes (Fig 3-5c). We found that the average cell body size of the GFP+ astrocytes surrounding the antennal lobe is smaller than that of astrocytes surrounding the mushroom body (induced by the MB247 driver). When measured at the largest optical cross-section, the GFP+ astrocytes labeled near the mushroom bodies of MB247 animals were 1.4 fold larger than those near the antennal lobe in orco animals (Fig. 3-6c) (orco: 96.08μm2, S.D.=+/-25.90μm2, n=35 from 10 animals; MB247: 135.71μm2, S.D.=+/-32.0μm2, n=64 from 6 animals; t-test, $p<0.0001$).

Interestingly, these GFP+ astrocytes infiltrate not only the antennal lobes, but also the dorsal part of the subesophageal zone (arrowhead in middle panel of Fig. 3-5c), consistent with previous finding of astrocytes in larval central brain (Omoto et al., 2015). The location and number of astrocytes induced by the ligand in OSNs varied between individuals examined. Depending on the animal, GFP was observed in one to three astrocytes straddling each antennal lobe. The cell bodies of the astrocytes were most commonly medial or ventrolateral, but never dorsolateral, to the antennal lobes (Fig. 3-6b), also consistent with previous finding (Omoto et al., 2015). As such, I define the medial/dorsomedial and ventral/ventrolateral sectors as “common sectors”. To analyze the variation

of GFP induction across individuals, I categorized the labeling pattern of astrocytes in 50 antennal lobes of 25 larval brains based on the number and location of astrocytes. I observed recurrent patterns, which I formulated into 6 broad categories. Most commonly, (A) a single astrocyte was labeled in a common sector (medial/dorsomedial or ventral/ventrolateral) (34%), or (B) two astrocytes were labeled in two opposite common sectors (e.g. dorsomedial and ventral) (30%). Similarly to (B) but less common, (C) two astrocytes were labeled, one of them in a common sector and the other in an opposite, non-common sector (e.g. dorsomedial and lateral) (6%). In some antennal lobes examined, three astrocytes were labeled (D), two of them in opposing common sectors and another in a non-common sector (e.g. medial, ventral, and ventrolateral) (10%). In other antennal lobes, (E) a single astrocyte was labeled outside the common sector (10%) or (F) multiple astrocytes were labeled in proximal sectors (10%).

When CD19mch was expressed under the pdf-LexA driver, we observed GFP induction in astrocytes near the larval optic lobe (white arrows in right panel of Fig. 3-5d1) and in the distal end of the ventral nerve cord (white arrows in right panel of Fig. 3-5d2). This distribution of GFP+ astrocytes is consistent with the location of the two groups of PDF+ neurons in larval nervous system: (i) lateral neurons in the central brain close to the optic lobe (blue arrows in middle panel of Fig. 3-5d1), which receive input from photoreceptors (Sprecher et al., 2011), and

(ii) motor neurons in the last two segments of ventral nerve cord (blue arrows in middle panel of Fig. 3-5d2) that innervate the hindgut to control muscle contraction (Helfrich-Forster, 1997; Talsma et al., 2012; Zhang et al., 2014).

To evaluate the consistency of TRACT, we counted the number of the GFP-labeled astrocytes in the ventral nerve cord terminal of pdf animals and the antennal lobes of orco animals, where it was possible to count the number of GFP+ accurately. The GFP induction patterns in the antennal lobes of orco driver animals and ventral nerve cord of pdf driver animals are highly consistent among individuals (Fig. 3-6a). There were between 5 and 8 (average= 6.57, S.D.= +/-0.87, n=21 larvae) astrocytes labeled in the ventral nerve cord terminal of pdf animals, and between 1 and 3 (average= 1.68, S.D.= +/-0.74, n=25 larvae) astrocytes in the antennal lobes of orco animals. These experiments demonstrate that directing expression of the ligand into a subset of neurons localized to a restricted area of the nervous system activates transcription in a very selective subset of astrocytes that make contact with those neurons in a reliable manner.

DISCUSSION

Our experiments demonstrate that it is possible to take advantage of the molecular mechanisms of the Notch pathway to genetically record cell-cell interactions in vivo. We have generated transgenic animals where cells expressing an artificial ligand (“emitter” cells) activate a genetically-modified Notch receptor on their interacting partners (“receiver” cells). Using TRACT we have shown that expressing the ligand in glial cells activates transcription in neurons throughout the Drosophila brain and ventral nerve cord. For these experiments, we used the repo driver, which is highly active in subperineurial, perineurial, cortex, and ensheathing glia, but weak in astrocytes, and the alrm driver which is active in astrocytes, but much weaker in other glial types (Freeman et al., 2003). As expected, the set of neurons activated is different when the ligand is expressed under the repo or alrm drivers. These different patterns of GFP induction are likely due to several factors. First, alrm and repo drivers are active in different brain regions. For instance, strong ligand expression can be detected in the larval optic lobe with the repo (Figs. 3-1c and 3-3) but not the alrm driver (Fig. 3-1b). Consequently, the GFP induction is robust in the larval optic lobe of repo (Figs. 3-1c and 3-3) but not alrm animals (Fig. 3-1b). Second, even within the same region, the repo and alrm drivers are active in different populations of glial cells (Stork et al., 2012). In particular, the alrm driver is active in astrocytes (Freeman et al., 2003), which have a large membrane

surface because they have highly branched processes that occupy a large fraction of the neuropil. The contact area between neurons and astrocytes is large because their interaction occurs between highly ramified processes from neurons (dendrites and axonal arborizations) and astrocytes (astrocyte processes) (Stork et al., 2012). Consistent with this observation, although the overall expression of CD19mch in the central brain with the alrm driver (Figs. 3-1b and 3-2) was weaker than with the repo driver (Figs. 3-1c and 3-2), the expression of CD19mch in astrocytes with the alrm driver may account for the robust GFP induction in mushroom body, antennal lobe, and subesophageal zone neurons (Fig. 3-1b and 3-2). Third, it is possible that not all areas of the cell membrane that participate in the interaction between neurons and glia have the same ability to activate the receptor. For example, in the optic lobe with the repo driver there is strong GFP induction in the medulla and lamina neurons, but the CD19mch+ ligand signal close to the cell bodies of GFP+ neurons is very weak, or absent (Fig. 3-3). In contrast, there is clear contact between the neurites of the GFP+ neurons and CD19mch+ glial cells clustered in two bands in the optic lobe, the marginal and medulla glia, and the epithelial glia (Figs. 3-3b and c). As a counterexample, in that same image there is strong CD19mch expression in glial cells in the central brain in areas where there are many neuronal cell bodies, but there is no GFP induction in neurons in those areas (Fig. 3-3a). Interestingly, those central brain areas with no GFP+ neuronal induction also contain cortex glia, which primarily make contact with the cell bodies of neurons, and the repo

driver is expected to direct ligand expression into these cortex glia. These observations suggest that the interaction between neurites and glial processes may be more effective at activating the receptor than interactions between cell bodies. This interpretation is also consistent with the observation of strong GFP induction in central brain neurons when the ligand is expressed in astrocytes (with the alrm driver), as astrocyte processes interact with neuronal processes in synapses (Figs. 3-1, 3-2, 3-4, 3-5 and 3-6). Finally, although our data indicate that the ligand CD19mch is present throughout the neuronal membrane, including cell bodies, axons and dendrites, its distribution may not be strictly uniform along the plasma membrane (Fig. 3-4c). Besides, depending on the cell surface size, the density of the ligand in different cells might also vary. Varying density of the ligand in the plasma membrane could account for the ability to detect some neuron-glia interactions, but not others.

Furthermore, we demonstrate that directing expression of the ligand into a subset of neurons localized to a restricted area of the nervous system activates transcription in a very selective subset of astrocytes that make contact with those neurons. We were able to selectively activate transcription in specific subsets of astrocytes located in the following regions: (i) antennal lobe (with a neuronal driver for OSNs), (ii) mushroom body (with a neuronal driver for Kenyon cells), and (iii) central brain regions next to the optic lobe and terminal end of the ventral nerve cord (with a driver for PDF neurons). This observation indicates that even if

there are no specific promoters capable of directly driving expression of transgenes into certain cell types (such as antennal lobe or mushroom body astrocytes), this strategy makes it possible to genetically manipulate highly specific populations of cells based, not on the genes that they express, but on the cells with which they interact.

TRACT has allowed us to gain new insights about neuron-glia interaction. We have observed that the distribution of glial cells can have a high degree of stereotypy. For example, we have observed that the astrocytes that interact with olfactory sensory neurons are preferentially localized in certain sectors of the antennal lobe, but are rarely, if ever, present in other sectors (Fig. 3-6b). The localizations of the astrocyte cell bodies have been reported previously by clone analysis (Omoto 2015). Because the randomness of the labeling by clone analysis, there is no direct evidence to show how different astrocytes coordinate together to cover larval antennal lobe or whether there is any consistency of astrocyte process patterns across different individuals. Peco et al., (2016) recently found that the arborizations of astrocytes in larval VNC stereotypically cover specific regions of neuropil. However, due to the repetitive structures of segmentation in larval VNC, it is still questionable whether this finding can also apply to the central brain, whose structure is relatively sophisticated. Our preliminary data suggest that the infiltration patterns of the astrocytes surrounding the larval antennal lobes are variable, unlike the patterns of the ones

in the VNC. However, it might be necessary to confirm whether all the astrocytes that branch into the antennal lobe were labeled by analyzing the co-localization between GFP signals and astrocytic membrane marker, such as GABA transporter. Moreover, due to the complexity of the combinations of cell body distribution, more sophisticated analysis should be considered in the future, such as more precise alignment of the images from different individuals or unbiased computational analysis.

In addition, we have observed that the astrocytes surrounding the medial sectors of the antennal lobe also extend branches into the subesophageal zone. This suggests that this particular astrocyte may bridge the function between the antennal lobe and the subesophageal zone, consistent with previous publications that imply a close functional relationship between these 2 brain areas in the larval brain (Omoto, et al 2015).

Finally, we have observed that the size of the cell bodies of astrocytes that branch in the mushroom body are larger than those that branch in the antennal lobe. The structural variation between these subpopulations of astrocytes could reflect an underlying functional heterogeneity among astrocytes localized to different areas. Traditionally glial cells are considered to be homogenous population deployed throughout different brain regions. However, different types of neurons in different brain regions process different neuronal properties and perform diverse functions. For instance, in mammals, a group of astrocytes in

subventricular zone and dentate gyrus are specialized to function as adult neural stem cells. Recently, in a review article, Magnusson and Frisen, (2016) raise the questions of why there is a regional difference for astrocytes and which factor regulates the specialization of their cell fate. In our case, by using our system with other tools, such as translating ribosome affinity purification (TRAP, Heiman et al., 2008), we might be able to analyze in details the differences of the gene profiles from astrocytes contacting different types of neurons.

TRACT, with the design described in this chapter, is not optimized to monitor glia-neuron contacts in the adult stage because of several issues. For instance, when the ligand was expressed in astrocytes and the receptor expressed pan-neuronally by elav promoter, there was no induction in the adult brains. However, once the same experiment was performed with the modified receptor, which has the Drosophila Neuroligin intracellular domain located between the TMD and GAL4 and will be discussed in Chapter 4, a strong induction of GFP expression was observed in the entire adult brain (data not shown). This might be due to the improvement of the sensitivity or the neurite localization of the receptor proteins. Moreover, for selectively labeling a group of astrocytes by TRACT, *alrm-SNTG4* generates strong ligand-independent background in many regions of the adult brain, which makes it difficult to analyze the real induction. This phenomena might be caused by higher expression level of the receptor proteins in adult vs. larval astrocytes. For this issue, I will have

more discussion in detail in Chapter 4, but one possible way to improve it is to replace *alrm* promoter with another pan-astrocytic one.

Previous research focusing on astrocytes involved in CNS functions mostly used astrocyte-specific drivers to perturb the cell properties or gene expression profiles in all astrocytes. For example, Ng et al., (2011) used astrocyte-specific or pan-glia drivers to block endocytosis or allow calcium signaling, respectively, to find that glial cells modulate circadian behavior in Drosophila. In another study, Liu et al., 2014 expressed TRPA1 in all astrocytes in larvae to show that the astrocytes regulate the synaptic strength and response between OSNs and PNs. Care should be taken to interpret these results and the possibility of the effects from other circuits. In the future, we anticipate to use TRACT to selectively manipulate the functions of astrocytes infiltrating specific neuropils or contacting specific types of neurons to precisely pinpoint their roles in neural circuits and animal behavior. For example, I am planning to use TRACT to express the dominant negative *Shibir*e selectively in the antennal lobe astrocytes to block endocytosis, which has been shown to be important for astrocytic regulation of synaptic function and animal behavior (Ma et al., 2016; Ng et al., 2011). I will test those animals' olfaction and olfactory learning and memory to characterize the impact on the antennal lobe circuit. In addition, to characterize the role of astrocytes in circadian rhythm, I will use TRACT to express an ebony RNAi in the astrocytes associated with *pdf* or other circadian neurons. *ebony* in *Drosophila*

glial cells has been shown to be essential for normal circadian behavior (Suh and Jackson, 2007). Hopefully, with those manipulations in selected astrocytes, we can get more precise insight into the roles of astrocytes on controlling neural circuit functions.

MATERIALS AND METHODS

Transgenic flies. For all experiments using transgenic flies we modified the SNTGV receptor described above for in vitro experiments and we generated a receptor called SNTG4, which contains the following: (i) SCAD, (ii) Drosophila notch NRR and notch TMD (residues 1460 to 1767) , and the transcriptional regulator GAL4esn (defined as G4 thereafter). GAL4esn includes the DNA binding domain and the transactivation domain, but it lacks the GAL80 binding domain (Sprinzak et al., 2010).

- elav-SNTG4: We introduced the SNTG4 receptor in a pCasper vector containing the 3.5 kb fragment of the elav promoter (Yao and White, 1991). Transgenic elav-SNTG4 flies were produced by standard P-element integration. elav-SNTG4 transgenic flies were screened by GAL4 immunostaining, and the lines with the highest expression level of SNTG4 were chosen for the future experiments.

-The alrm-SNTG4 construct was generated by amplifying a 4,973 bp region of alrm promoter from alrm-Gal4 cassette (Doherty et al. 2009), which then replaced the elav promoter in pCasper-elav-SNTG4. Transgenic alrm-SNTG4 flies were produced by standard P-element integration. alrm-SNTG4 transgenic flies were screened by GAL4 immunostaining, and the lines with the optimal expression level of SNTG4 were chosen for the future experiments. For transgenic flies we modified the CD19 ligand to carry the CD19 ECD and TMD

fused to the red fluorescent marker mCherry to allow identification of the emitter cells. In addition, we included an endocytosis signal from the human LDL receptor (Chen et al., 1990), as endocytosis is thought to be necessary to generate the pulling force that opens the NRR (Meloty-Kapella et al., 2012). The ligand containing CD19, mcherry, and the LDL endocytosis signal will be referred to as CD19mch. We compared the activity of SNTGV (with gal4VP16, human notch NRR and TMD) and SNTG4 (with GAL4esn, Drosophila NRR and TMD) receptors, as well as CD19 and CD19mch ligand, in CHO cells, and we observed that the level of inducibility (maximal induction levels normalized to ligand-independent background levels) were highly similar for these two receptors and two ligands (data not shown).

- LexAop-CD19mch: The CD19mch ligand was cloned in the LexAop pJFRC19 plasmid (Addgene). Transgenic LexAop-CD19mch flies were produced by attb site-specific integration in attP2 site.

- repo-LexA::GAD, alrm-LexA::GAD drivers, 5xUAS-mCD8::GFP and 5xUAS-CD4::tdGFP reporter were a gift from Marc Freeman, Umass Medical School.

- pdf-LexA were a gift from Quan Yuan, NINDS.

- MB247-LexA::VP16 were a gift from Tzumin Lee, Janelia Research Campus , HHMI. Genotypes of flies analyzed in the figures:

Fig. 3-1b and 3-2a: 5XUAS-CD4::tdGFP/elav-SNTG4 ; alrm-LexA::GAD/LexAop-

CD19mch

Fig. 3-1c, 3-3 and 3-2b: 5XUAS-CD4::tdGFP/elav-SNTG4 ; repo-LexA::GAD/LexAop-CD19mch

Fig. 3-1d: 5XUAS-CD4::tdGFP/elav-SNTG4 ; LexAop-CD19mch/TM3

Fig. 3-4a (top-right, top-left and bottom-left panel), 3-4b, 3-4d and 3-6c (bottom panel): 5XUASmCD8::GFP/alrm-SNTG4 ; MB247-LexA::VP16/LexAop-CD19mch

Fig. 3-4a (bottom-right) and 3-5b: 5XUAS-mCD8::GFP/alrm-SNTG4 ; LexAop-CD19mch/TM3

Fig. 3-4c: 5XUAS-mCD8::GFP/CyO ; MB247-LexA::VP16/LexAop-CD19mch

Fig. 3-5c, 3-6a (left two panels), 3-6b (top panel) and 3-6c (top panel):5XUAS-mCD8::GFP/alrm-SNTG4

; orco-LexA::VP16/LexAop-CD19mch

Fig 3-5d and 3-6a (right two panel): 5XUAS-mCD8::GFP/alrm-SNTG4 ; pdf-LexA/LexAop-CD19mch

All the crosses were maintained at room temperature, and were repeated at least 3 times.

Immunostaining and microscopy of fly brain. The brains of the wandering larvae were dissected in 1x PBS under a dissection microscope. Brains were

fixed by immersing them in a 4% paraformaldehyde solution in PBS for 15 minutes at room temperature. Brains were washed in PBS three times for 10 mins each, followed by permeabilization with PBS/0.5% triton X-100 (PBST) for 30 mins and blocking with 5% serum in PBST for 30 mins. The brain samples were stained with antibodies against GFP (rabbit polyclonal from Millipore, AB3080, diluted at 1:1,000), mcherry (rat monoclonal, 5F8, from Chromotek diluted at 1:1,000), Repo (mouse monoclonal, 8D12, from DSHB diluted at 1:10) and Brp (mouse monoclonal, nc82, from DSHB diluted at 1:50) diluted in 5% serum/PBST. Brains were Incubated with 1ry antibodies overnight at 4C, washed 3 times in PBST, incubated with 2ry (goat secondary antibodies, Life Technologies, 1:500) for two hours at room temperature except the one for repo and brp at 4C overnight) , washed in PBST and mounted on glass slides with a clearing solution (Slowfade Gold antifade reagent, invitrogen).

Stained brains were imaged with confocal microscopes (Olympus Fluoview 300 or Zeiss 710) under a 40X or 60X objective. In a typical experiment, we imaged 150 sections with an optical thickness of 0.3-0.5 μm from dorsal or ventral sides. Confocal stacks were processed with Fiji to obtain maximal projections.

FIGURES

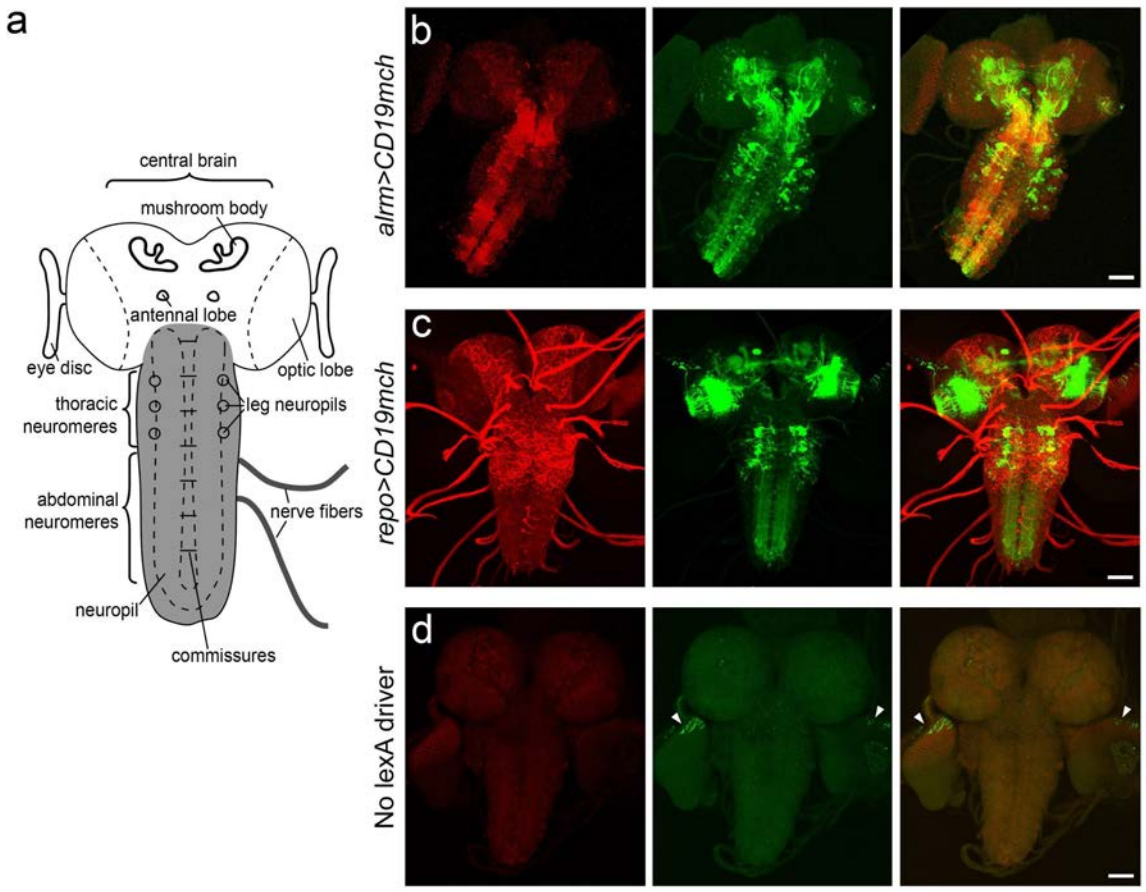
a
central brain
mushroom body
antennal lobe
eye disc
optic lobe
thoracic neuromeres
leg neuropils
abdominal neuromeres
nerve fibers
neuropil
commissures
b
alrm>CD19mch
c
repo>CD19mch
d
No lexA driver

FIGURE 3-1. Monitoring glia-neuron contacts in the Drosophila nervous system.

(a) Diagram of the Drosophila larval nervous system indicating the main regions and structures in the brain and ventral nerve cord (shadowed in grey). (b and c) Expression of the CD19mch ligand by the alrm (b) and repo (c) drivers lead to GFP expression in elav-SNTG4 neurons throughout the larval nervous system. (d) control flies without the lexA driver have weak GFP background expression (ligand-independent) in the larval eye discs (arrows). For all panels, left shows distribution of CD19mch+ emitter cells; middle shows distribution of GFP+ neurons; right shows merged imaged of CD19mch (red), GFP (green) . Scale bar= 50 μm.

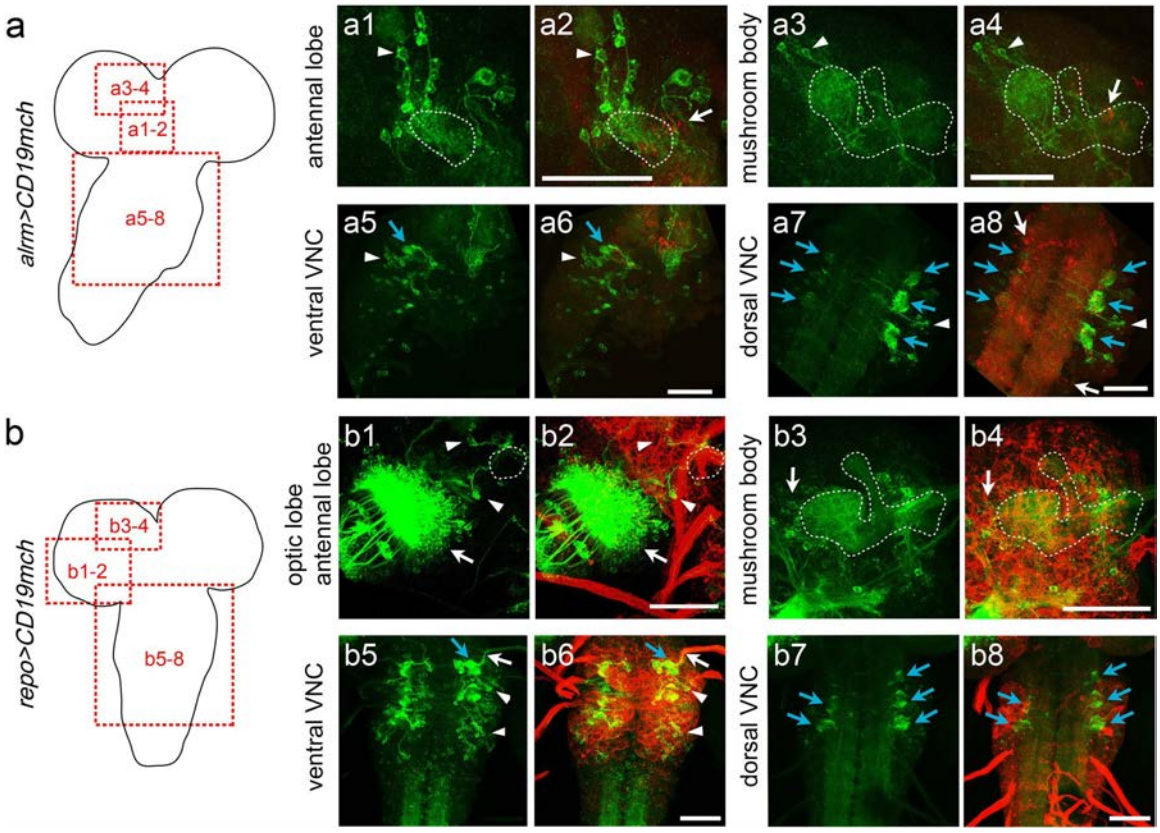
a
alrm>CD19mch
a3-4
a1-2
a5-8
antennal lobe
a1
a2
mushroom body
a3
a4
ventral VNC
a5
a6
dorsal VNC
a7
a8
b
repo>CD19mch
b3-4
b1-2
b5-8
optic lobe
antennal lobe
b1
b2
mushroom body
b3
b4
ventral VNC
b5
b6
dorsal VNC
b7
b8

FIGURE 3-2. Expression of the ligand in different glial subtypes produces different patterns of induction.

(a) Induction of GFP in neurons triggered by the *alrm* driver. Top, middle, and bottom squares in the diagram indicate high magnification views of the antennal lobe, mushroom body, and ventral nerve cord shown in Fig. 3b, and are shown in 4a1-a2, 4a3-a4, and 4a5-a8, respectively. The cell bodies of CD19mch+ glia cells (white arrows) are located in both the central brain (a2, a4), and ventral nerve cord (a6, a8). (a1, a2) GFP+ neurons (arrowheads) surround the antennal lobe (marked by a stippled oval). (a3, a4) GFP+ cells bodies of Kenyon cells (arrowheads) surround the mushroom body (contours traced by stippled line), which is filled with GFP+ processes. (a5-a8) ventral and dorsal view of the thoracic neuromeres in the ventral nerve cord. GFP+ cell bodies had neurites that traverse throughout the neuropil and commissures. (a7, a8) Some of the GFP+ neurons (white arrowhead) form clusters in the thoracic neuromeres that innervate into 3 pairs of leg neuropils (blue arrows). (b) Induction of GFP in neurons triggered by the *repo* driver. Right, top, and bottom squares in the diagram indicate high magnification views of the optic lobe, central brain, and ventral nerve cord from Fig. 3c and are shown in 4b1-b2, 4b3-b4, and 4b5-b8, respectively. (b1, b2) GFP induction in the optic lobe (arrow), and in a small number of neurons (arrowhead) surrounding the antennal lobe (circle). Rectangle in b2 outlines the position of a CD19mch band of glial cells in the border between

the lamina and medulla in the optic lobe. (b3, b4) Kenyon cells (arrows) surrounding the mushroom body (outlined by stippled line). (b5-b8) Ventral and dorsal view of the thoracic neuromeres in the ventral nerve cord. Neurites from GFP+ neurons traverse throughout neuropil, commissures, and fiber tracts in the ventral nerve cord. Leg neuropils (blue arrows) contain branches of strongly expressing GFP neurites, whose cell bodies are located surrounding the neuropils (arrowhead). Notice that the nerve fibers are wrapped by strongly labeled CD19mch+ glia (b6) and contain axons that are GFP+ (b5) , and connect with leg neuropils (blue arrows). All images are confocal maximal projection images of the larval nervous system. Emitter cells (expressing CD19mch) are labeled in red. Receiver cells (expressing GFP) are labeled in green. Scale Bar: 50 μm.

repo>CD19mch

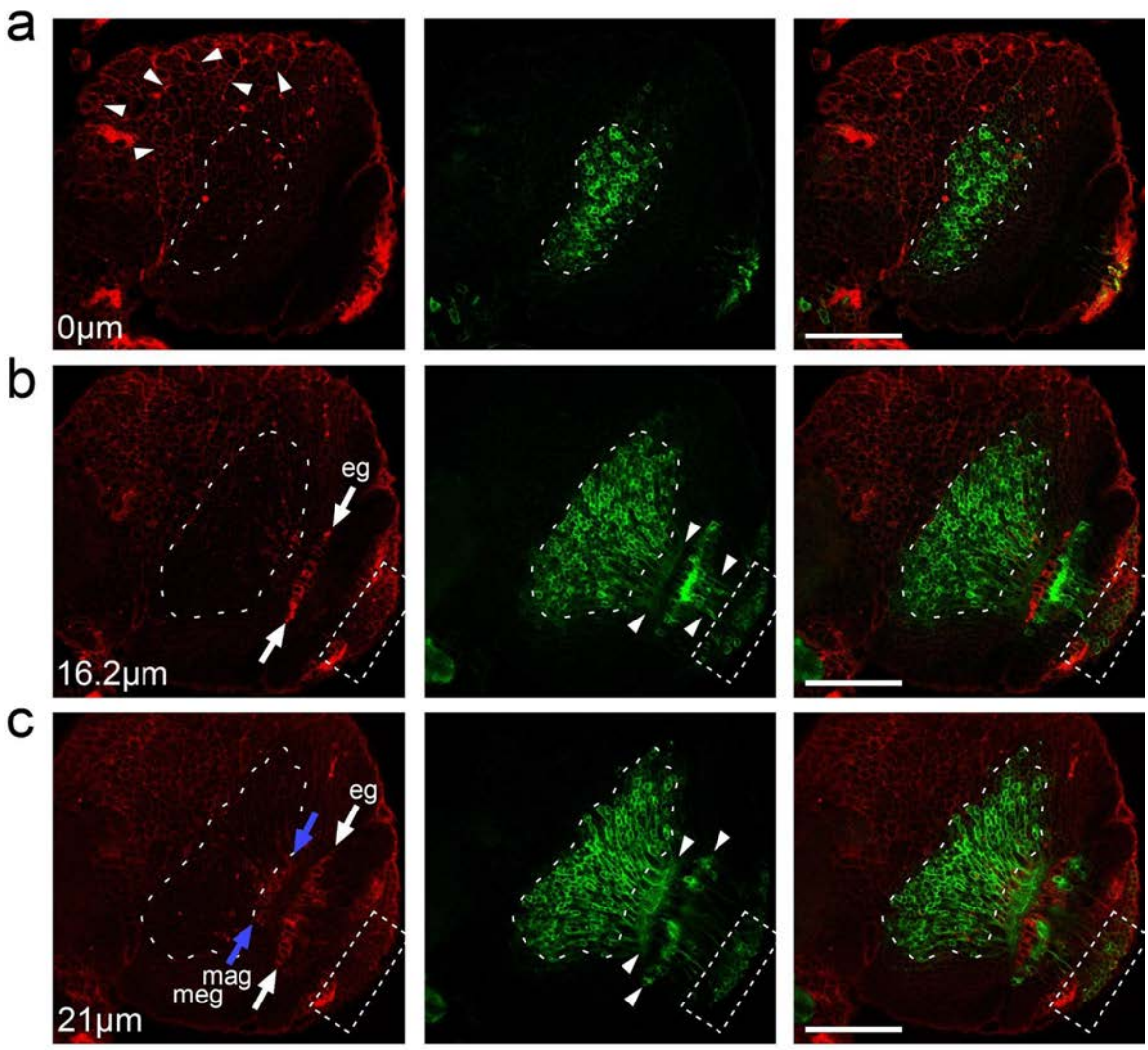

FIGURE 3-3. Differential induction of GFP in the central brain and optic lobe by expression of CD19mch ligand by a repo driver.

GFP expression was induced in the neurons of larval optic lobe (stippled ovals and rectangles) when CD19mch was expressed in larval optic lobe glia cells (b and c, white and blue arrows in b and c) by the repo driver. In contrast, CD19mch expression in the central brain (a, white arrowheads) did not induce GFP expression in neurons in those areas. Serial single optical sections (a: z=0μm; b: z=16.2μm and c: z=21μm) of larval optic lobe from confocal images show the distribution of CD19mch+ glia cells and GFP+ optic lobe neurons. (a) The cell bodies of medulla neurons express GFP strongly and form a cluster (stippled oval), with sparse, weakly expressing CD19mch+ glial cells inside of the cluster. (b) The cell bodies of lamina neurons are also GFP+ and form a second cluster (stippled rectangle on the right lower corner of the images) with weakly expressing CD19mch+ glial cells present inside of the cluster. The neurites of GFP+ lamina and medulla neurons (arrowheads) make contact with a row of epithelial glia (eg, white arrows) that express high levels of CD19mch. (c) The neurites of GFP+ neurons (arrowheads) interact with a second row of strongly expressing CD19mch+ marginal (mag) and medulla (meg) glia (blue arrows). For all panels, left shows distribution of CD19mch+ emitter cells; middle shows GFP+ neurons; right shows merged imaged of CD19mch (red), GFP (green). Scale bar= 20 μm.

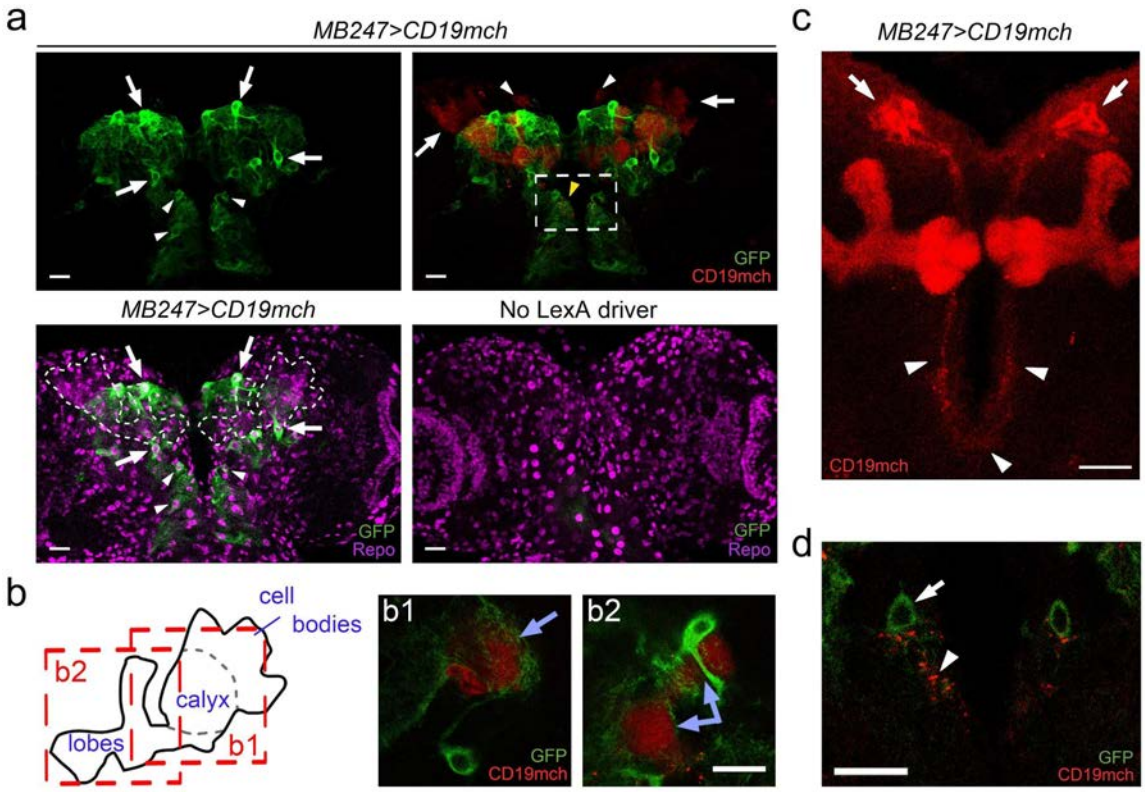
a
MB247>CD19mch
GFP
CD19mch
MB247>CD19mch
No LexA driver
GFP
Repo
GFP
Repo
b
cell
bodies
b2
calyx
lobes
b1
b1
GFP
CD19mch
b2
c
MB247>CD19mch
CD19mch
d
GFP
CD19mch

FIGURE 3-4. Monitoring neuron-astrocyte contacts selectively in Drosophila larval mushroom bodies.

(a) Induction of GFP in central brain astrocytes (arrows and arrowheads in top left panel) triggered by CD19mch expressed under the MB247 driver (red signals in top right panel). SNTG4 receptor was expressed in all astrocytes using the alrm promoter. The majority of the CD19mch+ neurons driven by MB247 are Kenyon cells (KCs) in mushroom bodies (arrows in top right panel), and are located next to GFP+ astrocytes (arrows in top left panel). In addition to KCs, the MB247 driver also expresses CD19mch in other neurons outside of the mushroom body (cell bodies indicated by white arrowheads and neurites by yellow arrowheads in top right panel), which lead to GFP expression in astrocytes located in the subesophageal zone and antennal lobe (arrowheads in top left). The enlarged image of the stippled rectangle region is shown in (d) Bottom left: immunostaining against REPO shows the location of all glial cell nuclei. The mushroom bodies are contoured by a stippled line. Bottom right: control larva without the LexA driver has no GFP expression. (b) Scheme showing the three domains of the right mushroom body in (a): KC cell bodies are located in the top right corner. Dendrites from KCs branch in the calyx, and their axons project to the lobes. Single optical sections of the calyx and dorsal lobe are shown in (b1) and (b2), respectively. In (b1) and (b2) the branches of the GFP positive astrocytes surround the mushroom body. The arrows indicate the

dendrites (branching in the calyx (b1)) and axons (branching in the dorsal lobe (b2)) of CD19mch+ KCs. (c) CD19mch expression pattern driven by MB247. In addition to the KCs in the mushroom bodies, CD19mch was also expressed in some neurons in the dorsomedial aspect of the central brain (arrows). The neurites (arrowheads) of these neurons project along the midline into the subesophageal zone. (d) Single optical section from the stippled rectangle region shown in the top right panel in (a). The GFP induction in astrocytes near the antennal lobe and subesophageal zone (arrow) was in the vicinity of projections from CD19mch+ neurons (arrowheads). The images in (a) and (c) are maximum projections of confocal microscopy images. Scale bar= 20 μm.

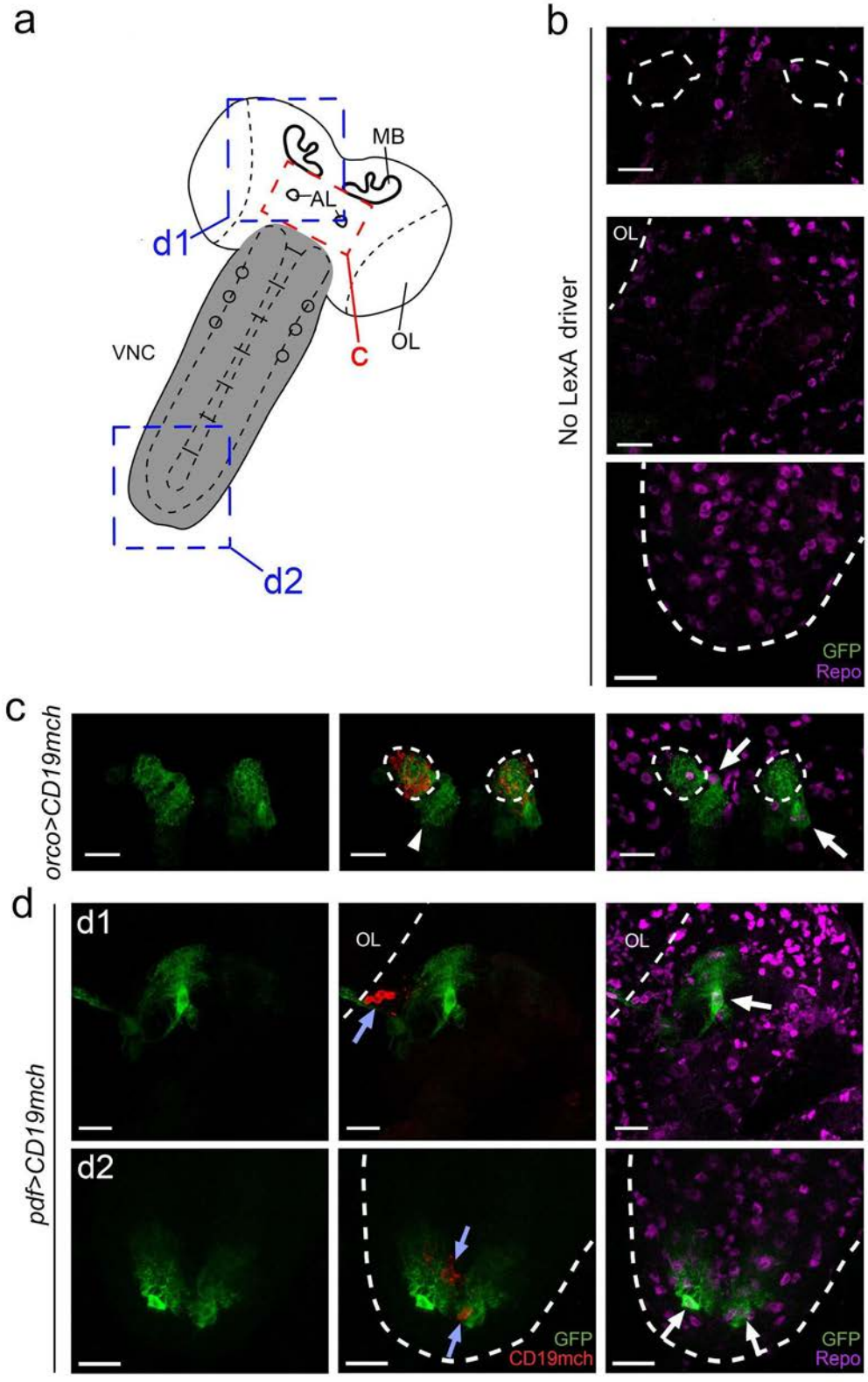
a
MB
AL
d1
VNC
c
OL
d2
b
No LexA driver
OL
GFP
Repo
c
orco>CD19mch
d
pdf>CD19mch
d1
OL
OL
d2
GFP
CD19mch
GFP
Repo

FIGURE 3-5. Monitoring neuron-astrocyte contacts selectively in larval antennal lobe, central brain, and ventral nerve cord.

(a) Diagram of the Drosophila larval nervous system indicating the regions shown in b-d. The region in the red stippled rectangle including antennal lobe is shown in top panel of (b) and (c). The region in the top blue stippled square in the central brain is shown in middle panels of (b) and (d1). The distal part of VNC in the bottom blue stippled square is shown in the bottom panel of (b) and (d2). (b) Control larva without the LexA driver has no GFP expression in the antennal lobes (top, stippled contours), central brain (middle) or the distal part of VNC (bottom, stippled contour). (c) The orco driver induces CD19mch expression in most OSNs. CD19mch+ axons from OSNs projecting into the antennal lobe (red in the stippled circles) induced GFP expression in antennal lobe astrocytes (white arrows in the right panel). The GFP+ astrocytes located in the medial sector of the larval antennal lobes also infiltrate into the subesophageal zone (white arrowhead in middle panel). (d) GFP induction in selective astrocytes in the central brain (d1) and ventral nerve cord (d2) when pdf driver directed CD19mch expression into PDF neurons. In (d1) the dashed lines mark the boundaries between the larval optic lobe (OL) and central brain, and in (d2) the dashed line contours the ventral nerve cord. The CD19mch+ PDF neurons (blue arrows in middle panels) induce GFP expression in a small set of astrocytes in their vicinity (white arrows in right panels). All images in this figure are maximum projections

of confocal microscopy stacks. Scale bar= 20µm.

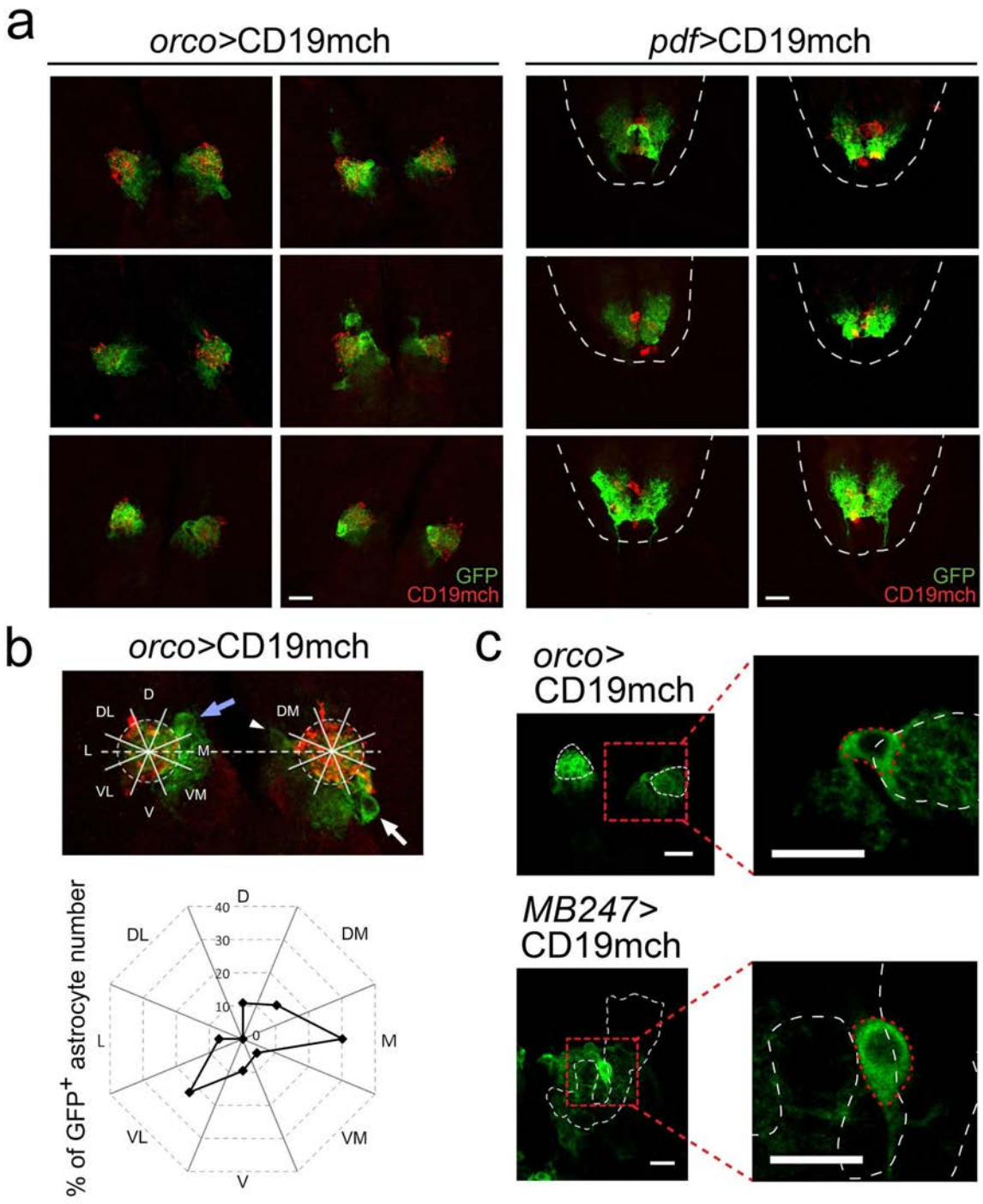
a
orco>CD19mch
pdf>CD19mch
GFP
CD19mch
GFP
CD19mch
b
orco>CD19mch
D
DL
DM
L
M
VL
VM
V
% of GFP+ astrocyte number
40
30
20
10
0
c
orco>
CD19mch
MB247>
CD19mch

FIGURE 3-6. Distribution and characteristics of astrocytes interacting with ligand-expressing neurons.

(a) Examples of the GFP expression patterns induced in astrocytes in the antennal lobe (with ligand expressed in OSNs with orco driver (left two panels)) and ventral nerve cord (with ligand expressed by pdf driver (right two panels)) show highly similar distribution of induced astrocytes and GFP intensity between hemispheres and animals. Maximum projections of confocal microscopy images. (b) The top panel shows an example illustrating how the locations of astrocyte cell bodies were determined in the antennal lobe. The two antennal lobes from each animal were aligned to generate the horizon line. Each antennal lobe was equally divided into 8 sectors: dorsal (D), dorsolateral (DL), lateral (L), ventrolateral (VL), ventral (V), ventromedial (VM), medial (M) and dorsomedial (DM). The sectors where the cell bodies of the GFP+ astrocytes located were recorded. In this example one astrocyte cell body at the left antennal lobe is in the DM sector (blue arrow); two astrocyte cell bodies at the right antennal lobe are in the M (white arrow head) and VL (white arrow) sectors. The bottom panel shows the percentage of the astrocytes located in the different sectors. The GFP+ astrocytes in the antennal lobes are most commonly located in the M (29.8%) and VL (22.6%) sectors, but no astrocytes were located in the DL sector (total 84 astrocytes from 25 larval brains). (c) Size of cell bodies of GFP+ astrocytes in the antennal lobe and mushroom body. Exemplars of two astrocyte

cell bodies (red dotted contours) in the antennal lobe (top, stippled contours) of an orco animal and in the mushroom body (bottom, stippled contour) of a MB247 animal. Left panels show the maximum projection images of each GFP+ astrocyte; right panels show the enlarged single optical sections, where the area size of cell bodies (red dotted contours) were measured. Scale bar= 20 μm.

Chapter 4: Application of TRACT to investigate connectivity between neurons in the Drosophila nervous system

This chapter was composed by Ting-Hao Huang's unpublished data.

ABSTRACT

To test TRACT in tracing neuronal circuits, the original receptor, expressed pan-neuronally, was first used in Drosophila olfactory and visual systems, which have been well-studied in EM levels. When the ligand was expressed in the OSN or specific types of optic lobe neurons, the induction of the reporter gene expression was observed in only a few cases, such as the OSN/LN contacts in the larval antennal lobes and L5/other optic lobe neurons in the adult brains. These results indicate that the original TRACT works inefficiently to monitor synaptic contacts. Furthermore, the original designs of the ligand and the receptor are not targeted at synaptic terminals. Therefore, the induction observed might also reflect non-synaptic contacts. To improve TRACT sensitivity and synaptic specificity, we managed to target the receptor to the postsynaptic sites by fusing SNTG4 with Drosophila Nlg2 intracellular domain. Interestingly, Nlg2 intracellular domain helped the receptor proteins localize to the neurites, and also increased the sensitivity of TRACT. However, when we restricted the ligand expression in single glomerulus, we found ectopic induction of GFP expression in non-ligand positive glomeruli, indicating the receptor is still present outside the synaptic sites. Therefore, we further attempted to target the ligand to presynaptic sites by fusing with presynaptic transmembrane proteins. We found the ligand fused with the synaptic vesicle protein, synaptobrevin, has better presynaptic localization, but is only able to induce GFP expression in a few antennal lobe neurons when it

is expressed in most of OSNs. Therefore, more sophisticated characterizations are still required to improve the efficacy of our system.

INTRODUCTION

There is an urgent need of tools to determine the connectome of the nervous system. Therefore, our main goal is to apply TRACT to monitor synaptic contacts in Drosophila central nervous system. Drosophila melanogaster has many powerful genetic tools available, which will help us to test TRACT *in vivo*. Moreover, the Drosophila nervous system shares many features with the mammalian nervous system, such as information transfer mediated by action potentials and most neurotransmitters and genes involved in synaptic functions are conserved. In addition, the relatively sophisticated brain with different functional compartments and a variety of behaviors make Drosophila an excellent model to study the relationship between neural circuits and behavioral outputs. In this chapter, we focused on the olfactory and visual systems in the *Drosophila* brain (Borst, 2009; Wilson, 2013). These two systems have been extensively studied using approaches such as EM, electrophysiology and GECI, both during development and in the adult, and several cell-type specific drivers are available to uniquely identify each cell type in them. Furthermore, the organization of these circuits is highly stereotyped (i.e., invariant from animal to animal). Together, these properties allow us to evaluate whether the connection revealed by TRACT in these circuits is consistent with previous findings.

The optic lobe is the insect analog of the mammalian visual center, which receive visual information from the photoreceptors R1-R8 in compound eyes, and

consists of four main structures: the lamina, medulla, lobula, and lobula plate (Fig. 5). Due to the stereotypic structures and the presence of different types of neurons, the Drosophila optic lobe is an excellent model to study neural circuit computation. Circuits in the lamina (La) and medulla (Me) of the optic lobe are organized into repeating, stereotyped modules called cartridges (in the La) and columns (in the Me) (Borst, 2009). In the La, there are 12 laminal neurons: 5 of them (L1-L5) are output neurons; 6 are feedback neurons and one intrinsic neuron. Each La cartridge contains the neurites of one L1-L5 neurons and other feedback neurons, T1, C2 and C3, whose cell bodies are located in the Me. Each La cartridge receive visual input from R1-R6 photoreceptors (mostly synapsing with L1, L2 and L3 laminal neurons) sensing the light from the same spot in the visual field (Meinertzhagen and O'Neil, 1991; Rivera-Alba et al., 2011). After processing in the La, the visual information is sent downstream to the Me columns. The Me not only receive color visual input directly from photoreceptors R7 and R8, but also is considered the first relay of motion related activity (Morante and Desplan, 2004; Takemura et al., 2013; Tuthill et al., 2013; Vogt et al., 2016). Each Me column receives the input from a single La cartridge. The color and motion specific information is further conveyed to the higher visual neuropils, lobula, and lobula plate (Morante and Desplan, 2008).

In the Drosophila olfactory system (see review Gerber et al., 2009), the olfactory information is received by the olfactory sensory neurons (OSNs), of which the cell bodies are located in larval dorsal organs or adult antenna and

maxillary pulps. Each OSN expresses one type of olfactory receptors responding to odor compounds and other stimuli, such as pheromone and CO2. The OSNs expressing the same olfactory receptor gene project their axons convergently to specific single glomerulus in each antennal lobe, the insect analog of the mammalian olfactory bulb, on each side, where the OSN axons form synapses with the projection neurons (PNs) and local interneurons (LNs) (Berck et al., 2016; Rybak et al., 2016). While most of PNs are cholinergic excitatory neurons, LNs are either excitatory (cholinergic or glutamatergic) or inhibitory (GABAergic). PN cell bodies are located in three clusters near the anterodorsal, lateral and ventral sides of the antennal lobes. According to the dendritic arborizations of the PNs, there are two types of PNs: uniglomerular PNs (uPNs) and multiglomerular PNs (mPNs). While mPNs, which mostly come from the ventral cluster, innervate multiple glomeruli, uniglomerular PNs with the same cell fates project their dendrites convergently into a specific glomerulus (Lai et al., 2008). Therefore, the olfactory information conveyed from the OSNs is still convergent from OSNs to uPNs in antennal lobes. In contrast, the dendritic arborizations of the axonless LNs branch widely and make synaptic contacts in multiple glomeruli to provide interglomerular communications in antennal lobes (Hong and Wilson, 2015). To convey the olfactory information to higher olfactory brain regions, the mPNs send axons directly to the lateral horn through the middle antennal tract (mACT); the uPNs send axons in the inner antennal tract (iACT) to the calyx of the mushroom bodies and the lateral horn subsequently (Butcher et al., 2012;

Jefferis et al., 2007). Mushroom body has known to be involved in olfactory learning and memory in Drosophila. Recently Caron et al. (2013) showed that a Kenyon cell (KC), the intrinsic neuron in mushroom bodies, might receive divergent olfactory information from random combinations of input from antennal lobe glomeruli. Although the olfactory circuit in Drosophila is stereotypical from the larval stage to adult stage, the complexity of the circuit does increase dramatically according to the number of cells, and the olfactory circuits are disassembled and reassembled during the metamorphosis. For example, the larval Drosophila antennal lobe is composed by around 21 glomeruli, which receives axon projections from around 21 OSNs, and make synapses with 25 PNs and unknown number of LNs. The larval PNs project their axons to around 35 glomeruli in the mushroom body calyx to connect to ~600 KCs. In adult brains, ~1,300 olfactory sensory neurons converge in some 50 glomeruli to both sides, and make synaptic contacts with some 150 projection neurons and 200 local interneurons on each side. In the adult mushroom body calyx, there are hundreds of glomeruli, where adult PNs form synapses with around 2500 KCs.

In this Chapter, we first tested the original TRACT with CD19-SNTG4 in Drosophila antennal lobes and optic lobes. The inductions were able to be observed in the contacts between larval OSNs/LNs and adult L5 lamina neurons/other optical lobe neurons. However, in theory, there are other types of connections that were predicted to be detected, such as the connections between

OSNs and PNs. Therefore, the initial results indicate that TRACT is not efficient at detecting all types of neuron-neuron contacts.

To further improve TRACT to map neuronal circuits by monitoring neuron-neuron contacts in synaptic sites, we generated new synthetic ligands and receptors specifically targeted to synaptic terminals. Our results show that improving the efficiency of transporting the receptor protein to neurites by fusing it with the intracellular domain of Drosophila neuroligin2 increases the sensitivity of the system. However, the induction caused by non-synaptic contacts was still able to be detected. To test whether targeting the ligand to pre-synaptic sites could increase specificity, we generated several new transgenic fly strains with the ligand fused with different pre-synaptic markers, such as synaptobrevin, syntaxin and neurexin1. We found the ligand fused with synaptobrevin have good pre-synaptic localization, and, as the initial test, it can generate moderate induction in the antennal lobes. Hopefully, targeting the ligand to the pre-synaptic terminals will allow TRACT to trace transsynaptic contacts specifically.

RESULTS

Monitoring neuron-neuron interactions in the brain *in vivo*

To test the capability of TRACT to monitor neuron-neuron contacts, we used the GMR64B 07-lexA driver to direct the expression of the ligand within the optic lobe. This driver is both selectively and robustly expressed in the L5 lamina neurons of the adult fly brain (Fig. 4-1). Previous EM data revealed that the L5 neurons make synaptic connections mainly with Mi1, C2, and TM3 neurons in the medulla, and L1 neurons in the lamina (Takemura et al., 2013). In addition, L5 neurons also make contacts with L2, L4, Lai and Lawf neurons in the lamina, and Mi4, Mi5, Dm2, Tm1, Tm6, Tm2, and C3 neurons in the medulla (Takemura et al., 2013). All of the putative interacting partners of L5 neurons have axons and dendrites that ramify in the lamina and medulla, but Tm1, Tm2, Tm3, Tm6 and T2 neurons also have axons that project into the optic lobe lobula (Fig. 4-1a) (Rivera-Alba et al., 2011).

In the absence of ligand (no lexA driver) there was a low level of ligand-independent GFP background expression in some cell bodies in the posterior surface of the medulla (Fig. 4-1b). When the CD19mch ligand (under GMR64B07-lexA driver) was expressed in L5 neurons, we observed robust GFP induction consistent with the distribution of the cells that interact with L5 neurons in the optic lobe as revealed by serial EM (Fig. 4-1c). GFP+ cell bodies localized exclusively to the lamina and medulla of the optic lobe, but GFP+ neurites (axons and

dendrites) also extended into the lobula (Figs. 4-1c, c1, and c2). Interestingly, although all neurons (including the emitter L5 lamina neurons) supposedly express the SNTG4 receptor we observed that CD19mch+ neurons did not express GFP, indicating the lack of *cis*-activation between ligand and receptor in the membrane of individual neurons (Fig. 4-1c1, right, inset).

Synapses between neurons in the antennal lobe occur only in the glomeruli, and electrophysiological studies have confirmed that neurons that extend processes into a common glomerulus (OSNs, LNs and PNs) are synaptically connected (Hong and Wilson, 2014). Thus, this prior information regarding the connectivity of this circuit can be used as a reference to evaluate the cell-cell interactions revealed by TRACT.

To investigate whether TRACT could also be used to investigate neuron-neuron interactions in the olfactory system, we used lexA drivers to express the CD19mch ligand in two populations of antennal lobe neurons: (1) *Orco*-lexA, which expresses in all OSNs in larvae (Lai et al., 2008) (Fig. 4-2), and (b) *GH146*-lexA, which expresses in a large subset of PNs (Lai et al., 2008) (Fig. 4-3), and in some optic lobe cells. We also included a UAS-GFP allele to report SNTG4 activation and combined these alleles by conventional genetic crosses (*ela*-SNTG4; *Orco* or *GH146*>CD19mch; UAS-GFP). When the emitter cells were OSNs, we observed labeling in neurons surrounding the antennal lobe (Fig. 4-2b). Antennal lobe PNs can be identified by the presence of axons arising from their cell bodies that project outside of the antennal lobe towards the mushroom body

and lateral horn (Wilson, 2013). Most antennal lobe LNs can be identified with antibodies that recognize GABA (Hong and Wilson, 2014). We observed that expressing the CD19mch ligand in OSNs (with the *orco*-LexA driver) activated GFP expression both in PNs (Fig. 4-2b), and in GABA-immunopositive antennal lobe LNs (Fig. 4-2c). The induction of GFP in these two cell types is in accord with known connectivity of the system, as both PNs and LNs in the antennal lobe are known targets of OSNs (Fig. 4-2a).

When the emitter cells were PNs (using the GH146 driver to express CD19mch) (Fig. 4-3a), we observed GFP induction in antennal lobe PNs (with axons projecting into the mushroom body) (Figs. 4-3b, d, and e), antennal lobe LNs (immunopositive for GABA) (Fig. 4-3c), and in mushroom body Kenyon cells (Fig. 4-3e), all known targets of PNs (Fig. 4-3a). Because the GH146 driver also labels cells in the optic lobe in addition to the PNs in the antennal lobe, we also observed strong GFP induction in neurons that project their axons towards the central brain (Figs. 4-3d and e). No GFP induction was observed in the antennal lobe or mushroom body in the absence of ligand (no lexA driver, data not shown). As indicated above for the L5 neurons, we observed that the CD19mch positive neurons did not express GFP (Fig. 4-3b), indicating that the CD19mch ligand and the SNTG4 receptor do not interact in *cis* in the membrane of individual neurons.

The components of the TRACT system described so far are likely expressed throughout the entire neuronal surface, without specific targeting. Therefore, it is important to note that in its current version, the induction of GFP expression is

broadly reporting cell-cell interactions, not limited to specific synaptic contacts. In addition, we had also tested TRACT with the ligand expressed in different types of neurons in the adult optic lobe, L1/L2 and T1 neurons and in adult OSNs. However, there was no induction in these cases implying that TRACT is not yet optimized to detect all neuron-neuron contacts and need further modifications.

Synaptic targeting the synthetic ligand and receptor

To synaptically target SNTG4 and CD19, we fused them with synaptic proteins. First, we tested the receptor SNTG4 fused to a postsynaptic marker, neuroligin. Neuroligins are generally thought to play an important role in synaptic formation and maintenance while binding to its ligand, neurexin (Bang and Owczarek, 2013; Knight et al., 2011). The intracellular domain of neuroligin contains a PDZ (postsynaptic density-95 (PSD-95)/Discs large (Dlg)/zona occludens-1) binding motif, which binds to several postsynaptic scaffolding protein with PDZ-domain, e.g. PSD-95 (Irie et al., 1997). Moreover, it has been suggested the neuroligin intracellular domains can also directly bind to other non-PDZ scaffolding protein, such as gephyrin at the inhibitory synapses (Iida et al., 2004; Shipman et al., 2011). Neuroligins and their ligand, Neurexins, have been also used in many cases to target exogenous proteins at synaptic sites, such as GRASP and iBlinc, without detectable effect on the distribution of endogenous synaptic markers (Desbois et al., 2015; Kim et al., 2011; Yamagata and Sanes, 2012). Therefore, we included 260 amino acid residues of the intracellular domain

of Drosophila neuroligin 2 (dnlg2) between TMD and Gal4 of STNG4, SNT::dNlg2ICD::G4, and generated a new transgenic strain, elav-SNT::dNlg2ICD::G4.

While crossing elav-SNT::dNlg2ICD::G4 with 5xUAS-mCD8::GFP alone, surprisingly, we noticed strong ligand-independent background of GFP in mushroom bodies, optic lobes and part of antennal mechanosensory and motor center (AMMC), and weak background GFP in larval neuroblasts (Fig. 4-4, star markers). To further test the inducibility of this new synthetic receptor, CD19mch was expressed in OSNs driven by Orco LexA driver. Because the ligand-independent background doesn't appear near the antennal lobes, we were able to observe strong GFP induction in several of the antennal lobe neurons both in the larvae (Fig. 4-4a and b) and in the adult (Fig. 4-4c and d). This indicate TRACT with the new receptor, SNT::dNlg2ICD::G4, might have higher sensitivity. However, the GFP+ neurons of the antennal lobe did not have axons, which is consistent with the arborization of the axonless LNs. The counterstaining results show that they are all negative for the PN marker, choline acetyltransferase (ChAT), but some of them are positive for the LN marker, GABA, which confirms they are the LNs (Fig. 4-4b and d). Therefore, TRACT in this case only labeled the antennal lobe LNs, but not the PNs.

Why is there no induction in PNs of antennal lobes? Why is there strong background in the optic lobe and mushroom body? One possibility is that the activity of elav promoter is not homogenous across different neuron types

although it is general considered as a pan-neuronal promoter. For example, perhaps the expression levels of SNT::dNlg2ICD::G4 under elav promoter might be low in the PNs and high in the mushroom bodies. To test whether the results are due to the promoter, we generated several new transgenic strains carrying different variants of the receptor under the control of nSyb (neural synaptobrevin) promoter, which is also considered as a pan-neuronal promoter in postmitotic neurons. Those variants include STNG4, SNT::dNlg2ICD::G4 and $SNT_{CD4/dN}$::dNlg2ICD::G4 (the comparable version of $SNT_{CD4/hN1}$G4 tagged with V5 epitope at the C-terminals behind Gal4 to facilitate immunostaining. In addition, to enable direct comparisons between strains carrying different receptors, the new transgenic flies were generated by site-specific insertion at the attP40 site to avoid insertion position effects. First, to confirm the effect of the dNlg2ICD on the subcellular localization of the receptor, we performed immunostaining against V5 tag to compared the expression patterns of $STNG4^{V5}$ and SNT::dNlg2ICD::$G4^{V5}$. While $STNG4^{V5}$ preferentially accumulates in cell bodies and is largely absent in the neuropil, most of SNT::dNlg2ICD::$G4^{V5}$ is transported to the neurites (Fig. 4-5). In the Drosophila neuromuscular junction, dNlg2 is localized in both pre- and post-synaptic sites (Sun et al., 2011). Thus, it is possible that SNT::dNlg2ICD::G4 is also present in both the pre- and post-synaptic sites. This possibility is, however, difficult to disentangle. Nonetheless, flies carrying both one of the receptor variant and the reporter 5xUAS-CD4::tdGFP, show no detectable ligand-independent background in either the

larval (data not shown) or the adult brain (Fig. 4-6a) .

To further test the inducibility of different receptors, STNG4^{V5}, SNT::dNlg2ICD::G4^{V5} and SNT$_{CD4/dN}$::dNlg2ICD::G4^{V5} were individually combined with the ligand, orco>CD19mch, and the reporter, 5xUAS-CD4::tdGFP. STNG4^{V5} nor SNT$_{CD4/dN}$::dNlg2ICD::G4^{V5} showed any induction in adult or larval stages (data not shown). SNT::dNlg2ICD::G4^{V5}, on the other hand, showed induction of the reporter in a few LNs in the larval stage (data not shown). Interestingly, in the adult brain, we observed strong induction in PNs and LNs in the antennal lobes. The PN cell bodies are located at the dorsal and lateral regions near the antennal lobes (arrows in Fig. 4-6d left panels), and the majority of the GFP+ PN axons are running through mACT (arrowhead in Fig. 4-6c bottom panels), and small portion of them through iACT (arrow in Fig. 4-6c bottom panels). The results of the counterstaining with ChAT confirmed that some of the GFP+ are ChAT positive PNs (arrows in Fig. 4-6d top panels), and some of them at the lateral region might be the ChAT negative LNs (arrows in Fig. 4-6d bottom panels). Unexpectedly, control adult brains lacking the LexA driver also show strong GFP expression in AMMC and in few neurites in the antennal lobes (Fig. 4-6b). This GFP signal, which has not been observed in the nSyb-SNT::dNlg2ICD::G4^{V5}/5xUAS-CD4::tdGFP brain, might be due to the basal expression of CD19 even without LexA driver.

To investigate whether the response mediated by the receptor SNT::dNlg2ICD::G4^{V5} is specific enough to monitor synaptic contacts , we further

tested the induction in a single antennal lobe glomerulus. At this level the synaptic contacts between OSNs and PNs is restricted to the glomeruli. Therefore, if TRACT with SNT::dNlg2ICD::G4^{V5} enables to specifically monitor the synaptic contacts, in theory, the induction would only occur in the ligand positive glomerulus. To restrict the CD19 expression to groups of OSNs innervating only a few glomeruli, we have screened the database of LexA driver library from HHMI Janelia Farm, and found several candidates having LexA activity limited to 1-4 glomeruli (Table 4-1). Furthermore, we also generated a strain in which SNT::dNlg2ICD::G4^{V5} is driven by GH146 enhancer, GH146-SNT::dNlg2ICD::G4^{V5}, that is restricted to PNs. The results from different combinations of ligand and receptor variants were, however, very inconsistent. In the brain of flies where the ligand is controlled by Ir84a and GMR13C03-LexA drivers, there was no or extremely weak ligand-induced reporter expression (data not shown). In the combinations with other drivers, whether CD19 is expressed or not, DA1 glomerulus, which has low level of ligand-independent background, was always positive (Fig. 4-7 star marks in the left panels). When CD19 was driven by GMR28H10 or GMR17H02-LexA, reporter induction was observed in one mPN (Fig. 4-7c and f). Moreover, the induction pattern in the samples with GMR19F06-LexA was excluded from the CD19 positive VA1lm glomerulus. In summary, even though the ICD of dNlg2 appears to improve the trafficing of the receptor to to neurites and away from the cell body, it was not sufficient to specifically target the receptor just to the synaptic sites.

To further pursue the goal of monitoring synaptic-specific contacts, we also tried to target the ligand (CD19) to pre-synaptic sites. To this purpose, we fused CD19 with several different pre-synaptic markers, including synaptobrevin (nSyb), syntaxin (Syx) and Neurexin1 (Nrx1). Synaptobrevin and syntaxin are both type II transmembrane proteins, and play important roles in synaptic vesicle ducking and fusion at the active zone of pre-synapses (Jahn and Fasshauer, 2012; Sudhof, 2013). For these two markers, since their c-terminals is at the extracellular site, both of them were fused by the extracellular domain of CD19 at their C-terminals. For Nrx1, the type I transmembrane ligand protein of neuroligin at the synaptic sites, we replaced its extracellular part with the extracellular domain of CD19. Comparing all these three new ligands with the original CD19mch when driven by orco driver, we notice that, in nSyb::CD19 antennal lobes, the expression levels of the ligand proteins in the glomeruli were more intense than the regions between each glomerulus, which shows clear glomerular boundaries in the antennal lobes (Fig. 4-8b1 and b1'), and might be due to the lower expression in the OSN axon processes (arrow and arrowhead in Fig. 4-8b1') than axon terminals. In contrast, in CD19mch, Syx::CD19 and CD19::Nrx1, the ligand expression levels in the axons are as strong as the levels in the antennal lobe glomeruli, for example, the axon fascicles of OSNs from maxillary palps (arrows in Fig. 4-8 panels 1') and the antennal commissure, which the OSN axons cross to reach the contralateral antennal lobe (arrowheads in Fig. 4-8 panels 1'). These observations indicate that nSyb:CD19 might have better presynaptic localization. After testing all these

ligands driven by orco driver with nSyb-SNT::dNlg2ICD::G4 and 5xUAS-CD4::tdGFP, we found Syx::CD19 and CD19::Nrx1 only triggered weak inductions in the antennal lobe LNs. In contrast, nSyb::CD19 in OSNs induced strong GFP expression in several mPNs and perhaps LNs, but these are still relatively fewer than the neurons get inductions by CD19mch+ OSNs.

DISCUSSION

In the original design, despite reliable ligand-mediated induction in larval antennal lobes and adult optic lobes, neither the ligand, CD19mch, nor the receptor, SNTG4, was targeted to synaptic sites. This lack of proper targeting limits the use of TRACT to map synaptic connections. More specifically, TRACT does not label all the known synaptic partners of the emitter neurons. For example, in flies expressing the ligand in most larval OSNs (with the orco driver), we expected ~21 PNs of the antennal lobe to be labeled as postsynaptic partners; instead, we observe only one PN labeled *(Fig. 4-2b)*. In addition, only L5 lamina neurons expressing CD19 were able to trigger the induction of GFP expression in the adult optic lobes, even though CD19 expression levels in L1/L2 and T1 were comparable. Finally, TRACT as described so far can only be used to broadly report cell-cell interactions, not specific to synaptic contacts.

These limitations indicate that to enable the use of this strategy for tracing brain circuits it is necessary to localize the receptor and/or ligand specifically into presynaptic and postsynaptic sites (Sheng, 2001; Sudhof, 2013). Targeting the ligand and receptor selectively into synaptic sites could have two important benefits. First, it could increase the effective concentration of the signaling components in the synaptic membrane potentially leading to stronger signaling between synaptically connected neurons. Second, it could also minimize the potential for activation of the reporter between neurons whose membranes are

close to each other (for instance, between fasciculating axons), but are not connected by synapses.

Therefore, we have modified TRACT by fusing the ligand and the receptor to known synaptic markers. For the receptor, by inserting the dNlg2 ICD between notch TMD and Gal4 facilitate its transport to the neurites, and increase the sensitivity of the system. However, the reason for the improvement is still unknown. One possibility is that the more efficient trafficking of SNT::dNlg2ICD::G4 to neurites can increase surface expression of the receptor. Such an increase in surface expression could result in a higher number of ligand-receptor interactions and generate stronger signaling. Alternatively, more receptor proteins on the neuronal surface could lead to increased total amount of internalized proteins and ligand-independent cleavage of GAL4 fragments. A higher basal level of freed GAL4 fragments could take it closer to the threshold for the reporter to induce detectable GFP expression, and only a small amount of ligand-mediated GAL4 cleavage is required to monitor the contact events. This possibility could also explain why, with the same elav promoter, SNT::dNlg2ICD::G4 has stronger ligand-independent background in the mushroom bodies and optic lobes than the original SNTG4 does, which is similar to S(LZ)NTGV receptor mentioned previously in Chapter I. To test this hypothesis, my colleague has introduced the temperature-sensitive shibire mutant, shi^{ts}, into the KCs of the elav-SNT::dNlg2ICD::G4/5xUAS-mCD8::GFP flies to attempt to

block the endocytosis in the KCs. He found, that after incubating the flies into non-permissive temperature, the ligand-independent background of GFP expression level decrease dramatically (Donghyung Lee unpublished data). This finding indicates that the stronger ligand-independent background in SNT::dNlg2ICD::G4 compared to SNTG4 might result from the better surface expression in an endocytosis-dependent manner. However, we still have to keep in mind the possibility that by including the dNlg2 ICD makes this receptor is more susceptible to be cleaved by metalloprotease in S2 site.

One thing that needs careful consideration for SNT::dNlg2ICD::G4 are the potential effects on synaptic function from the overexpression of dNlg2ICD. For many synaptic markers, especially neuroligin, it was shown that overexpression can cause significant changes in synaptic functions and animal behavior (Hoy et al., 2013). Therefore, although so far the flies carrying any variant of the SNT::dNlg2ICD::G4 are generally healthy, and there is no aberrant behaviors shown in any of them, care should be still taken to confirm the synaptic properties in those flies are normal. In the current version of SNT::dNlg2ICD::G4, it includes full length of dNlg2ICD. It would be interesting to test different fragments of dNlg2ICD to find the minimal domain required to guide the receptor to neurites. Such measure could help to reduce the possible side effects from other domains of dNlg2ICD.

According to the results from single glomerular experiments,

SNT::dNlg2ICD::G4 does not appear to be properly targeted to synaptic sites. Therefore, in this case, one way to get TRACT to work in a synaptic-specific manner is to localize the ligand at the pre-synaptic sites. Targeting the ligand to pre-synaptic sites is relatively simpler compared to the receptor. Here we fused CD19 ECD with different pre-synaptic markers, nSyb, Syx and Nrx1. In general, all these synaptic targeted ligands provided weaker activation compared to the original CD19mch. However, only nSyb-CD19, which seems to have better synaptic localization, triggers the induction in a few PNs. nSyb is normally localized on synaptic vesicles. Only when synaptic vesicles dock and fuse to presynaptic plasma membranes at the active zone, nSyb will be transiently present on the plasma membrane surface. Soon after fusion, the ligand will be recycled by endocytosis back to the synaptic vesicles. This feature of nSyb has been utilized on the activity-dependent GRASP, which the reconstitution of split GFP only happens when the neuron is actively firing (Macpherson et al., 2015). Therefore, we hypothesize that at the normal status only low amount of nSyb-CD19 present at the pre-synaptic membrane, and only the labeled PNs, which are mPNs, have enough contacts with OSNs due to the broad arborizations all over the antennal lobes to reach the threshold of the sensitivity of TRACT. In contrast, because the contacts between the uPNs and OSNs are restricted in single glomerulus, although they make strong connection, the total area of the contacts per uPN might be still lower than the one per mPN. In the future, I’m planning to artificially boost the neuronal activity of OSNs by odors, dTRPA1 or

channelrhodopsin to investigate whether we can label more neurons in different types.

In summary, the preliminary results shown in this Chapter provide promising evidence that the TRACT is capable to trace neuron-neuron contacts. Importantly, we have shown that in cells that supposedly express both the ligand and the receptor on the same membrane in *cis* show no activation of the reporter (Fig. 4-1 and 4-2). This observation indicates that in situations where a cell expresses both the receptor and the ligand, the activation of the reporter will indicate a trans-activation, between interacting neighboring cells. We anticipate in the future with further optimization TRACT might enable to dissect the neural circuits not only in Drosophila but also in other species.

MATERIALS AND METHODS

Transgenic flies.

- elav-SNT::dNlg2ICD::G4: The SNT::dNlg2ICD::G4 constructs were generated by ligating three PCR fragments of SNT, dNlg2 ICD and Gal4. The SNT and Gal4esn fragment was amplified by PCR from FU-SdNTG4-W, and the dNlg2 ICD was from Drosophila EST RH63339. These three fragments were subcloned into the vector, which elav-SNTG4 was digested by NotI and KpnI, by Gibson Assembly® Cloning Kit. Transgenic elav-SNT::dNlg2ICD::G4 flies were produced by standard P-element integration, and were screened by GAL4 immunostaining, and the lines with the highest expression level of SNTG4 were chosen for the future experiments.

- GH146-SNT::dNlg2ICD::G4^{V5}: The SNT::dNlg2ICD::G4^{V5} construct was generated by amplifying SNT::dNlg2ICD::G4 from elav-SNT::dNlg2ICD::G4 with the reverse primer having V5 tag sequence, and subcloning into pCasper-GH146QF digested by XbaI. Transgenic GH146-SNT::dNlg2ICD::G4^{V5} flies were produced by standard P-element integration, and were screened by V5 immunostaining, and the lines with the highest expression level of SNTG4 were chosen for the future experiments.

- nSyb-SNT::dNlg2ICD::G4^{V5} and nSyb-SNTG4^{V5}: The SNT::dNlg2ICD::G4^{V5} fragment was directly amplifyied from GH146-SNT::dNlg2ICD::G4^{V5}, and was

subcloned into pattNSYBBN digested by EcoRI and AatII. The SNTG4^{V5} construct was generated by amplifying from FU-SdNTG4-W with the reverse primer having V5 tag sequence, and the SNTG4^{V5} PCR fragment was subcloned into pattNSYBBN digested by EcoRI and AatII. Transgenic nSyb-SNT::dNlg2ICD::G4^{V5} and nSyb-SNTG4^{V5} flies were produced by attb site-specific integration in attP40 site.

- LexAop-Syx::CD19 and LexAop-nSyb::CD19: The synthetic DNA fragments of Syx1A, nSyb and CD19 with OLLAS tag were generated by gBlocks® Gene Fragments. Syx1A or nSyb were, then, ligated with CD19::OLLAS and pJFRC19 digested by XhoI and XbaI by Gibson Assembly kit. Transgenic LexAop-Syx::CD19 and LexAop-nSyb::CD19 flies were produced by attb site-specific integration in attP2 site.

- LexAop-CD19::Nrx1: The synthetic DNA fragments of CD19 extracellular domain and Nrx1 transmembrane and intracellular domains with OLLAS tag were generated by gBlocks® Gene Fragments. These two fragments were, then, ligated with pJFRC19 digested by XhoI and XbaI by Gibson Assembly kit. Transgenic LexAop-CD19::Nrx1 flies were produced by attb site-specific integration in attP2.

- Janelia LexA driver lines: GMR13C03, GMR13F03, GMR17H02, GMR19F06, GMR28H10, GMR46B01 and GMR64B07-LexA are requested from Bloomington fly stocks.

Genotypes of flies analyzed in the figures:

Fig. 4-1b: 5XUAS-CD4::tdGFP/elav-SNTG4; LexAop-CD19mch/TM3

Fig. 4-1c, c1 and c2: 5XUAS-CD4::tdGFP/elav-SNTG4; LexAop-CD19mch/GMR64B07-LexA

Fig. 4-2: 5XUAS-CD4::tdGFP/elav-SNTG4; LexAop-CD19mch/orco-LexA::VP16

Fig. 4-3b and c: 5XUAS-CD4::tdGFP/GH146-LexA::GAD, elav-SNTG4; LexAop-CD19mch/TM3

Fig. 4-3d and e: GH146-LexA::GAD, 5XUAS-CD4::tdGFP/GH146-LexA::GAD, elav-SNTG4; LexAop-CD19mch/LexAop-CD19mch

Fig. 4-4a, b, c and d: 5XUAS-mCD8::GFP/elav-SNT::dNlg2ICD::G4; orco-LexA::VP16/LexAop-CD19mch

Fig. 4-4a’ and c’: 5XUAS-mCD8::GFP/elav-SNT::dNlg2ICD::G4; LexAop-CD19mch/TM3

Fig 4-5 (left panels): nSyb-SNTG4^{V5}/CyO; +/+

Fig 4-5 (right panels): nSyb-SNT::dNlg2ICD::G4^{V5}/CyO; +/+

Fig 4-6a: nSyb-SNT::dNlg2ICD::G4^{V5}/5XUAS-CD4::tdGFP; TM3/+

Fig 4-6b and d (left panels): nSyb-SNT::dNlg2ICD::G4^{V5}/5XUAS-CD4::tdGFP; LexAop-CD19mch/TM3

Fig 4-6c, d (right panels) and 4-8a: nSyb-SNT::dNlg2ICD::G4^{V5}/5XUAS-CD4::tdGFP; LexAop-CD19mch/orco-LexA::VP16

Fig 4-7a: 5XUAS-CD4::tdGFP/CyO; LexAop-CD19mch/GH146-SNT::dNlg2ICD::G4^{V5}

Fig 4-7b: 5XUAS-CD4::tdGFP/CyO; orco-LexA::VP16, LexAop-CD19mch/GH146-SNT::dNlg2ICD::G4^{V5}

Fig 4-7c: 5XUAS-CD4::tdGFP/GMR17H02-LexA; LexAop-CD19mch/GH146-SNT::dNlg2ICD::G4^{V5}

Fig 4-7d: 5XUAS-CD4::tdGFP/GMR13F03-LexA; LexAop-CD19mch/GH146-SNT::dNlg2ICD::G4^{V5}

Fig 4-7e: 5XUAS-CD4::tdGFP/GMR19F06-LexA; LexAop-CD19mch/GH146-SNT::dNlg2ICD::G4^{V5}

Fig 4-7f: 5XUAS-CD4::tdGFP/GMR28H10-LexA; LexAop-CD19mch/GH146-SNT::dNlg2ICD::G4^{V5}

Fig 4-8b: nSyb-SNT::dNlg2ICD::G4^{V5}/5XUAS-CD4::tdGFP; LexAop-nSyb::CD19/orco-LexA::VP16

Fig 4-8c: nSyb-SNT::dNlg2ICD::G4^{V5}/5XUAS-CD4::tdGFP; LexAop-nSyx::CD19/orco-LexA::VP16

Fig 4-8d: nSyb-SNT::dNlg2ICD::G4^{V5}/5XUAS-CD4::tdGFP; LexAop-

CD19::Nrx1/orco-LexA::VP16

All the crosses were maintained at room temperature, and were repeated at least 3 times.

Immunostaining and microscopy of fly brain. The brains of the wandering larvae or adult drosophila were dissected in 1x PBS under a dissection microscope. Brains were fixed by immersing them in a 4% paraformaldehyde solution in PBS for 15 minutes at room temperature. Brains were washed in PBS three times for 10 mins each, followed by permeabilization with PBS/0.5% triton X-100 (PBST) for 30 mins and blocking with 5% serum in PBST for 30 mins. The brain samples were stained with antibodies against GFP (rabbit polyclonal from Millipore, AB3080P, diluted at 1:1,500), mcherry (rat monoclonal, 5F8, from Chromotek diluted at 1:1,000), Brp (mouse monoclonal, nc82, from DSHB diluted at 1:50), ChAT (mouse monoclone 4B1, from DSHB diluted at 1:200), V5 (mouse monoclone from invitrogen, R960-25, diluted at 1:300; rabbit polyclone from GenScript, A00623-100, diluted at 1:500), OLLAS (rat monoclone L2 from Novus, NBP106713, diluted at 1:300) diluted in 5% serum/PBST. Brains were Incubated with 1ry antibodies overnight at 4C, washed 3 times in PBST, incubated with 2ry (goat secondary antibodies, Life Technologies, 1:500, except for rabbit anti-GFP AB3080P, which 1:750 was used) for 1.5 hours at room temperature, washed in PBST and mounted on glass slides with a clearing solution (Slowfade Gold antifade reagent, invitrogen).

Stained brains were imaged with confocal microscopes (Olympus Fluoview 300 or Zeiss 710) under a 40X or 60X objective. In a typical experiment, we imaged 150 sections with an optical thickness of 0.3-0.5 μm from dorsal or ventral sides. Confocal stacks were processed with Fiji to obtain maximal projections.

FIGURES

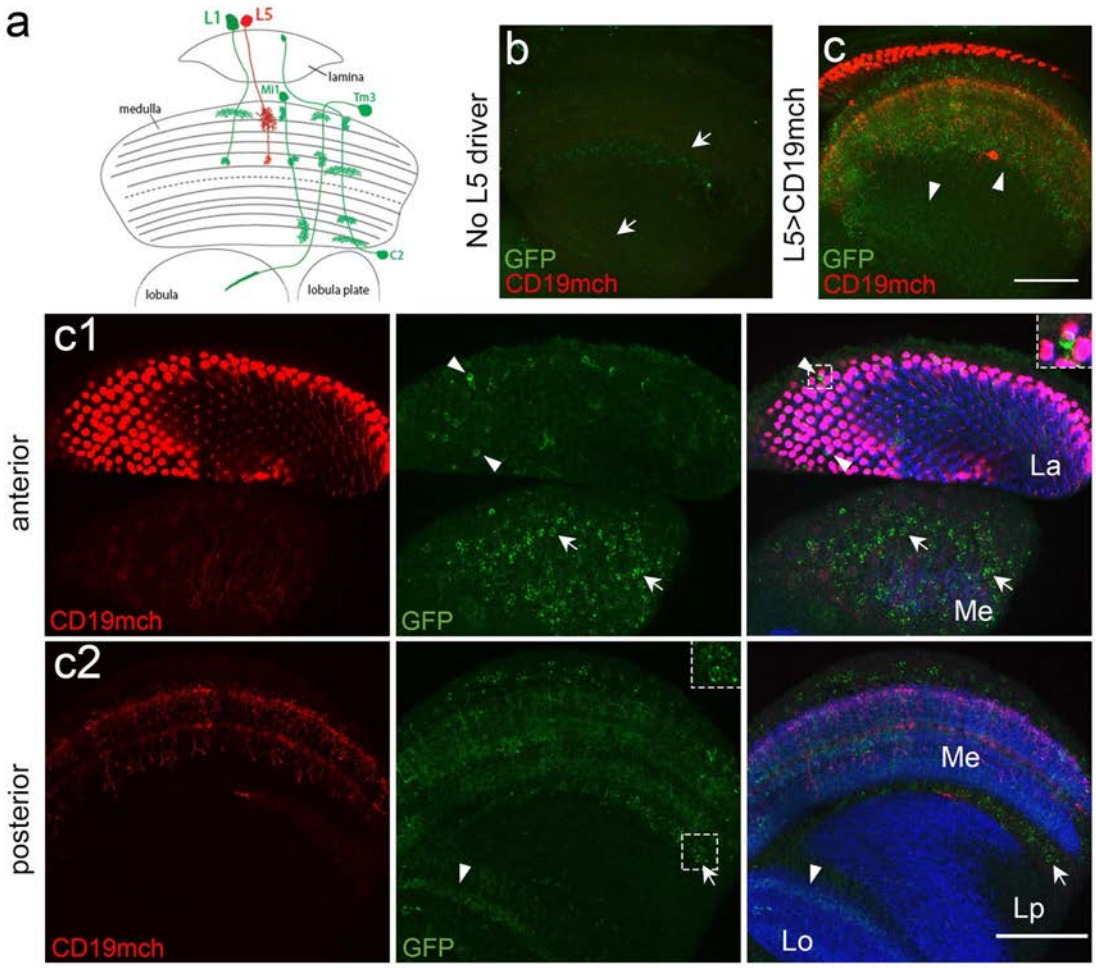
a
L1
L5
lamina
Mi1
Tm3
medulla
C2
lobula
lobula plate
b
No L5 driver
GFP
CD19mch
c
L5>CD19mch
GFP
CD19mch
c1
anterior
CD19mch
GFP
La
Me
c2
posterior
CD19mch
GFP
Me
Lo
Lp

FIGURE 4-1. Monitoring neuron-neuron contacts in the optic lobe

(a) Diagram of the anatomy of the optic lobe of the Drosophila brain indicating the distribution of neurites of the L5 neurons (red), and their preferred synaptic partners, L1, Mi1, C2 and Tm3 neurons (green). (b and c) Maximum projection images from posterior view of optic lobe without (b) and with the GMR64B07-LexA driver (c). (b) The control optic lobe had weak ligand-independent GFP expression, (arrows) in the deeper layers of the optic lobe. (c) Induction of GFP expression in the lamina and medulla neurons of the optic lobe upon expression of the CD19mch ligand in L5 neurons with the GMR64B07>lexA driver. Emitter cells (expressing CD19mch) are labeled in red. Receiver cells (expressing GFP) are labeled in green. (c1 and c2) GFP expression induced by the GMR64B07>CD19mch in the optic lobe shown in (c) from an anterior (c1) and posterior (c2) view. left: distribution of CD19mch+ emitter cells; middle: distribution of GFP+ neurons; right: merged imaged of CD19mch (red), GFP (green) and neuropil (blue). Neuropil is revealed by the antibody Nc82, which labels the presynaptic active zone protein bruchpilot and reveals sites of synaptic contacts. Maximum projection of 10 confocal optical sections. (c1) GFP expression was induced in a few neurons with cell bodies located at the lamina (La) (arrowheads), and a much greater number of neurons in the medulla (arrows). Inset in the merged image (top right corner) shows a high magnification view of the lamina indicating that the GFP signals of the lamina neurons did not

colocalize with CD19mch, indicating there is no *cis*-activation in the system. (c2) GFP+ neurons (arrow in the merged image) in the medulla close to the lobula plate (Lp). Inset in the middle (top right corner) shows a high magnification view of the GFP+ neuronal cell bodies in the deeper layers of the medulla (arrow). GFP+ neurites (arrowhead) projecting into the lobula (Lo) were also observed. La=lamina; Me=medulla; Lo= lobula; Lp=lobula plate. Scale Bar: 50 μm.

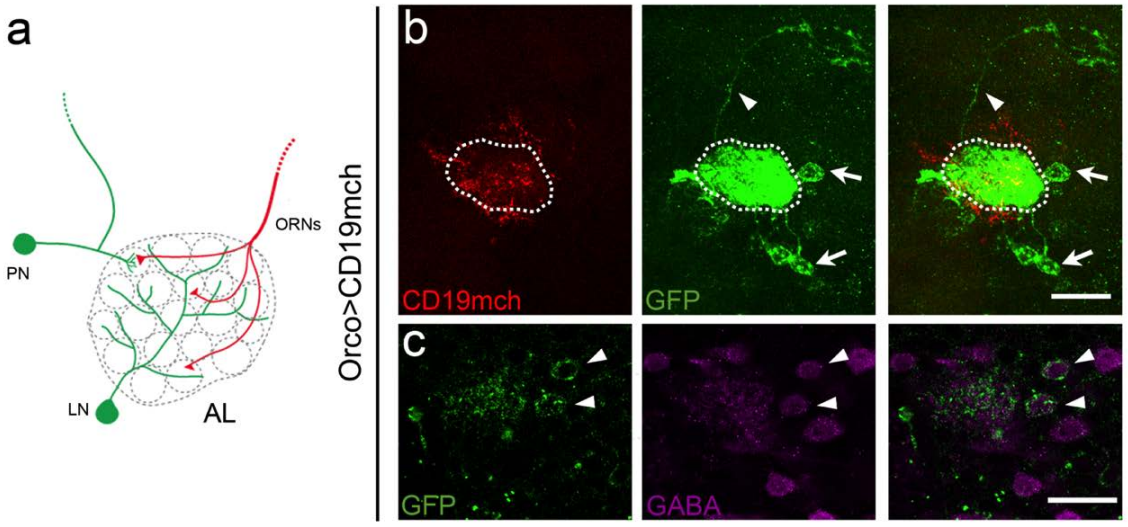
a
ORNs
PN
LN
AL
Orco>CD19mch
b
CD19mch
GFP
c
GFP
GABA

FIGURE 4-2. Monitoring neurons-neuron contacts between the olfactory receptor neurons and the antennal lobe

(a) Diagram of the anatomy of the antennal lobe (AL) in the larval *Drosophila* brain. Axons from olfactory receptor neurons (OSNs)=red; Projections neurons (PN) and local interneurons (LN) =green. (b) Induction of GFP expression in neurons surrounding the antennal lobe (stippled circle) when the ligand (CD19::mch) was driven by orco-LexA::VP16. left: distribution of CD19mch+ emitter axons; middle: distribution of GFP+ neurons; right: merged imaged of CD19mch (red), GFP (green) . An axon (arrowhead) from a GFP+ PN projecting towards the mushroom body. Cell bodies of GFP+ neurons (arrows) surrounding the antennal lobe (stippled circle). (c) GABA immunostaining (magenta) confirmed that some of the GFP+ neurons (green) induced by orco-LexA::VP16 are LNs. Scale bar= 20 μm.

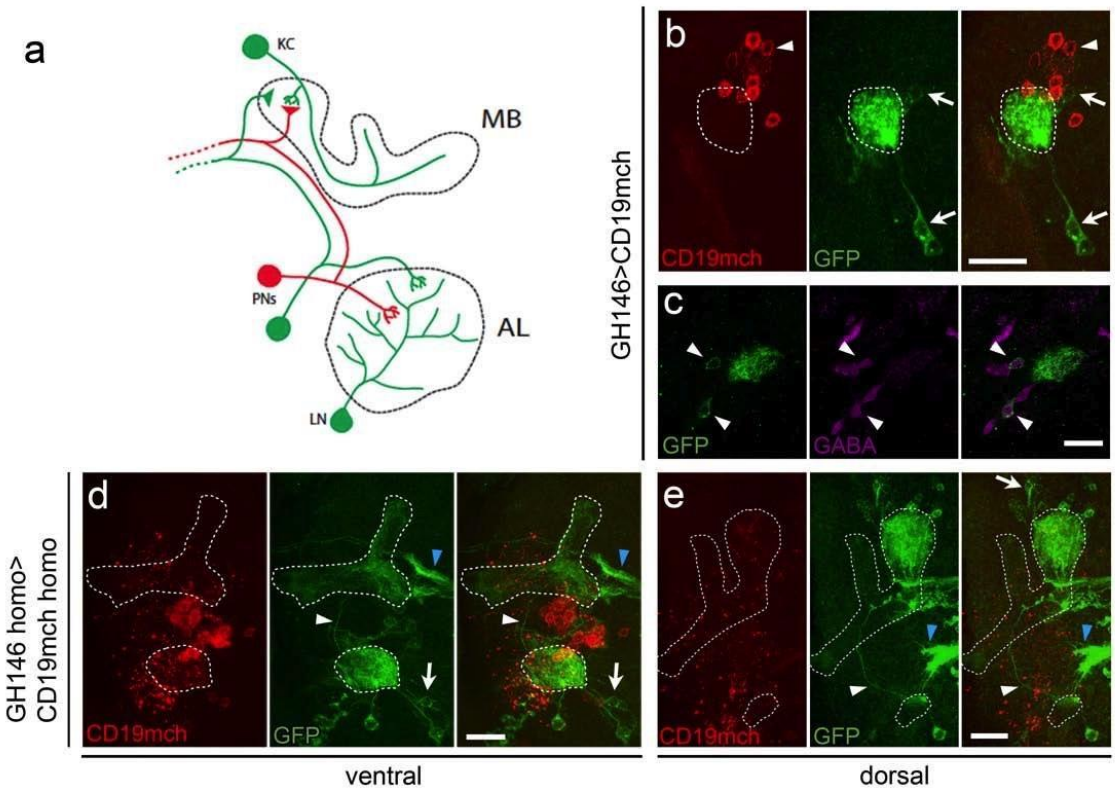
a
KC
MB
PNs
AL
LN
GH146>CD19mch
b
CD19mch
GFP
c
GFP
GABA
GH146 homo>
CD19mch homo
d
CD19mch
GFP
e
CD19mch
GFP
ventral
dorsal

FIGURE 4-3. Monitoring neurons-neuron contacts between the antennal lobe and the mushroom body

(a) Diagram of the anatomy of the olfactory system in the larval *Drosophila* brain. AL= antennal lobe; MB=mushroom body. PNs= projection neurons; LN=local interneurons; KC=Kenyon cells. Emitter PNs (red); receiver PNs, LNs and KCs (green). (b) Expression of the ligand into PNs (GH146-lexA::GAD) induced GFP expression in LNs. mcherry+ PNs (arrowheads) surround the antennal lobe (circle). The antennal lobe is occupied by the GFP+ branching neurites from the GFP+ neurons (arrows). (c) GABA immunostaining (purple) confirmed that some of the GFP+ neurons (arrowheads) induced by the ligand are LNs. (d, e) Connections between the antennal lobe to the mushroom body. To increase the sensitivity of the system to reveal these connections, both the lexA driver and the CD19mch were used in this case in a double homozygote stock. left: distribution of CD19mch+ emitter cells and their neurites; middle: distribution of GFP+ neurons and their neurites; right: merged imaged of CD19mch (red) and GFP (green). (d) Several cell bodies of GFP+ neurons (arrows) surround the antennal lobe (stippled circle). An axon (arrowhead) from a PN surrounding the antennal lobe projects into and branches in the mushroom body (contours outlined by stippled line). (e) GFP+ KC (arrow) surrounding the mushroom body (outlined with a line). Axon (arrowhead) from a PN surrounding the antennal lobe (oval) projects into and branches in the mushroom body. Axons originating from the optic lobe

are indicated by a blue arrow in d and e. Scale bar= 20 μm

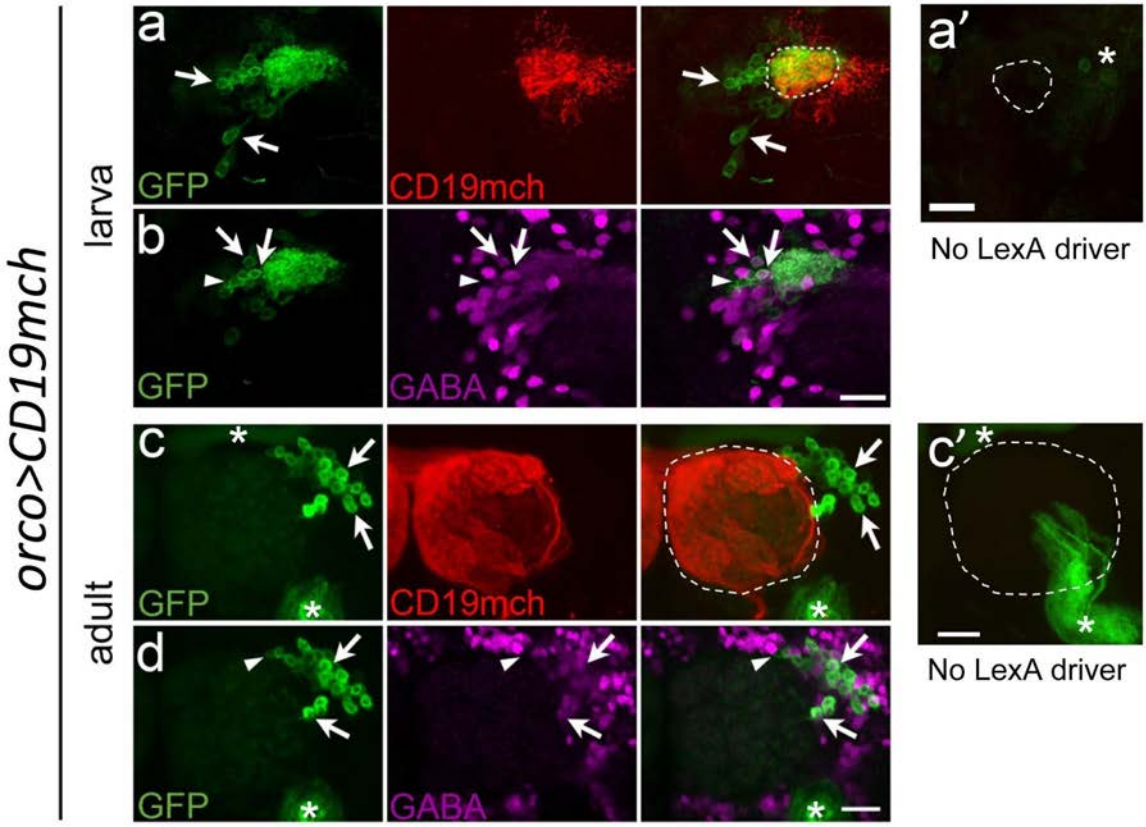
orco>CD19mch
larva
adult
a
GFP
CD19mch
b
GFP
GABA
c
GFP
CD19mch
d
GFP
GABA
a'
No LexA driver
c'
No LexA driver

FIGURE 4-4. Monitoring neurons-neuron contacts between the olfactory receptor neurons and the antennal lobe neurons by SNT::dNlg2ICD::G4 (elav promoter).

SNT::dNlg2ICD::G4 driven by elav promoter was tested to detect the neuron-neuron contacts in the larval (a, b) and the adult (c, d) antennal lobes. In (a) and (c), induction of mCD8::GFP expression in neurons (arrows) surrounding the antennal lobe (stippled circle) when the ligand (CD19::mch) was driven by orco driver in OSNs. Left: distribution of mCD8::GFP+ neurons; middle: distribution of CD19mch+ axons of OSNs; right: merged images of CD19mch (red), mCD8::GFP (green). (a') and (c') show no induction in neurons near the antennal lobes (stippled circle) of the control samples without orco driver. The stars mark the ligand-independent background in the larval optic lobe (a') and the mushroom bodies and the axons of Johnson's organ neurons (c and c'). In (b) and (d), the images of a single optical section from (a) and (c) show GABA immunostaining (magenta) to confirm that some of the mCD8::GFP+ neurons (green) induced by CD19mch+ OSNs are GABAergic LNs (arrows). The arrowheads indicate the GABA negative neurons. left: distribution of mCD8::GFP+ neurons; middle: GABA immunostaining; right: merged images of GABA (magenta), mCD8::GFP (green). Scale bar= 20 μm.

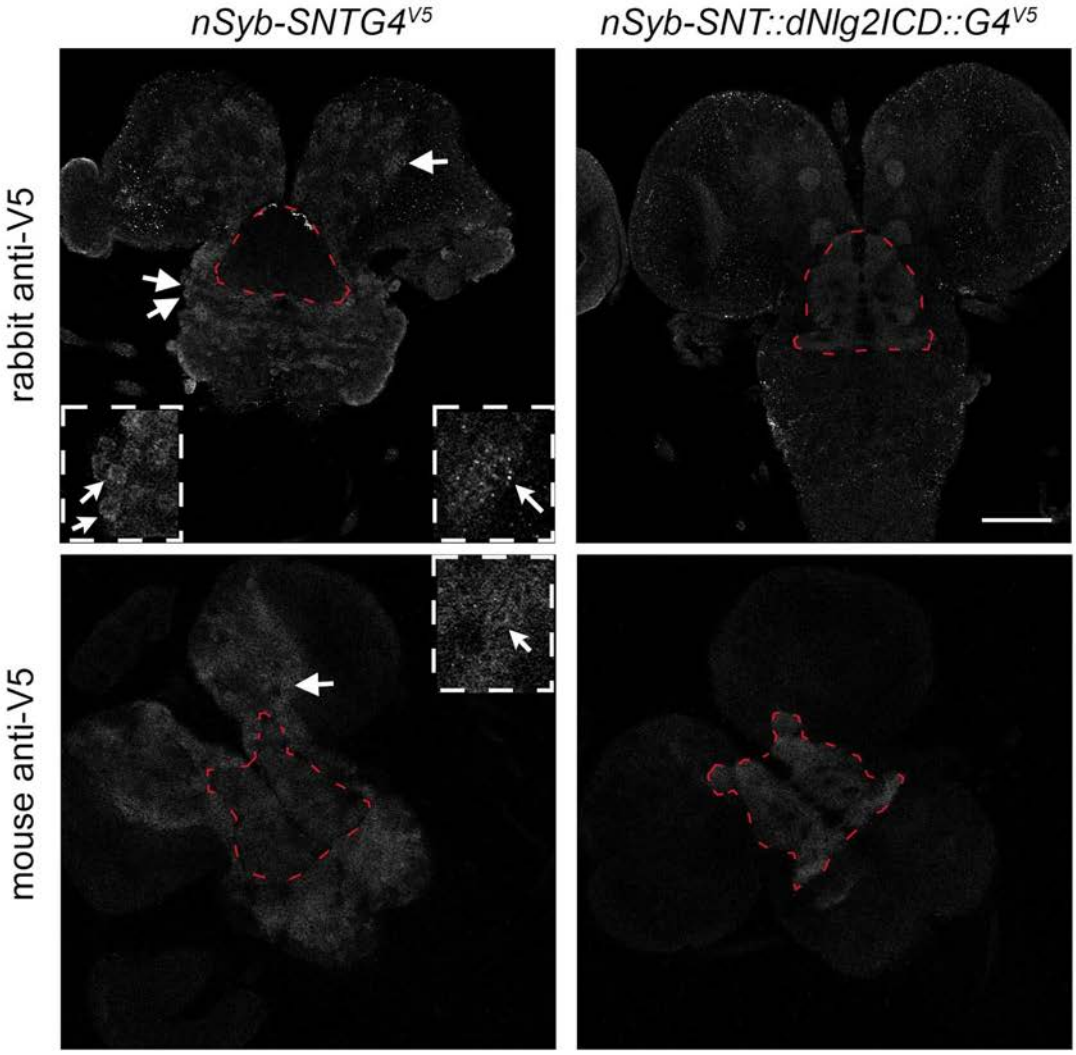
nSyb-SNTG4V5
nSyb-SNT::dNlg2ICD::G4V5
rabbit anti-V5
mouse anti-V5

FIGURE 4-5. The distribution of the receptor expression in Drosophila CNS. The receptors driven by nSyb promoter are tagged by V5 epitope tag (left: nSyb-SNTG4^{V5}; right: nSyb-SNT::dNlg2ICD::G4^{V5}). The immunostaining was performed with two V5 antibodies separately, rabbit anti-V5 (top panels) and mouse anti-V5 (bottom panels). The single optical sections of the confocal images with comparable levels are shown here. nSyb-SNTG4^{V5} proteins (left) were accumulated in the cell bodies (arrows), but relatively weaker in the neuropils (red stippled outlines), especially in the sample staining by rabbit anti-V5 antibody (top left). Insets in the left panels show a high magnification view of the SNTG4^{V5}+ cell bodies (arrows). In contrast, SNT::dNlg2ICD::G4^{V5} was concentrated in the neuropils (red stippled outlines), but there is no detectable SNT::dNlg2ICD::G4^{V5} in the cell bodies outside the neuropils (right). Scale bar= 50 μm.

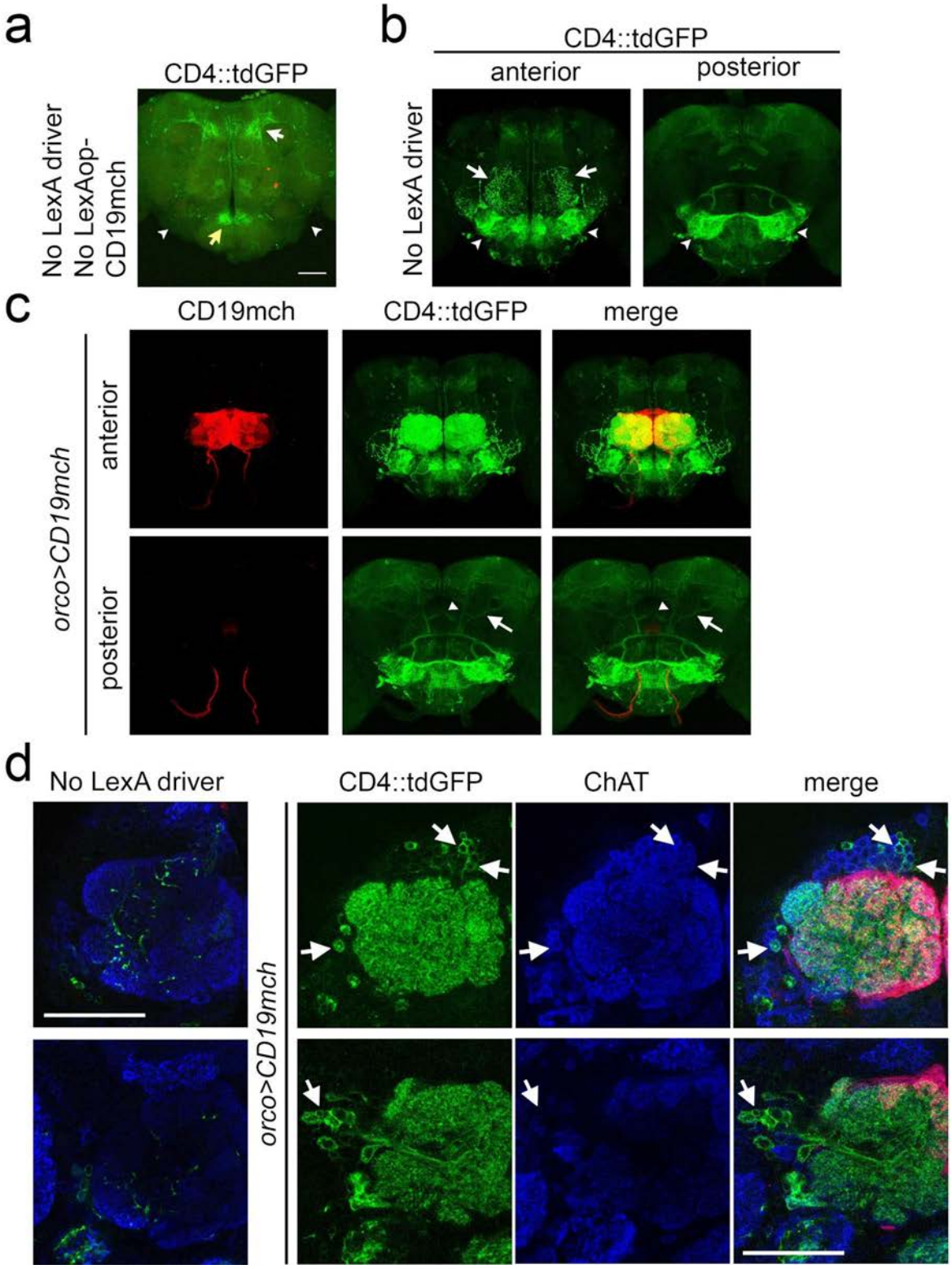
a
CD4::tdGFP
No LexA driver
No LexAop-CD19mch
b
CD4::tdGFP
anterior
posterior
No LexA driver
c
CD19mch
CD4::tdGFP
merge
orco>CD19mch
anterior
posterior
d
No LexA driver
CD4::tdGFP
ChAT
merge
orco>CD19mch

FIGURE 4-6. Monitoring neurons-neuron contacts between the olfactory receptor neurons and the antennal lobe neurons by SNT::dNlg2ICD::G4 (nSyb promoter).

(a) The image shows that the flies carrying both nSyb-SNT::dNlg2ICD::G4^{V5} and 5xUAS-CD4::tdGDP had moderate GFP signals in the dorsal brain (white arrow) and the subesophageal ganglions (yellow arrow), which is from the reporter lines itself, but not in the antennal and mechanosensory motor center (AMMC, arrowheads). (b) However, once the fly carrying the ligand transgene (LexAop-CD19::mch) together with the receptor and the reporter in (a), strong CD4::tdGFP expression was induced in AMMC (arrowheads), even without LexA driver to specifically drive the ligand expression. Several neurite arborizations from the antennal lobe neurons can also be observed (arrows). The left shows the image of anterior half of the brain; the right shows the rest of the posterior brain. (c) Induction of CD4::tdGFP expression in neurons (arrows) having the arborizations covered the whole antennal lobe when CD19::mch was driven by orco driver in OSNs. The top panels show the anterior half of the brain; the bottom panels show the rest of the posterior brain. In the bottom panels, the arrowhead indicates the axons of the uPNs having the induction of CD4::tdGFP expression run through the iACT while the arrow indicates the axons from the CD4::tdGFP+ mPNs in the mACT. Left: distribution of CD19mch+ emitter axons; middle: distribution of CD4::tdGFP+ neurons; right: merged images of CD19mch (red), CD4::tdGFP (green). (d) the images of two single optical section (right top and bottom panels)

in different depth show ChAT immunostaining (blue) to confirm that some of the CD4::tdGFP+ neurons (green) induced by CD19mch+ OSNs are non-cholinergic LNs (arrow in the right top panels), and some are cholinergic PNs (arrows in the right bottom panels). The images in the left panels show the antennal lobe of the no driver control brain (CD4::tdGFP in green, ChAT in blue). In the right panels, the left: distribution of CD4::tdGFP+ neurons; the middle: ChAT immunostaining; right: merged images of ChAT (blue), CD4::tdGFP (green) and CD19mch (red). Scale bar= 50 μm.

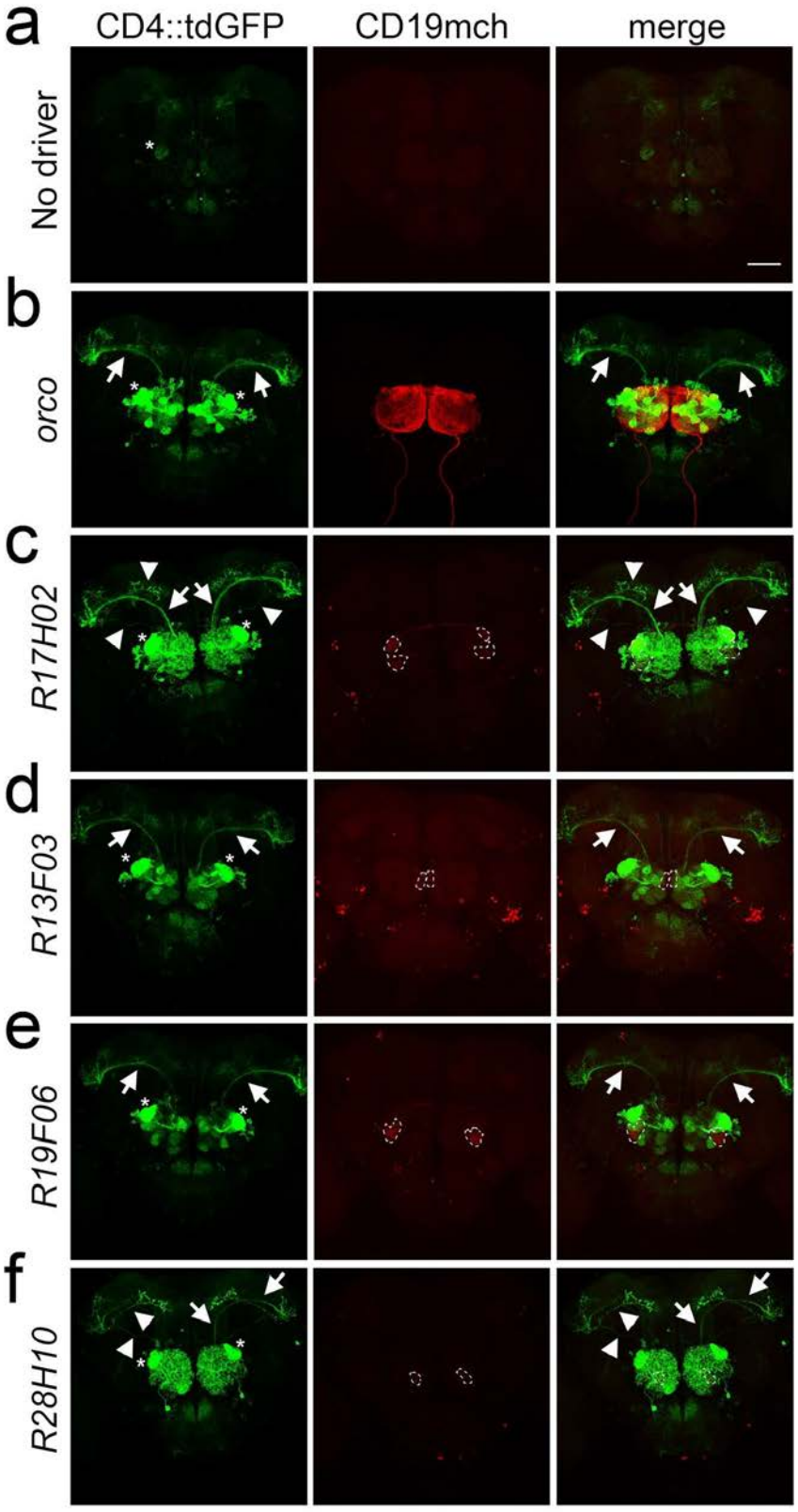
a
CD4::tdGFP
CD19mch
merge
No driver
b
orco
c
R17H02
d
R13F03
e
R19F06
f
R28H10

FIGURE 4-7. Monitoring neurons-neuron contacts between the olfactory receptor neurons and the PNs by SNT::dNlg2ICD::G4^{V5} (GH146 enhancer) in single glomerular level.

SNT::dNlg2ICD::G4^{V5} used in this figure was expressed in part of PNs driven by GH146 enhancer. To selectively express the ligand in few glomeruli, several LexA driver lines, which have LexA activity in 1-3 antennal lobe glomeruli, were selected from the Janelia LexA stocks (see Table 3-1). (a) The images are the no driver control sample. Only low level of CD4::tdGFP can be barely observed in several brain regions, including DA1 glomerulus (star in the right). (b) the induction of CD4::tdGFP expression (left) was triggered by CD19+ OSNs driven by orco driver (middle). The axon bundles of the CD4::tdGFP+ PNs in the iACT (arrows) can be clearly seen. (c-f) The images show the distributions of CD4::tdGFP expression (the left panels) induced by CD19mch+ OSN axons that innervate in one to three specific glomeruli (stippled circles in the middle panels). The LexA divers used here are R17H02 (c), R13F03 (d), R19F06 (e) and R28H10 (f). Although the ligand proteins were only present in specific glomeruli, strong ectopic CD4::tdGFP inductions (left panels) were detected outside the ligand+ glomeruli, especially the DA1 (stars) in all the cases. In (d) and (e), The PNs having CD4::tdGFP inductions are likely to be the uPNs, which their axons run through the iACT (arrows in the left). In (e), the ligand driven by R19H06 driver was expressed in VA1lm glomerulus, in which there is no CD4::tdGFP+ signals. In (c) and (f), except of the uPNs, few mPNs were labeled as well. Their dendrite

arborizations cover the entire antennal lobes, and their axons are projected along the mACT (arrowheads) to the lateral horn directly and subsequently toward the anterior medial brain regions. The right panels show the merged images of CD4::tdGFP (green) and CD19mch (red). Scale bar= 50μm

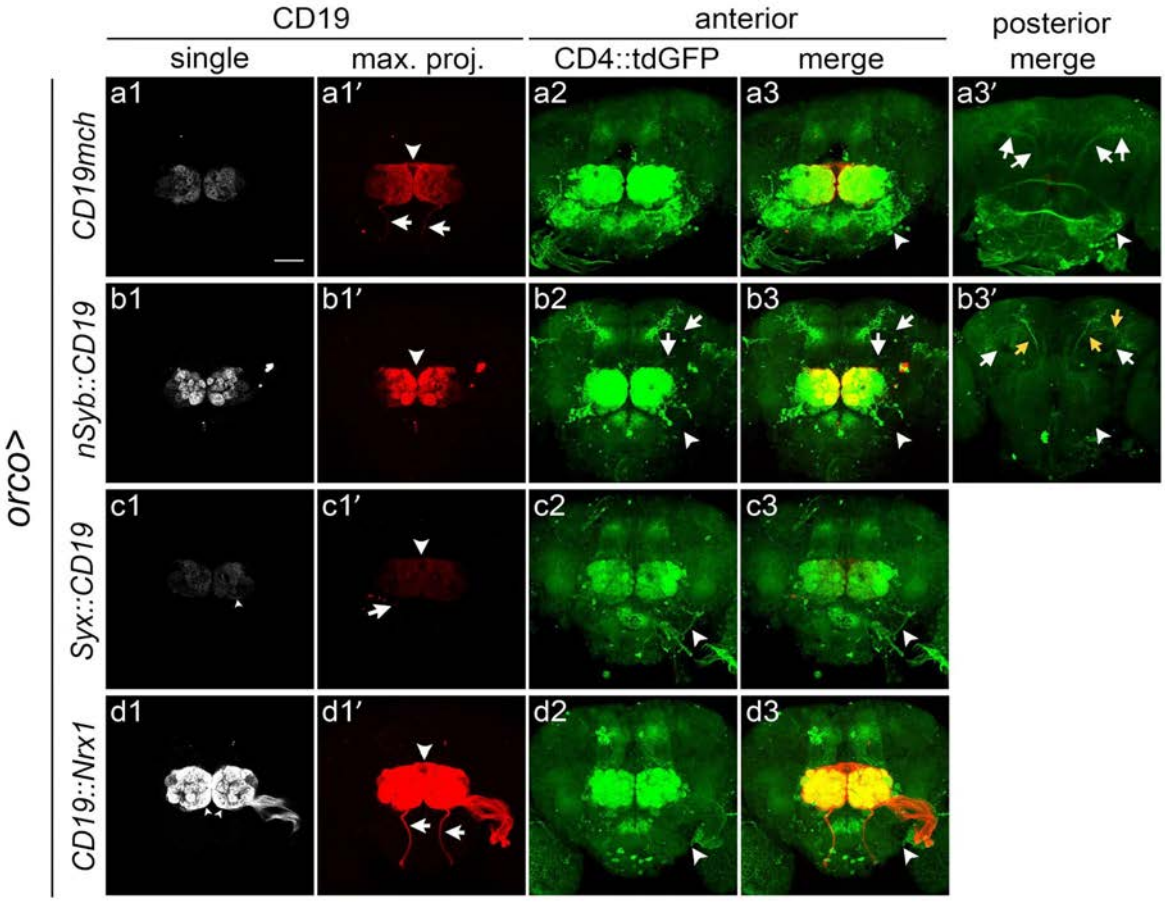
CD19
anterior
posterior
single
max. proj.
CD4::tdGFP
merge
merge
orco>
CD19mch
nSyb::CD19
Syx::CD19
CD19::Nrx1
a1
a1′
a2
a3
a3′
b1
b1′
b2
b3
b3′
c1
c1′
c2
c3
d1
d1′
d2
d3

FIGURE 4-8. Monitoring neurons-neuron contacts between the olfactory receptor neurons and the AN neurons by nSyb-SNT::dNIg2ICD::G4^{V5} and pre-synaptic targeted CD19.

The ligand, CD19, was fused with different pre-synaptic markers, nSyb (b), Syx (c) and Nrx1 (d). In panel (1) and panel (1'), the distributions of the different ligands expressed in OSN axons driven by orco driver are shown in single optic sections (1) or maximum projection (1'). CD19mch (a1, a1'), Syx::CD19 (c1, c1') and CD19::Nrx1 (d1, d1') are homogeneously distributed in the axon terminals in the antennal lobe glomeruli and the axon shafts, such as the antennal commissure (arrowheads in a1', c1' and d1') and axon fascicles of OSNs from maxillary palps (arrows in a1', c1' and d1'). In contrast, nSyb::CD19 (second panels from the top) was more accumulated at the axon terminals in the antennal lobe glomeruli, which causes the weak signals in the axon shafts (arrowhead in b1') and clear boundaries between each glomerulus (b1). The induction of CD4::tdGFP patterns by the CD19+ OSNs are shown in panel (2) and (3) for the anterior half of the brains and in panel (3') for the rest of the posterior brains. In a2, a3 and a3', the induction patterns are identical to the foundings in Fig. 3-7 with strong background in the AMMC (arrowheads in a2 and a3') and the good induction in PNs (arrows indicate the green+ mACT). Interestingly, the background GFP expression in the AMMC (arrowhead in b2, c2, d2) is not existing when the three new ligands were used. In (c2) and (b2), Stx::CD19 and CD19::Nrx1 in OSNs only induced weak CD4::tdGFP expression in the antennal

lobe neurons. Those antennal lobe neurons do not have the axons go to higher order of the brain regions, which indicates that they might be the LNs. In contrast, nSyb::CD19 in the OSNs triggered strong CD4::tdGFP expression in some of the mPNs, whose axons were projected to lateral horns directly through mACT (white arrows in b3'), and weak GFP in a few other PN as well, whose axons are in iACT (yellow arrows in b3') .

Table 4-1. The LexA driver lines used for single glomerular expression of CD19.

LexA driver	labeled glomeruli
Ir84a	VL2a
GMR13c03	VL1
GMR13F03	DM2
GMR17H02	VA1lm DA1 DA4l
GMR19F06	VA1lm
GMR28H10	VC1
GMR46B01	VA7l or (VA7m and VM5d)?

.

CHAPTER 5: CONCLUSION AND PERSPECTIVE

After Ramon y Cajal (1899) published his first work regarding the elegant observation that neurons are the fundamental building blocks of the nervous system, neuroscientists have been trying to understand the link between neuronal wiring, computation and animal behavior. Most functional brain regions contain not only one type of principal neuron receiving and sending information between their partners in other brain regions, but also interneurons and glial cells to modulate the communications inside this region. Therefore, in order to comprehensively understand how the neural networks process information, first, we need to know which elements, neurons and glial cells, are involved in the circuit (Cazemier et al., 2016; Fornito et al., 2015; Schreiner et al., 2016). Currently there are several ongoing projects attempting to systematically dissect and map the entire brain circuits from Drosophila to Human and from macroscale to microscale, e.g. the FlyEM, the MouseLight, the Mouse Connectome Project, Allen Mouse Brain Connectivity Atlas and the Human Connectome Project, etc.

Many studies have also indicated that the abnormal changes in the neural circuits could result in several psychiatric disorders. For example, the imbalance of excitation/inhibition activity in brains might be the common mechanism involved in schizophrenia and autism (Peca and Feng, 2012; Gao and Penzes, 2015). Moreover, it has been hypothesized that the synaptic loss and inflammation reactions of glial cells might be the early sign of the neuronal death in brain diseases such as Alzheimer’s disease, prion disease and amyotrophic

lateral sclerosis (Hilton et al., 2013; Hong et al., 2016; Wishart et al., 2006). The detailed knowledge of neural circuits and networks can help us not only to understand the mysteries of the nervous system but also to identify the circuit-level changes that accompany brain disease. Such findings may allow investigators to design new treatments focusing on the correct targets that were otherwise unknown.

In addition, a comprehensive map of neural circuits of different species could also allow us to understand the beauty of the designs in different animals. Animals have evolved for millions years to build extremely efficient machinery for particular tasks, such as flight and swimming. For instance, how do the motor neurons of insects or fishes control and coordinate the muscle movements during flight or swimming, respectively? How do the sensory feedback inputs fine-tune the slight change to achieve the maximum outputs to immediately turn the direction to avoid predators? To understand the detailed connectome of these circuits could provide a blueprint for scientists to design a more efficient and tinier device or robot that might be able to operate some special tasks or benefit human beings in the future (Liu et al., 2016a; Raj and Thakur, 2016).

As mentioned in the introduction, each of the methods for tracing the neuronal connections has its advantages and disadvantages (Table 1-1). In choosing the appropriate method for tracing nervous system connectivity, it is crucial to first identify the nature of the question at hand. The main advantages

of signaling systems based on ligand-induced membrane proteolysis are the following: (a) They are fully genetically-encoded, and therefore could be used with high reproducibility in transgenic animals. Moreover, as we demonstrate here, the ligand and/or the receptor could be driven with promoters specific to selective cell populations to enable monitoring of cell-cell interactions from specific cell types and developmental stages, (b) They can be used in any species in which transgenesis is possible. This is particularly important for mice (Anderson and Ingham, 2003), Drosophila (Bellen et al., 2010) and zebrafish (Fetcho and Liu, 1998), three model organisms of great interest to developmental biologists and neurobiologists with extremely powerful genetics, (c) The interacting cells can be studied both in vivo (combined with live imaging, electrophysiological recordings and optical monitoring of activity) or in fixed tissue (by fluorescent or electron microscopy), (d) They can be used in high-throughput experiments because unlike electron microscopy, it is not labor intensive. In addition, as we have shown here, it is reproducible between animals because it does not require injections of the signaling components or any other chemical. (e) The system can be used to genetically modify the interacting cells. For instance it could be used to induce the expression of transgenes such as TRPA1, genetically-encoded calcium sensors (Tian et al., 2012; Yizhar et al., 2011) or optogenetic constructs (Yizhar et al., 2011) based on synaptic contact for functional analysis of newly identified circuits. (f) Lastly, it could be used to control cell fate or function by regulating endogenous genes indirectly through

nuclear translocation of drivers such as cre, flp, lexA, or tetA (del Valle Rodriguez et al., 2011; Lewandoski, 2001; Venken et al., 2011), or directly by fusing endogenous transcription factors to the artificial receptor. We anticipate that these synthetic genetic systems will be particularly useful to investigate cell-cell interactions during development in vivo.

In its current implementation, our results clearly demonstrate that TRACT is capable of detecting neuron-glia contact in *Drosophila*. In addition, this application of TRACT serves as a much-needed tool for selectively labeling groups of glial cells. Though systems such as MARCM or Flip-Out can be used to sparsely label glial cells in mosaic clones, both systems are inherently stochastic and cannot be used to control gene expression in a stereotypical set of cells. With TRACT, we have shown that it is now possible to readily identify and consistently label subpopulations of glial cells based on their contact with known neuronal types. For neuron-neuron contacts, because it does not require prior knowledge of the neurotransmitters used or putative synaptic partners, TRACT with optimization would be ideal for unbiased identification of novel synaptic connections. However, more detailed analysis is still required to confirm the efficiency of the synaptic targeted ligand, nSyb::CD19. Ideally, nSyb::CD19 could minimize the potential for activation of the reporter between neurons whose membranes are close to each other (for instance, between fasciculating axons) but are not connected by synapses.

In addition, we also anticipate that TRACT will be able to be used in studying several crucial cell-cell contact events during animal development or cancer progression, such as cell migrations or metastasis. Because those cell-cell contacts are very dynamic and transient, one of the major drawbacks of TRACT is that the readout requires several steps, including proteolytic cleavages, nuclear translocation, DNA transcription and RNA translation. Therefore, it might take around 1 day to generate detectable changes of the induction. Moreover, how long the signals would last, which depends on the half-lives of the reporter proteins, also needs to be addressed because prolonged half-life could increase the chance of overlapping of that two individual signals, and influence the readout or mislead the analysis. In this case, perhaps, instead of regular GFP, destabilized GFP or split horseradish peroxidase can be considered for the final readout (Corish and Tyler-Smith, 1999; Li et al., 1998).

Moreover, it is important to note that, according to the results we have shown in the previous chapters, the promoter driving receptor expression needs to be carefully chosen as it will likely influence whether TRACT can work successfully *in vivo*. For example, elav-SNTG4 could be activated by contact with ligand-expressing cells in the larval antennal lobe as described in Chapter 3 and 4, but not in the adult antennal lobe (data not shown). In contrast, induction experiments with the nSyb-SNT::dNlg2ICD::G4 receptor only labeled a few LNs in the larval antennal lobe(data not shown), but many PNs and LNs in the adult

antennal lobe. It is tempting to attribute the opposite patterns of inducibility to differentially regulated activities of elav and nSyb promoters through development. In addition, SNT::dNlg2ICD::G4 driven by different promoters, elav or nSyb, resulted in different patterns of ligand-independent background and inducibility. This indicates that promoters determine the expression levels of receptors in different neuronal types. Finally, although alrm-SNTG4 worked efficiently in the larval stage to selectively label astrocytes contacting given groups of neurons, in the adult brain, this receptor led to high ligand-independent background (in the optic lobes and ventral central brains) and lacked inducibility in the antennal lobes (data not shown). The variability introduced by the promoters seems to restrict the system to narrow developmental time windows or neuronal types. Therefore, to achieve a more homogenous expression of the receptor, I plan to implement a flp-out system in which SNT::dNlg2ICD::G4 cassette is under the control of a housekeeping gene promoter that theoretically has more consistent activity across different cell types. A cell type-specific Flp will be used to selectively express SNT::dNlg2ICD::G4. For example, tubP>stop>SNT::dNlg2ICD::G4 in conjunction with nSyb-Flp could be used for pan-neuronal expression.

Another drawback that we encounter is the ligand-independent activity of the receptor. The ligand-independent activity of Notch is generated through endosomal trafficking of Notch proteins to lysosome. Therefore, to secure

development processes from ectopic Notch ligand-independent signaling, the internalization of Notch protein on plasma membrane is tightly regulated by endosomal sorting, ubiquitination and *cis*-inhibition of the ligand (Fortini and Bilder, 2009; Palmer and Deng, 2015). In addition, several studies have demonstrated that, to trigger notch signaling, only a small strength of force is required (Gordon et al., 2015; Wang and Ha, 2013). Therefore, perhaps the natural design of the Notch NRR and TMD is very sensitive to small change of protein structure that could cause ligand-independent activity, and it is possible that there is not much room for us to reduce the background while preserving strong inducibility. Moreover, this system still relies on the activity of ADAM and γ-secretase to release the intracellular transcription factor. Although it is thought that these proteases are expressed ubiquitously, there is no direct evidence proving that their activity levels are comparable in different cells or throughout different developmental stages. This possibility could cause the variations in the current TRACT system. Currently, our group is attempting to generate a new synthetic receptor carrying a motif, instead of the Notch NRR, that can be recognized and proteolytically cleaved by an exogenous protease, which would act as the ligand. The idea is, once the ligand protease is bound or close to the new receptor, it will cut and shorten the receptor proteins, and subsequently the intracellular GAL4 will be released. We anticipate that this will allow us to gain more control over the system. According to our preliminary results, the new synthetic receptor has good surface expression and minimal background in vitro,

and after adding the protease in the culture medium, it triggers strong induction within hours (Antuca unpublished data). Furthermore, surprisingly, the induction was also able to be triggered once the antibody recognizing the extracellular domain of the new receptor was anchored on the surface of the culture plates (Donghyung Lee unpublished data). It indicates that, even without NRR, if the structural folding is suitable, mechanical force can also trigger a transmembrane protein to be also cleaved by metalloprotease. Therefore, this new receptor might provide us two future directions by utilizing either endogenous or exogenous protease.

In conclusion, as connectomic methods continue to be developed for higher organisms, one day we may more fully understand the details of the nervous system, especially there are still many types of neurons are not well-characterized yet. However, there is a lesson to be learned from the precedent in *C. elegans*: the connectome alone, no matter how complete, cannot explain how brain circuits work in real time. What more importantly is, with electrophysiological or optical recordings, etc., to establish an understanding of the dynamics of neural circuits in parallel.

REFERENCES

Adams, S.R., Mackey, M.R., Ramachandra, R., Palida Lemieux, S.F., Steinbach, P., Bushong, E.A., Butko, M.T., Giepmans, B.N., Ellisman, M.H., and Tsien, R.Y. (2016). Multicolor Electron Microscopy for Simultaneous Visualization of Multiple Molecular Species. Cell chemical biology *23*, 1417-1427.

Akin, O., and Zipursky, S.L. (2016). Frazzled promotes growth cone attachment at the source of a Netrin gradient in the Drosophila visual system. eLife *5*.

Anderson, K.V., and Ingham, P.W. (2003). The transformation of the model organism: a decade of developmental genetics. Nature genetics *33 Suppl*, 285-293.

Andretic, R., Kim, Y.C., Jones, F.S., Han, K.A., and Greenspan, R.J. (2008). Drosophila D1 dopamine receptor mediates caffeine-induced arousal. Proceedings of the National Academy of Sciences of the United States of America *105*, 20392-20397.

Artavanis-Tsakonas, S., and Muskavitch, M.A. (2010). Notch: the past, the present, and the future. Current topics in developmental biology *92*, 1-29.

Bachmair, A., Finley, D., and Varshavsky, A. (1986). In vivo half-life of a protein is a function of its amino-terminal residue. Science *234*, 179-186.

Banerjee, S., and Bhat, M.A. (2007). Neuron-glial interactions in blood-brain barrier formation. Annual review of neuroscience *30*, 235-258.

Bang, M.L., and Owczarek, S. (2013). A matter of balance: role of neurexin and neuroligin at the synapse. Neurochemical research *38*, 1174-1189.

Barnea, G., Strapps, W., Herrada, G., Berman, Y., Ong, J., Kloss, B., Axel, R., and Lee, K.J. (2008). The genetic design of signaling cascades to record receptor activation. Proceedings of the National Academy of Sciences of the United States of America *105*, 64-69.

Begemann, I., and Galic, M. (2016). Correlative Light Electron Microscopy: Connecting Synaptic Structure and Function. Frontiers in synaptic neuroscience *8*, 28.

Bellen, H.J., Tong, C., and Tsuda, H. (2010). 100 years of Drosophila research and its impact on vertebrate neuroscience: a history lesson for the future. Nature reviews Neuroscience *11*, 514-522.

Berck, M.E., Khandelwal, A., Claus, L., Hernandez-Nunez, L., Si, G., Tabone, C.J., Li, F., Truman, J.W., Fetter, R.D., Louis, M.*, et al.* (2016). The wiring diagram of a glomerular olfactory system. eLife *5*.

Berger-Muller, S., Sugie, A., Takahashi, F., Tavosanis, G., Hakeda-Suzuki, S., and Suzuki, T. (2013). Assessing the role of cell-surface molecules in central synaptogenesis in the Drosophila visual system. PloS one *8*, e83732.

Berlin, S., Carroll, E.C., Newman, Z.L., Okada, H.O., Quinn, C.M., Kallman, B., Rockwell, N.C., Martin, S.S., Lagarias, J.C., and Isacoff, E.Y. (2015). Photoactivatable genetically encoded calcium indicators for targeted neuronal imaging. Nature methods *12*, 852-858.

Blaumueller, C.M., Qi, H., Zagouras, P., and Artavanis-Tsakonas, S. (1997). Intracellular cleavage of Notch leads to a heterodimeric receptor on the plasma membrane. Cell *90*, 281-291.

Blazquez-Llorca, L., Hummel, E., Zimmerman, H., Zou, C., Burgold, S., Rietdorf, J., and Herms, J. (2015). Correlation of two-photon in vivo imaging and FIB/SEM microscopy. Journal of microscopy *259*, 129-136.

Borst, A. (2009). Drosophila's view on insect vision. Current biology : CB *19*, R36-47.

Bosch, J.A., Tran, N.H., and Hariharan, I.K. (2015). CoinFLP: a system for efficient mosaic screening and for visualizing clonal boundaries in Drosophila. Development *142*, 597-606.

Bowtell, D.D., Lila, T., Michael, W.M., Hackett, D., and Rubin, G.M. (1991). Analysis of the enhancer element that controls expression of sevenless in the developing Drosophila eye. Proceedings of the National Academy of Sciences of the United States of America *88*, 6853-6857.

Broadwell, R.D., and Balin, B.J. (1985). Endocytic and exocytic pathways of the neuronal secretory process and trans-synaptic transfer of wheat germ agglutinin-horseradish peroxidase in vivo. The Journal of comparative neurology *242*, 632-650.

Brou, C., Logeat, F., Gupta, N., Bessia, C., LeBail, O., Doedens, J.R., Cumano, A., Roux, P., Black, R.A., and Israel, A. (2000). A novel proteolytic cleavage involved in Notch signaling: the role of the disintegrin-metalloprotease TACE.

Molecular cell *5*, 207-216.

Butcher, N.J., Friedrich, A.B., Lu, Z., Tanimoto, H., and Meinertzhagen, I.A. (2012). Different classes of input and output neurons reveal new features in microglomeruli of the adult Drosophila mushroom body calyx. The Journal of comparative neurology *520*, 2185-2201.

Callaway, E.M., and Luo, L. (2015). Monosynaptic Circuit Tracing with Glycoprotein-Deleted Rabies Viruses. The Journal of neuroscience : the official journal of the Society for Neuroscience *35*, 8979-8985.

Caron, S.J., Ruta, V., Abbott, L.F., and Axel, R. (2013). Random convergence of olfactory inputs in the Drosophila mushroom body. Nature *497*, 113-117.

Cavanaugh, D.J., Geratowski, J.D., Wooltorton, J.R., Spaethling, J.M., Hector, C.E., Zheng, X., Johnson, E.C., Eberwine, J.H., and Sehgal, A. (2014). Identification of a circadian output circuit for rest:activity rhythms in Drosophila. Cell *157*, 689-701.

Cazemier, J.L., Clasca, F., and Tiesinga, P.H. (2016). Connectomic Analysis of Brain Networks: Novel Techniques and Future Directions. Frontiers in neuroanatomy *10*, 110.

Chen, T.W., Wardill, T.J., Sun, Y., Pulver, S.R., Renninger, S.L., Baohan, A., Schreiter, E.R., Kerr, R.A., Orger, M.B., Jayaraman, V.*, et al.* (2013). Ultrasensitive fluorescent proteins for imaging neuronal activity. Nature *499*, 295-300.

Chen, Y., Akin, O., Nern, A., Tsui, C.Y., Pecot, M.Y., and Zipursky, S.L. (2014).

Cell-type-specific labeling of synapses in vivo through synaptic tagging with recombination. Neuron *81*, 280-293.

Chklovskii, D.B., Vitaladevuni, S., and Scheffer, L.K. (2010). Semi-automated reconstruction of neural circuits using electron microscopy. Current opinion in neurobiology *20*, 667-675.

Christiansen, F., Zube, C., Andlauer, T.F., Wichmann, C., Fouquet, W., Owald, D., Mertel, S., Leiss, F., Tavosanis, G., Luna, A.J.*, et al.* (2011). Presynapses in Kenyon cell dendrites in the mushroom body calyx of Drosophila. The Journal of neuroscience : the official journal of the Society for Neuroscience *31*, 9696-9707.

Clarke, L.E., and Barres, B.A. (2013). Emerging roles of astrocytes in neural circuit development. Nature reviews Neuroscience *14*, 311-321.

Clowney, E.J., Iguchi, S., Bussell, J.J., Scheer, E., and Ruta, V. (2015). Multimodal Chemosensory Circuits Controlling Male Courtship in Drosophila. Neuron *87*, 1036-1049.

Collman, F., Buchanan, J., Phend, K.D., Micheva, K.D., Weinberg, R.J., and Smith, S.J. (2015). Mapping synapses by conjugate light-electron array tomography. The Journal of neuroscience : the official journal of the Society for Neuroscience *35*, 5792-5807.

Corish, P., and Tyler-Smith, C. (1999). Attenuation of green fluorescent protein half-life in mammalian cells. Protein engineering *12*, 1035-1040.

DeFalco, J., Tomishima, M., Liu, H., Zhao, C., Cai, X., Marth, J.D., Enquist, L., and Friedman, J.M. (2001). Virus-assisted mapping of neural inputs to a feeding

center in the hypothalamus. Science *291*, 2608-2613.

del Valle Rodriguez, A., Didiano, D., and Desplan, C. (2011). Power tools for gene expression and clonal analysis in Drosophila. Nature methods *9*, 47-55.

Denk, W., and Horstmann, H. (2004). Serial block-face scanning electron microscopy to reconstruct three-dimensional tissue nanostructure. PLoS biology *2*, e329.

Desbois, M., Cook, S.J., Emmons, S.W., and Bulow, H.E. (2015). Directional Trans-Synaptic Labeling of Specific Neuronal Connections in Live Animals. Genetics *200*, 697-705.

DiAntonio, A. (1999). Learning something ORIGINal at the Drosophila neuromuscular junction. Neuron *23*, 1-2.

Doherty, J., Logan, M.A., Tasdemir, O.E., and Freeman, M.R. (2009). Ensheathing glia function as phagocytes in the adult Drosophila brain. The Journal of neuroscience : the official journal of the Society for Neuroscience *29*, 4768-4781.

Edwards, T.N., and Meinertzhagen, I.A. (2010). The functional organisation of glia in the adult brain of Drosophila and other insects. Progress in neurobiology *90*, 471-497.

Fabian, R.H., and Coulter, J.D. (1985). Transneuronal transport of lectins. Brain research *344*, 41-48.

Feinberg, E.H., Vanhoven, M.K., Bendesky, A., Wang, G., Fetter, R.D., Shen, K., and Bargmann, C.I. (2008). GFP Reconstitution Across Synaptic Partners

(GRASP) defines cell contacts and synapses in living nervous systems. Neuron *57*, 353-363.

Feng, L., Zhao, T., and Kim, J. (2012). Improved synapse detection for mGRASP-assisted brain connectivity mapping. Bioinformatics *28*, i25-31.

Fetcho, J.R., and Liu, K.S. (1998). Zebrafish as a model system for studying neuronal circuits and behavior. Annals of the New York Academy of Sciences *860*, 333-345.

Fields, R.D. (2015). A new mechanism of nervous system plasticity: activity-dependent myelination. Nature reviews Neuroscience *16*, 756-767.

Fisek, M., and Wilson, R.I. (2014). Stereotyped connectivity and computations in higher-order olfactory neurons. Nature neuroscience *17*, 280-288.

Fornito, A., Zalesky, A., and Breakspear, M. (2015). The connectomics of brain disorders. Nature reviews Neuroscience *16*, 159-172.

Fortini, M.E., and Bilder, D. (2009). Endocytic regulation of Notch signaling. Current opinion in genetics & development *19*, 323-328.

Fouquet, W., Owald, D., Wichmann, C., Mertel, S., Depner, H., Dyba, M., Hallermann, S., Kittel, R.J., Eimer, S., and Sigrist, S.J. (2009). Maturation of active zone assembly by Drosophila Bruchpilot. The Journal of cell biology *186*, 129-145.

Freeman, M.R. (2015). Drosophila Central Nervous System Glia. Cold Spring Harbor perspectives in biology *7*.

Freeman, M.R., Delrow, J., Kim, J., Johnson, E., and Doe, C.Q. (2003).

Unwrapping glial biology: Gcm target genes regulating glial development, diversification, and function. Neuron *38*, 567-580.

Gabius, H.J., Andre, S., Jimenez-Barbero, J., Romero, A., and Solis, D. (2011). From lectin structure to functional glycomics: principles of the sugar code. Trends in biochemical sciences *36*, 298-313.

Gao, R., and Penzes, P. (2015). Common mechanisms of excitatory and inhibitory imbalance in schizophrenia and autism spectrum disorders. Current molecular medicine *15*, 146-167.

Gonda, D.K., Bachmair, A., Wunning, I., Tobias, J.W., Lane, W.S., and Varshavsky, A. (1989). Universality and structure of the N-end rule. The Journal of biological chemistry *264*, 16700-16712.

Gordon, M.D., and Scott, K. (2009). Motor control in a Drosophila taste circuit. Neuron *61*, 373-384.

Gordon, W.R., Vardar-Ulu, D., Histen, G., Sanchez-Irizarry, C., Aster, J.C., and Blacklow, S.C. (2007). Structural basis for autoinhibition of Notch. Nature structural & molecular biology *14*, 295-300.

Gordon, W.R., Zimmerman, B., He, L., Miles, L.J., Huang, J., Tiyanont, K., McArthur, D.G., Aster, J.C., Perrimon, N., Loparo, J.J.*, et al.* (2015). Mechanical Allostery: Evidence for a Force Requirement in the Proteolytic Activation of Notch. Developmental cell *33*, 729-736.

Gorostiza, E.A., Depetris-Chauvin, A., Frenkel, L., Pirez, N., and Ceriani, M.F. (2014). Circadian pacemaker neurons change synaptic contacts across the day.

Current biology : CB *24*, 2161-2167.

Grabher, C., von Boehmer, H., and Look, A.T. (2006). Notch 1 activation in the molecular pathogenesis of T-cell acute lymphoblastic leukaemia. Nature reviews Cancer *6*, 347-359.

Gradinaru, V., Zhang, F., Ramakrishnan, C., Mattis, J., Prakash, R., Diester, I., Goshen, I., Thompson, K.R., and Deisseroth, K. (2010). Molecular and cellular approaches for diversifying and extending optogenetics. Cell *141*, 154-165.

Griesbeck, O., Baird, G.S., Campbell, R.E., Zacharias, D.A., and Tsien, R.Y. (2001). Reducing the environmental sensitivity of yellow fluorescent protein. Mechanism and applications. The Journal of biological chemistry *276*, 29188-29194.

Hakim, Y., Yaniv, S.P., and Schuldiner, O. (2014). Astrocytes play a key role in Drosophila mushroom body axon pruning. PloS one *9*, e86178.

Hamanaka, Y., and Meinertzhagen, I.A. (2010). Immunocytochemical localization of synaptic proteins to photoreceptor synapses of Drosophila melanogaster. The Journal of comparative neurology *518*, 1133-1155.

Hasegawa, E., Truman, J.W., and Nose, A. (2016). Identification of excitatory premotor interneurons which regulate local muscle contraction during Drosophila larval locomotion. Scientific reports *6*, 30806.

Hayworth, K.J., Xu, C.S., Lu, Z., Knott, G.W., Fetter, R.D., Tapia, J.C., Lichtman, J.W., and Hess, H.F. (2015). Ultrastructurally smooth thick partitioning and volume stitching for large-scale connectomics. Nature methods *12*, 319-322.

Cell 135, 738–748, November 14, 2008

Heiman, M., Schaefer, A., Gong, S., Peterson, J.D., Day, M., Ramsey, K.E., Suárez-Fariñas, M, Schwarz, C., Stephan, D.A., Surmeier, D.J., Greengard, P., Heintz, N. (2008) A translational profiling approach for the molecular characterization of CNS cell types. Cell *135*, 738-748.

Helfrich-Forster, C. (1997). Development of pigment-dispersing hormone-immunoreactive neurons in the nervous system of Drosophila melanogaster. The Journal of comparative neurology *380*, 335-354.

Hell, S.W., and Wichmann, J. (1994). Breaking the diffraction resolution limit by stimulated emission: stimulated-emission-depletion fluorescence microscopy. Optics letters *19*, 780-782.

Hilton, K.J., Cunningham, C., Reynolds, R.A., and Perry, V.H. (2013). Early Hippocampal Synaptic Loss Precedes Neuronal Loss and Associates with Early Behavioural Deficits in Three Distinct Strains of Prion Disease. PloS one *8*, e68062.

Hong, E.J., and Wilson, R.I. (2015). Simultaneous encoding of odors by channels with diverse sensitivity to inhibition. Neuron *85*, 573-589.

Hong, S., Beja-Glasser, V.F., Nfonoyim, B.M., Frouin, A., Li, S., Ramakrishnan, S., Merry, K.M., Shi, Q., Rosenthal, A., Barres, B.A.*, et al.* (2016). Complement and microglia mediate early synapse loss in Alzheimer mouse models. Science *352*, 712-716.

Hoy, J.L., Haeger, P.A., Constable, J.R., Arias, R.J., McCallum, R., Kyweriga, M.,

Davis, L., Schnell, E., Wehr, M., Castillo, P.E.*, et al.* (2013). Neuroligin1 drives synaptic and behavioral maturation through intracellular interactions. The Journal of neuroscience : the official journal of the Society for Neuroscience *33*, 9364-9384.

Huang, B., Babcock, H., and Zhuang, X. (2010). Breaking the diffraction barrier: super-resolution imaging of cells. Cell *143*, 1047-1058.

Huang, H., and Kornberg, T.B. (2015). Myoblast cytonemes mediate Wg signaling from the wing imaginal disc and Delta-Notch signaling to the air sac primordium. eLife *4*, e06114.

Huh, Y., Oh, M.S., Leblanc, P., and Kim, K.S. (2010). Gene transfer in the nervous system and implications for transsynaptic neuronal tracing. Expert opinion on biological therapy *10*, 763-772.

Iida, J., Hirabayashi, S., Sato, Y., and Hata, Y. (2004). Synaptic scaffolding molecule is involved in the synaptic clustering of neuroligin. Molecular and cellular neurosciences *27*, 497-508.

Irie, M., Hata, Y., Takeuchi, M., Ichtchenko, K., Toyoda, A., Hirao, K., Takai, Y., Rosahl, T.W., and Sudhof, T.C. (1997). Binding of neuroligins to PSD-95. Science *277*, 1511-1515.

Itakura, Y., Kohsaka, H., Ohyama, T., Zlatic, M., Pulver, S.R., and Nose, A. (2015). Identification of Inhibitory Premotor Interneurons Activated at a Late Phase in a Motor Cycle during Drosophila Larval Locomotion. PloS one *10*, e0136660.

Jacobs, S., and Doering, L.C. (2010). Astrocytes prevent abnormal neuronal development in the fragile x mouse. The Journal of neuroscience : the official journal of the Society for Neuroscience *30*, 4508-4514.

Jagadish, S., Barnea, G., Clandinin, T.R., and Axel, R. (2014). Identifying functional connections of the inner photoreceptors in Drosophila using Tango-Trace. Neuron *83*, 630-644.

Jahn, R., and Fasshauer, D. (2012). Molecular machines governing exocytosis of synaptic vesicles. Nature *490*, 201-207.

Jefferis, G.S., Potter, C.J., Chan, A.M., Marin, E.C., Rohlfing, T., Maurer, C.R., Jr., and Luo, L. (2007). Comprehensive maps of Drosophila higher olfactory centers: spatially segregated fruit and pheromone representation. Cell *128*, 1187-1203.

Ke, M.T., Nakai, Y., Fujimoto, S., Takayama, R., Yoshida, S., Kitajima, T.S., Sato, M., and Imai, T. (2016). Super-Resolution Mapping of Neuronal Circuitry With an Index-Optimized Clearing Agent. Cell reports *14*, 2718-2732.

Kim, J., Zhao, T., Petralia, R.S., Yu, Y., Peng, H., Myers, E., and Magee, J.C. (2011). mGRASP enables mapping mammalian synaptic connectivity with light microscopy. Nature methods *9*, 96-102.

Klar, T.A., Engel, E., and Hell, S.W. (2001). Breaking Abbe's diffraction resolution limit in fluorescence microscopy with stimulated emission depletion beams of various shapes. Physical review E, Statistical, nonlinear, and soft matter physics *64*, 066613.

Knight, D., Xie, W., and Boulianne, G.L. (2011). Neurexins and neuroligins: recent insights from invertebrates. Molecular neurobiology *44*, 426-440.

Kochenderfer, J.N., Feldman, S.A., Zhao, Y., Xu, H., Black, M.A., Morgan, R.A., Wilson, W.H., and Rosenberg, S.A. (2009). Construction and preclinical evaluation of an anti-CD19 chimeric antigen receptor. Journal of immunotherapy *32*, 689-702.

Kopan, R., and Ilagan, M.X. (2009). The canonical Notch signaling pathway: unfolding the activation mechanism. Cell *137*, 216-233.

Kremer, M.C., Christiansen, F., Leiss, F., Paehler, M., Knapek, S., Andlauer, T.F., Forstner, F., Kloppenburg, P., Sigrist, S.J., and Tavosanis, G. (2010). Structural long-term changes at mushroom body input synapses. Current biology : CB *20*, 1938-1944.

Kriegstein, A., and Alvarez-Buylla, A. (2009). The glial nature of embryonic and adult neural stem cells. Annual review of neuroscience *32*, 149-184.

Lai, J.S., Lo, S.J., Dickson, B.J., and Chiang, A.S. (2012). Auditory circuit in the Drosophila brain. Proceedings of the National Academy of Sciences of the United States of America *109*, 2607-2612.

Lai, S.L., Awasaki, T., Ito, K., and Lee, T. (2008). Clonal analysis of Drosophila antennal lobe neurons: diverse neuronal architectures in the lateral neuroblast lineage. Development *135*, 2883-2893.

Lee, T., and Luo, L. (2001). Mosaic analysis with a repressible cell marker (MARCM) for Drosophila neural development. Trends in neurosciences *24*, 251-

254.

Leiss, F., Groh, C., Butcher, N.J., Meinertzhagen, I.A., and Tavosanis, G. (2009). Synaptic organization in the adult Drosophila mushroom body calyx. The Journal of comparative neurology *517*, 808-824.

Lewandoski, M. (2001). Conditional control of gene expression in the mouse. Nature reviews Genetics *2*, 743-755.

Li, X., Zhao, X., Fang, Y., Jiang, X., Duong, T., Fan, C., Huang, C.C., and Kain, S.R. (1998). Generation of destabilized green fluorescent protein as a transcription reporter. The Journal of biological chemistry *273*, 34970-34975.

Li, Y., Guo, A., and Li, H. (2016). CRASP: CFP reconstitution across synaptic partners. Biochemical and biophysical research communications *469*, 352-356.

Libbrecht, S., Van den Haute, C., Malinouskaya, L., Gijsbers, R., and Baekelandt, V. (2016). Evaluation of WGA-Cre-dependent topological transgene expression in the rodent brain. Brain structure & function.

Lin, C.W., Sim, S., Ainsworth, A., Okada, M., Kelsch, W., and Lois, C. (2010). Genetically increased cell-intrinsic excitability enhances neuronal integration into adult brain circuits. Neuron *65*, 32-39.

Lin, T.Y., Luo, J., Shinomiya, K., Ting, C.Y., Lu, Z., Meinertzhagen, I.A., and Lee, C.H. (2016). Mapping chromatic pathways in the Drosophila visual system. The Journal of comparative neurology *524*, 213-227.

Lioy, D.T., Garg, S.K., Monaghan, C.E., Raber, J., Foust, K.D., Kaspar, B.K., Hirrlinger, P.G., Kirchhoff, F., Bissonnette, J.M., Ballas, N.*, et al.* (2011). A role

for glia in the progression of Rett's syndrome. Nature *475*, 497-500.

Liu, H., Ravi, S., Kolomenskiy, D., and Tanaka, H. (2016a). Biomechanics and biomimetics in insect-inspired flight systems. Philosophical transactions of the Royal Society of London Series B, Biological sciences *371*.

Liu, H., Zhou, B., Yan, W., Lei, Z., Zhao, X., Zhang, K., and Guo, A. (2014). Astrocyte-like glial cells physiologically regulate olfactory processing through the modification of ORN-PN synaptic strength in Drosophila. The European journal of neuroscience *40*, 2744-2754.

Liu, S., Liu, Q., Tabuchi, M., and Wu, M.N. (2016b). Sleep Drive Is Encoded by Neural Plastic Changes in a Dedicated Circuit. Cell *165*, 1347-1360.

Liu, X., Buchanan, M.E., Han, K.A., and Davis, R.L. (2009). The GABAA receptor RDL suppresses the conditioned stimulus pathway for olfactory learning. The Journal of neuroscience : the official journal of the Society for Neuroscience *29*, 1573-1579.

Lo, L., and Anderson, D.J. (2011). A Cre-dependent, anterograde transsynaptic viral tracer for mapping output pathways of genetically marked neurons. Neuron *72*, 938-950.

Logeat, F., Bessia, C., Brou, C., LeBail, O., Jarriault, S., Seidah, N.G., and Israel, A. (1998). The Notch1 receptor is cleaved constitutively by a furin-like convertase. Proceedings of the National Academy of Sciences of the United States of America *95*, 8108-8112.

Lois, C., Hong, E.J., Pease, S., Brown, E.J., and Baltimore, D. (2002). Germline

transmission and tissue-specific expression of transgenes delivered by lentiviral vectors. Science 295, 868-872.

Ma, Z., Stork, T., Bergles, D.E., and Freeman, M.R. (2016). Neuromodulators signal through astrocytes to alter neural circuit activity and behaviour. Nature. 539, 428-432.

Macpherson, L.J., Zaharieva, E.E., Kearney, P.J., Alpert, M.H., Lin, T.Y., Turan, Z., Lee, C.H., and Gallio, M. (2015). Dynamic labelling of neural connections in multiple colours by trans-synaptic fluorescence complementation. Nature communications 6, 10024.

Maglione, M., and Sigrist, S.J. (2013). Seeing the forest tree by tree: super-resolution light microscopy meets the neurosciences. Nature Neuroscience 16, 790–797.

Magnusson, J.P., and Frisen, J. (2016). Stars from the darkest night: unlocking the neurogenic potential of astrocytes in different brain regions. Development 143, 1075-1086.

Malecki, M.J., Sanchez-Irizarry, C., Mitchell, J.L., Histen, G., Xu, M.L., Aster, J.C., and Blacklow, S.C. (2006). Leukemia-associated mutations within the NOTCH1 heterodimerization domain fall into at least two distinct mechanistic classes. Molecular and cellular biology *26*, 4642-4651.

Marshel, J.H., Mori, T., Nielsen, K.J., and Callaway, E.M. (2010). Targeting

single neuronal networks for gene expression and cell labeling in vivo. Neuron *67*, 562-574.

Masuda-Nakagawa, L.M., Ito, K., Awasaki, T., and O'Kane, C.J. (2014). A single GABAergic neuron mediates feedback of odor-evoked signals in the mushroom body of larval Drosophila. Frontiers in neural circuits *8*, 35.

Meinertzhagen, I.A., and Lee, C.H. (2012). The genetic analysis of functional connectomics in Drosophila. Advances in genetics *80*, 99-151.

Meinertzhagen, I.A., and O'Neil, S.D. (1991). Synaptic organization of columnar elements in the lamina of the wild type in Drosophila melanogaster. The Journal of comparative neurology *305*, 232-263.

Meloty-Kapella, L., Shergill, B., Kuon, J., Botvinick, E., and Weinmaster, G. (2012). Notch ligand endocytosis generates mechanical pulling force dependent on dynamin, epsins, and actin. Developmental cell *22*, 1299-1312.

Miyamichi, K., Amat, F., Moussavi, F., Wang, C., Wickersham, I., Wall, N.R., Taniguchi, H., Tasic, B., Huang, Z.J., He, Z.*, et al.* (2011). Cortical representations of olfactory input by trans-synaptic tracing. Nature *472*, 191-196.

Morante, J., and Desplan, C. (2004). Building a projection map for photoreceptor neurons in the Drosophila optic lobes. Seminars in cell & developmental biology *15*, 137-143.

Morante, J., and Desplan, C. (2008). The color-vision circuit in the medulla of Drosophila. Current biology : CB *18*, 553-565.

Morsut, L., Roybal, K.T., Xiong, X., Gordley, R.M., Coyle, S.M., Thomson, M.,

and Lim, W.A. (2016). Engineering Customized Cell Sensing and Response Behaviors Using Synthetic Notch Receptors. Cell *164*, 780-791.

Mosca, T.J., and Luo, L. (2014). Synaptic organization of the Drosophila antennal lobe and its regulation by the Teneurins. eLife *3*, e03726.

Mumm, J.S., Schroeter, E.H., Saxena, M.T., Griesemer, A., Tian, X., Pan, D.J., Ray, W.J., and Kopan, R. (2000). A ligand-induced extracellular cleavage regulates gamma-secretase-like proteolytic activation of Notch1. Molecular cell *5*, 197-206.

Nagai, Y., Sano, H., and Yokoi, M. (2005). Transgenic expression of Cre recombinase in mitral/tufted cells of the olfactory bulb. Genesis *43*, 12-16.

Nassi, J.J., Cepko, C.L., Born, R.T., and Beier, K.T. (2015). Neuroanatomy goes viral! Frontiers in neuroanatomy *9*, 80.

Ng, F.S., Tangredi, M.M., and Jackson, F.R. (2011). Glial cells physiologically modulate clock neurons and circadian behavior in a calcium-dependent manner. Current biology : CB *21*, 625-634.

Nichols, J.T., Miyamoto, A., Olsen, S.L., D'Souza, B., Yao, C., and Weinmaster, G. (2007). DSL ligand endocytosis physically dissociates Notch1 heterodimers before activating proteolysis can occur. The Journal of cell biology *176*, 445-458.

Nienhaus, K., and Nienhaus, G.U. (2014). Fluorescent proteins for live-cell imaging with super-resolution. Chemical Society reviews *43*, 1088-1106.

Oberdick, J., Smeyne, R.J., Mann, J.R., Zackson, S., and Morgan, J.I. (1990). A promoter that drives transgene expression in cerebellar Purkinje and retinal

bipolar neurons. Science *248*, 223-226.

Oland, L.A., and Tolbert, L.P. (2011). Roles of glial cells in neural circuit formation: insights from research in insects. Glia *59*, 1273-1295.

Omoto, J.J., Yogi, P., and Hartenstein, V. (2015). Origin and development of neuropil glia of the Drosophila larval and adult brain: Two distinct glial populations derived from separate progenitors. Developmental biology *404*, 2-20.

Palmer, W.H., and Deng, W.M. (2015). Ligand-Independent Mechanisms of Notch Activity. Trends in cell biology *25*, 697-707.

Patterson, G.H., and Lippincott-Schwartz, J. (2002). A photoactivatable GFP for selective photolabeling of proteins and cells. Science *297*, 1873-1877.

Peca, J., and Feng, G. (2012). Cellular and synaptic network defects in autism. Current opinion in neurobiology *22*, 866-872.

Peco, E., Davla, S., Camp, D., Stacey, S.M., Landgraf, M., and van Meyel, D.J. (2016). Drosophila astrocytes cover specific territories of the CNS neuropil and are instructed to differentiate by Prospero, a key effector of Notch. Development *143*, 1170-1181.

Petersen, S.A., Fetter, R.D., Noordermeer, J.N., Goodman, C.S., and DiAntonio, A. (1997). Genetic analysis of glutamate receptors in Drosophila reveals a retrograde signal regulating presynaptic transmitter release. Neuron *19*, 1237-1248.

Prinz, M., and Priller, J. (2014). Microglia and brain macrophages in the molecular age: from origin to neuropsychiatric disease. Nature reviews

Neuroscience *15*, 300-312.

Raj, A., and Thakur, A. (2016). Fish-inspired robots: design, sensing, actuation, and autonomy--a review of research. Bioinspiration & biomimetics *11*, 031001.

Rivera-Alba, M., Vitaladevuni, S.N., Mishchenko, Y., Lu, Z., Takemura, S.Y., Scheffer, L., Meinertzhagen, I.A., Chklovskii, D.B., and de Polavieja, G.G. (2011). Wiring economy and volume exclusion determine neuronal placement in the Drosophila brain. Current biology : CB *21*, 2000-2005.

Robinson, I.M., Ranjan, R., and Schwarz, T.L. (2002). Synaptotagmins I and IV promote transmitter release independently of Ca(2+) binding in the C(2)A domain. Nature *418*, 336-340.

Rolls, M.M., Satoh, D., Clyne, P.J., Henner, A.L., Uemura, T., and Doe, C.Q. (2007). Polarity and intracellular compartmentalization of Drosophila neurons. Neural development *2*, 7.

Roybal, K.T., Williams, J.Z., Morsut, L., Rupp, L.J., Kolinko, I., Choe, J.H., Walker, W.J., McNally, K.A., and Lim, W.A. (2016). Engineering T Cells with Customized Therapeutic Response Programs Using Synthetic Notch Receptors. Cell *167*, 419-432 e416.

Ruta, V., Datta, S.R., Vasconcelos, M.L., Freeland, J., Looger, L.L., and Axel, R. (2010). A dimorphic pheromone circuit in Drosophila from sensory input to descending output. Nature *468*, 686-690.

Rybak, J., Talarico, G., Ruiz, S., Arnold, C., Cantera, R., and Hansson, B.S. (2016). Synaptic circuitry of identified neurons in the antennal lobe of Drosophila

melanogaster. The Journal of comparative neurology *524*, 1920-1956.

Sasai, Y. (2013). Next-generation regenerative medicine: organogenesis from stem cells in 3D culture. Cell Stem Cell 12, 520-530.

Schmid, A., Hallermann, S., Kittel, R.J., Khorramshahi, O., Frolich, A.M., Quentin, C., Rasse, T.M., Mertel, S., Heckmann, M., and Sigrist, S.J. (2008). Activity-dependent site-specific changes of glutamate receptor composition in vivo. Nature neuroscience *11*, 659-666.

Schneider-Mizell, C.M., Gerhard, S., Longair, M., Kazimiers, T., Li, F., Zwart, M.F., Champion, A., Midgley, F.M., Fetter, R.D., Saalfeld, S*., et al.* (2016). Quantitative neuroanatomy for connectomics in Drosophila. eLife *5*.

Schreiner, D., Savas, J.N., Herzog, E., Brose, N., and de Wit, J. (2016). Synapse biology in the 'circuit-age'-paths toward molecular connectomics. Current opinion in neurobiology *42*, 102-110.

Sharpe, H.J., Stevens, T.J., and Munro, S. (2010). A comprehensive comparison of transmembrane domains reveals organelle-specific properties. Cell *142*, 158-169.

Sheng, M. (2001). Molecular organization of the postsynaptic specialization. Proceedings of the National Academy of Sciences of the United States of America *98*, 7058-7061.

Shipman, S.L., Schnell, E., Hirai, T., Chen, B.S., Roche, K.W., and Nicoll, R.A. (2011). Functional dependence of neuroligin on a new non-PDZ intracellular domain. Nature neuroscience *14*, 718-726.

Shu, X., Lev-Ram, V., Deerinck, T.J., Qi, Y., Ramko, E.B., Davidson, M.W., Jin, Y., Ellisman, M.H., and Tsien, R.Y. (2011). A genetically encoded tag for correlated light and electron microscopy of intact cells, tissues, and organisms. PLoS biology *9*, e1001041.

Singh, S., and Mittal, A. (2016). Transmembrane Domain Lengths Serve as Signatures of Organismal Complexity and Viral Transport Mechanisms. Scientific reports *6*, 22352.

Sprecher, S.G., Cardona, A., and Hartenstein, V. (2011). The Drosophila larval visual system: high-resolution analysis of a simple visual neuropil. Developmental biology *358*, 33-43.

Sprinzak, D., Lakhanpal, A., Lebon, L., Santat, L.A., Fontes, M.E., Anderson, G.A., Garcia-Ojalvo, J., and Elowitz, M.B. (2010). Cis-interactions between Notch and Delta generate mutually exclusive signalling states. Nature *465*, 86-90.

Spuhler, I.A., Conley, G.M., Scheffold, F., and Sprecher, S.G. (2016). Super Resolution Imaging of Genetically Labeled Synapses in Drosophila Brain Tissue. Frontiers in cellular neuroscience *10*, 142.

Stephenson, N.L., and Avis, J.M. (2012). Direct observation of proteolytic cleavage at the S2 site upon forced unfolding of the Notch negative regulatory region. Proceedings of the National Academy of Sciences of the United States of America *109*, E2757-2765.

Stephenson, N.L., and Avis, J.M. (2015). Mutational analysis of the Notch2 negative regulatory region identifies key structural elements for mechanical

stability. FEBS open bio *5*, 625-633.

Stocker, R.F., Heimbeck, G., Gendre, N., and de Belle, J.S. (1997). Neuroblast ablation in Drosophila P[GAL4] lines reveals origins of olfactory interneurons. Journal of neurobiology *32*, 443-456.

Stork, T., Bernardos, R., and Freeman, M.R. (2012). Analysis of glial cell development and function in Drosophila. Cold Spring Harbor protocols *2012*, 1-17.

Struhl, G., and Adachi, A. (1998). Nuclear access and action of notch in vivo. Cell *93*, 649-660.

Struhl, G., and Adachi, A. (2000). Requirements for presenilin-dependent cleavage of notch and other transmembrane proteins. Molecular cell *6*, 625-636.

Sudhof, T.C. (2013). Neurotransmitter release: the last millisecond in the life of a synaptic vesicle. Neuron *80*, 675-690.

Sugie, A., Hakeda-Suzuki, S., Suzuki, E., Silies, M., Shimozono, M., Mohl, C., Suzuki, T., and Tavosanis, G. (2015). Molecular Remodeling of the Presynaptic Active Zone of Drosophila Photoreceptors via Activity-Dependent Feedback. Neuron *86*, 711-725.

Suh, J., and Jackson, F.R. (2007). *Drosophila* ebony activity is required in glia for the circadian regulation of locomotor activity. Neuron, 55, 435–447

Sun, M., Xing, G., Yuan, L., Gan, G., Knight, D., With, S.I., He, C., Han, J., Zeng, X., Fang, M.*, et al.* (2011). Neuroligin 2 is required for synapse development and function at the Drosophila neuromuscular junction. The Journal of neuroscience :

the official journal of the Society for Neuroscience *31*, 687-699.

Tabuchi, K., Sawamoto, K., Suzuki, E., Ozaki, K., Sone, M., Hama, C., Tanifuji-Morimoto, T., Yuasa, Y., Yoshihara, Y., Nose, A.*, et al.* (2000). GAL4/UAS-WGA system as a powerful tool for tracing Drosophila transsynaptic neural pathways. Journal of neuroscience research *59*, 94-99.

Takemura, S.Y., Bharioke, A., Lu, Z., Nern, A., Vitaladevuni, S., Rivlin, P.K., Katz, W.T., Olbris, D.J., Plaza, S.M., Winston, P.*, et al.* (2013). A visual motion detection circuit suggested by Drosophila connectomics. Nature *500*, 175-181.

Talsma, A.D., Christov, C.P., Terriente-Felix, A., Linneweber, G.A., Perea, D., Wayland, M., Shafer, O.T., and Miguel-Aliaga, I. (2012). Remote control of renal physiology by the intestinal neuropeptide pigment-dispersing factor in Drosophila. Proceedings of the National Academy of Sciences of the United States of America *109*, 12177-12182.

Tian, L., Akerboom, J., Schreiter, E.R., and Looger, L.L. (2012). Neural activity imaging with genetically encoded calcium indicators. Progress in brain research *196*, 79-94.

Tiyanont, K., Wales, T.E., Aste-Amezaga, M., Aster, J.C., Engen, J.R., and Blacklow, S.C. (2011). Evidence for increased exposure of the Notch1 metalloprotease cleavage site upon conversion to an activated conformation. Structure *19*, 546-554.

Tsurudome, K., Tsang, K., Liao, E.H., Ball, R., Penney, J., Yang, J.S., Elazzouzi, F., He, T., Chishti, A., Lnenicka, G.*, et al.* (2010). The Drosophila miR-310 cluster

negatively regulates synaptic strength at the neuromuscular junction. Neuron *68*, 879-893.

Tuthill, J.C., Nern, A., Holtz, S.L., Rubin, G.M., and Reiser, M.B. (2013). Contributions of the 12 neuron classes in the fly lamina to motion vision. Neuron *79*, 128-140.

Uytterhoeven, V., Kuenen, S., Kasprowicz, J., Miskiewicz, K., and Verstreken, P. (2011). Loss of skywalker reveals synaptic endosomes as sorting stations for synaptic vesicle proteins. Cell *145*, 117-132.

Varnum-Finney, B., Wu, L., Yu, M., Brashem-Stein, C., Staats, S., Flowers, D., Griffin, J.D., and Bernstein, I.D. (2000). Immobilization of Notch ligand, Delta-1, is required for induction of notch signaling. Journal of cell science *113 Pt 23*, 4313-4318.

Venken, K.J., Simpson, J.H., and Bellen, H.J. (2011). Genetic manipulation of genes and cells in the nervous system of the fruit fly. Neuron *72*, 202-230.

Vogt, K., Aso, Y., Hige, T., Knapek, S., Ichinose, T., Friedrich, A.B., Turner, G.C., Rubin, G.M., and Tanimoto, H. (2016). Direct neural pathways convey distinct visual information to Drosophila mushroom bodies. eLife *5*.

Volterra, A., Liaudet, N., and Savtchouk, I. (2014). Astrocyte Ca(2)(+) signalling: an unexpected complexity. Nature reviews Neuroscience *15*, 327-335.

Vooijs, M., Ong, C.T., Hadland, B., Huppert, S., Liu, Z., Korving, J., van den Born, M., Stappenbeck, T., Wu, Y., Clevers, H.*, et al.* (2007). Mapping the consequence of Notch1 proteolysis in vivo with NIP-CRE. Development *134*,

535-544.

Wagh, D.A., Rasse, T.M., Asan, E., Hofbauer, A., Schwenkert, I., Durrbeck, H., Buchner, S., Dabauvalle, M.C., Schmidt, M., Qin, G.*, et al.* (2006). Bruchpilot, a protein with homology to ELKS/CAST, is required for structural integrity and function of synaptic active zones in Drosophila. Neuron *49*, 833-844.

Wang, W., Goswami, S., Sahai, E., Wyckoff, J.B., Segall, J.E., and Condeelis, J.S. (2005). Tumor cells caught in the act of invading: their strategy for enhanced cell motility. Trends in cell biology *15*, 138-145.

Wang, X., and Ha, T. (2013). Defining single molecular forces required to activate integrin and notch signaling. Science *340*, 991-994.

Wickersham, I.R., Lyon, D.C., Barnard, R.J., Mori, T., Finke, S., Conzelmann, K.K., Young, J.A., and Callaway, E.M. (2007). Monosynaptic restriction of transsynaptic tracing from single, genetically targeted neurons. Neuron *53*, 639-647.

Wilson, R.I. (2013). Early olfactory processing in Drosophila: mechanisms and principles. Annual review of neuroscience *36*, 217-241.

Wishart, T.M., Parson, S.H., and Gillingwater, T.H. (2006). Synaptic vulnerability in neurodegenerative disease. Journal of neuropathology and experimental neurology *65*, 733-739.

Yamagata, M., and Sanes, J.R. (2012). Transgenic strategy for identifying synaptic connections in mice by fluorescence complementation (GRASP). Frontiers in molecular neuroscience *5*, 18.

Yamanaka, M., Smith, N.I., and Fujita, K. (2014). Introduction to super-resolution microscopy. Microscopy *63*, 177-192.

Yizhar, O., Fenno, L.E., Davidson, T.J., Mogri, M., and Deisseroth, K. (2011). Optogenetics in neural systems. Neuron *71*, 9-34.

Zhang, W., Yan, Z., Li, B., Jan, L.Y., and Jan, Y.N. (2014). Identification of motor neurons and a mechanosensitive sensory neuron in the defecation circuitry of Drosophila larvae. eLife *3*.

Zhang, Y.Q., Rodesch, C.K., and Broadie, K. (2002). Living synaptic vesicle marker: synaptotagmin-GFP. Genesis *34*, 142-145.